Catalysis assisted by plasmon

Iyad Sarhid

université PARIS-SACLAY

NNT: 2019SACLS227

Thèse de doctorat

UNIVERSITÉ PARIS SUD
Comprendre le monde, construire l'avenir

Catalysis assisted by plasmon

Thèse de doctorat de l'Université Paris-Saclay
préparée à l'Université Paris-Sud

École doctorale n°571 Sciences chimiques : molécules, matériaux, instrumentation et biosystèmes (2MIB)
Spécialité de doctorat: chimie

Thèse présentée et soutenue à Orsay, le 30 août 2019 par

Iyad Sarhid

Composition du Jury :

Olivier Pluchery Professeur, Sorbonne Université (INSP– Unité de recherche)	Président
Sara Cavaliere Maître de conférences, Université de Montpellier (ICGM– UMR 5253)	Rapporteur
Souhir Boujday Professeure, Sorbonne Université (LRS– UMR 7197)	Rapporteur
Arnaud Etcheberry Directeur de Recherche Emerite, CNRS -UVSQ (ILV – UMR 8180)	Examinateur
Isabelle Lampre Professeure, Université Paris-Sud (LCP– UMR 8000)	Examinatrice
Hynd Remita Directrice de Recherche, CNRS - UPSud (LCP – UMR 8000)	Directrice de thèse

Titre : Catalyse Assistée par Plasmon

Mots clés : Nanoparticules, Plasmon, Catalyse, Or, Palladium

Résumé : Les nanoparticules (NPs) métalliques ont de nombreuses applications en catalyse. Certaines d'entre elle (or, argent, cuivre) présentent une absorption dans le visible résultant de l'excitation du plasmon de surface par un champ électromagnétique extérieur.
Nous proposons dans ce projet de coupler les proprietes catalytiques de nanoparticules à base d'or avec leurs propriétés de résonance de plasmon de façon à assister la réaction catalytique par les électrons chauds générés et par l'effet thermique qui en découle.
Cette approche de catalyse assiste par plasmon, est générale et peut être utilisée pour une variété de procèdes catalytique exothermiques et endothermiques impliquant des nanoparticules. Cette catalyse assistée par plasmon permet de réaliser des réaction catalytiques à moindre cout énergétique sous lumière solaire.

Les processus catalytique sucitent un interet majeur pour la recherhe et le developpement. Des processus catalytiques photo-actives naturels interviennent dans presque tous les aspets de notre environnement: les cycles de photosynthese nourrissent et colorent les plantes, les reactions enzymatiques essentielles à la suivre des especes, la decontamination d l'eau à la lumiere visible, etc.

Enfin, la conclusion generale met en evidence les principaux resultats obenus au cours de cete these avec des nanostructures plasmonique de Au et de Pd utilisiees pour catalyer differentes reactions. Ces travauz ouvrent des perpectives en catalyse exaltee par plasmon, en particulier pour les applications environnmentales.

Title : Catalysis Assisted by Plasmon

Keywords : Nanoparticles, Plasmon, Catalysis, Gold, Palladium

Abstract : Metallic nanoparticles (NPs) have many applications in catalysis. Some of them (gold, silver, copper) have a visible absorption resulting from the excitation of the surface plasmon by an external electromagnetic field.
In this project, we propose to couple the catalytic properites of gold-based nanoparticles with their plasmon resonance properties in order to assist the catalytic reaction with the generated hot electrons and the resulting thermal effect.
This plasmon-assisted catalysis approach is general and can be used for a variety of exothermic and endothermic catalytic processes involving nanoparticles. This plasmon-assisted catalysis makes it possible to carry out catalytic reactions at lower energy cost under sunlight.

Catalytic processes are a of major interst for research and development. Natural photoactivated catalytic processes are involved in almost every aspect of our environment: photosynthetic cycles feed and color plants, enzymatic reactions essential for species survival, decontamination of water with visible light, etc.

Finally, the general conclusion highlights the main results obtained during this thesis with plasmonic nanostructures of Au and Pd used to catalyze different reactions. This work opens perspectives for plasmon-enhanced catalysis, especially for environmental applications.

Acknowledgements

I would like to extend my deepest gratitude to my director Mrs. Hynd Remita, for having faith in our project from the starting point till completion of this manuscript. Working under Mme. Remita's supervision was such an immense privilege. We managed to achieve multiple successes and milestones in several aspects of my years in academia. I admire Hynd's patience and support, her guidance, and her great scientific and human qualities, and I wish to work with her for future collaborations to develop products and valorize our research.

My deepest thanks goes of course to Mrs. Isabelle Lampre for the co-supervision of this work. She was involved in all of the studied systems. Her great expertise on photochemistry and kinetics was crucial to the advancement of this project. Mrs Lampre always suggested new and innovative routs to achieve desired products, challenged my work with interesting hypothesis, and helped me a lot during the last stretches of manuscript writing. I sincerely hope we collaborate again in the future.

I acknowledge C'Nano IdF and the DIM NanoK pour the financial support of the project and for the PhD scholarship.

Many thanks to Mr. Bruno Palpant from LPQM (Ecole-Centrale Supelec) and Mrs. Catherine Louis and Laurent Delannoy from LRS (Sorbonne Université) for their great involvement in this project. They generously participated in multiple meetings to discuss data and perspectives, provided platforms to carry out laser experiments and photocatlaysis units, allowed my research to branch-out and evolve.

Our collaboration with ICMMO (Université Paris-Sud, Université Paris-Saclay) resulted in winning a spot on the cover on New Journal of Chemistry on 2019. This achievement would not have been possible without the great expertise in organic synthesis, catalysis, and characterization of Mr. Ibrahim Abdellah and Mr. Vincent Huc and Mr. Cyril Martini. I am very glad to have had the opportunity to work with such talented and results-oriented researchers. I thank Mrs. Diana Dragoe (ICMMO) for XPS analysis, data treatment, and discussions. I thank Mrs Patricia Beaunier (LRS, Sorbonne Université) for TEM characterization and discussions.

My warmest thanks go to Mrs. Marine de Person and Mr. Fathi Moussa from LCP-Orsay for collaborating on mass spectroscopy and helping us with analytical qualitative analysis of our

results. I specially thank Mrs De Person for her patience and aid. I also would like to thank Mrs Mireille Benoît for being a great colleague to work with and very helpful in finding chemical products and setting up experiments. Mr. Tfayli's collaboration was such a great opportunity to work at the Faculty of Pharmacy – University Paris Sud, where we performed very helpful SERS experiments. We wish to publish our work soon and look forward to collaborating in the future.

My colleagues in the lab were such a pleasure to work with. We were a big family and we all took care of each other's. My special thanks go to Tayseer Bahry, Luis Hernandez Adame, Cecila Coletta, Maria-Guadalupe Mendez Medrano, Xiaojiao Yuan, Zhengpeng Chui for their help, kindness, and great scientific discussions.

Finally, I would like to thank my former supervisors Mr. Oliver Nüsse (LCP) and Nabil Joudieh (Damascus University) for being an inspirational force during my bachelor and master's. My parents Khalil and Maha, my sister Noor, and my brother Ayman for their faith and support, my beloved and life partner Astrid Dunselman and her family for the love and support, and last but not least: Abdullah Al-Baba and Osama Qubaitary, RIP.

Table of content

General introduction

Catalytic processes are attracting a major interest for research and development. Naturally-occurring photo-activated catalytic processes are involved in almost every aspect of our surroundings: photosynthesis cycles provide nurture and color to plants, enzymatic reactions that are crucial for survival of species, decontamination of water under visible light, and the list goes on.

A catalyst, from a chemical point of view, can be simply defined as a chemical entity with specific physio-chemical properties to accelerate and favor the least-energy-demanding reaction route to achieve the desired products. Nowadays, nanostructures of noble and transition metals had been widely developed to serve as catalysts with controlled morphology, variable chemical functionalization, and wide-range of possible crystallographic structures, as well as unique optical properties. In fact, nanoparticles of metallic nature show different properties than metals in their bulk structure. Several factors contribute to the difference in physico-chemical properties such as size, morphology, functionalization, and surrounded environment. These tunable properties are studied and applied in a vast spectrum of applications: industrial and academic research [1]. In particular, plasmon properties of metal nanoparticles have attracted a lot of attention. Indeed, when nanoparticles are under excitation of light, electrons oscillate in phase when excited at a certain wavelength of the electromagnetic wave of incident beam; this phenomenon is called Localized Surface Plasmon Resonance (LSPR). This absorption triggers the intraband transitions and heat dissipation around nanoparticles and allows an efficient and instant energy storing and exchanging throughout a complex mechanisms of interactions between photons and condensed electron gas of the metal. This interesting phenomenon generates localized hot-spots that are rich with electrons and energy in the form of heat. These hot-spots encouraged researchers to find suitable applications in the field of catalysis namely for reactions for environmental protection [2].

Gold, as an inert noble metal in its bulk state, had attracted our interest. Its brilliance, value, and stability drew attention of humans since the beginning of formed communities and societies. Gold is still in the core of today's economics, fashion industry, industrial and medical applications, cosmetics, and even in space shuttles [3]. Michael Faraday was the first who has reported the first preparation of colloidal gold nanoparticles (Figure 1). In his notebook Faraday observes : "The cone was well defined in the fluid by the illuminated particles" [4]. He realized that this cone effect was made because the fluid contained suspended gold particles that were too small to be observed with the scientific apparatus of that time, but which scattered the light

to the side. This is known as the **Faraday-Tyndall effect**, and it is because of this discovery that Faraday is seen as one of the first researchers in nanoscience and nanotechnology [4]. Gold nanoparticles with controlled size, shape, and functionalization have shown promising applications in several domains due to their catalytic properties and their surface plasmon resonance (around 525 nm for quasi-spherical NPs). Different redox reactions activated by Au nanoparticles under illumination have been studied [5, 6].

Figure 1. Michael Faraday (left) and his first prepared solution of gold nanoparticles preserved in the British museum (London)(right). [2]

Palladium is a very attractive metal for its applications in different catalytic reactions such as: selective hydrogenation, Suzuki-Miyaura and Heck reactions [7]. Recently, palladium attracts also interest in the field of nanomedicine [8]. Spherical Pd nanoparticles of few nanometers exhibit a plasmon band in the UV while palladium nanosheets show a broad plasmon absorption band in the visible-near infrared domain.

Plasmon properties of metal nanoparticles can be used to enhance the kinetics of catalytic reactions. Few reviews [9-14] have already been published on catalysis assisted by plasmonic nanostructures raising several questions such as:

- What are the possible mechanisms by which the catalytic effect takes place?
- What are the optimum physico-chemical conditions for a reaction catalyzed by plasmon of nanostructures? And many more.

Within this context, in order to bring part of the answers, we chose to study four model reactions:

1- Plasmon induced photo-decomposition of adsorbed para-nitrothiophenol on the surface of spherical gold nanoparticles and nanorods.
2- Photoreduction of Hexacyanoferrate assisted by plasmon of spherical gold nanoparticles under visible light.

3- Suzuki-Miyaura reactions catalyzed by plasmon of palladium nanosheets under visible light.
4- Gas phase oxidation of CO to CO_2 assisted by plasmon of gold nanoparticles deposited on a solid support.

It is worth mentioning that catalysis assisted by plasmon of metal nanostructures is an interdisciplinary domain of research that incorporates physics, chemistry as well biology with applications in the medical field for instance. Hence, it is challenging not only to observe this phenomenon, but also to interpret the obtained results. This manuscript aims to provide experimental models of catalytic reactions assisted by plasmon of nanostructures as well as proposing mechanisms for these reactions.

This manuscript is organized as follows:

The **first chapter** is an introduction to nanoscience with a focus on gold nanoparticles, their synthesis and properties, in particular, the localized surface plasmon resonance phenomenon and its applications. This chapter outlines the state of the art in catalysis assisted by plasmon.

The **second chapter** is devoted to the materials, metal nanoparticle synthesis and the experimental setups used to study the catalytic reactions. The different techniques used for characterization of the nanoparticles and for analysis of the reaction products are also described.

In **the third chapter** degradation of para-nitrothiophenol assisted by gold plasmon is studied. This degradation is much effective with Au nanoparticles excited under visible light. The results show that the degradation mechanism is complex as several products are formed. However, evidence is given that surface-catalyzed reactions involving hot electrons occur as (part of) para-nitrothiophenol is reduced to para-aminothiophenol.

In the fourth chapter, we investigate the reduction of ferricyanide (III) ion into ferrocyanide (II) catalyzed by spherical gold nanoparticles (AuNPs) when excited at their localized plasmon resonance. This reduction takes place, at room temperature and under illumination of visible light even without using a reducing agent. This result indicates again that hot electrons are involved in the reaction mechanism.

Suzuki-Heck cross-coupling reactions catalyzed by Pd nanoflowers plasmon are studied in the **fifth chapter**. The reactions between halogenated benzene compounds and phenylboronic acid in the presence of various bases are carried out in the dark and under visible light

irradiation. It is shown that the photocatalytic activity of Pd nanoflowers for Suzuki-Miuyara reactions is remarkably enhanced under visible light irradiation [7].

Finally, the general conclusion highlights the main results obtained during this PhD work with plasmonic Au and Pd nanostructures used to catalyze different reactions. It also gives perspectives of this work, in particular for environmental applications.

In annex, preliminary work on the oxidation of CO to CO_2 assisted by plasmon of Au nanoparticles (deposited on different supports) in gas and liquid phase is presented.

References

1 Baffou, G.; Rigneault, H. Femtosecond-pulsed optical heating of gold nanoparticles. *Phys. Rev. B* **2011**, *84*, 035415

2 Mahmoud, M.A.; Garlyyev, B.; El-Sayed, M.A. Determining the Mechanism of Solution Metallic Nanocatalysis with Solid and Hollow Nanoparticles: Homogeneous or Heterogeneous. *J. Phys. Chem. C* **2013**, *117*, 21886-21893.

3. Pluchery, O.; Remita, H.; Schaming, D. Demonstrative experiments about gold nanoparticles and nanofilms: an introduction to nanoscience. *Gold Bulletin* **2013**, *46*, 319-327.

4. Tweney, R.D. Epistemic Artifacts: Michael Faraday's Search for the Optical Effects of Gold in Magnani L., Nersessian N.J. (eds) *Model-Based Reasoning*. Springer, Boston, MA, **2002**, pp 287-303.

5. Carregal-Romero, S.; Perez-Juste, J.; Herves, P.; Liz-Marzan, L.M.; Mulvaney, P. Colloidal gold-catalyzed reduction of ferrocyanate (III) by borohydride ions: a model system for redox catalysis. *Langmuir*, **2010**, *26*, 1271-1277.

6. Wang, C.; Astruc, D. Nanogold Plasmonic Photocatalysis for Organic Synthesis and Clean Energy Conversion. *Chem. Soc. Rev* **2014**, *43*, 7188–7216.

7. Sarhid, I.; Abdellah, I.; Martini, C.; Huc, V.; Dragoe, D.; Beaunier, P.; Lampre, I.; Remita, H. Plasmonic catalysis for the Suzuki–Miyaura cross-coupling reaction using palladium nanoflowers. *New J. Chem.* **2019**, *43*, 4349-4355.

8. Dumas, A.; Couvreur, P. Palladium: a future key player in the nanomedical field? *Chem. Sci.* **2015**, *6*, 2153–2157.

9 Linic, S.; Christopher, P.; Ingram, D. B. Plasmonic-Metal Nanostructures for Efficient Conversion of Solar to Chemical Energy. *Nat. Mater.* **2011**, *10*, 911–921.

10 Wang, C.; Astruc, D. Nanogold Plasmonic Photocatalysis for Organic Synthesis and Clean Energy Conversion. *Chem. Soc. Rev.* **2014**, *43*, 7188–7216.

11 Baffou, G.; Quidant, R.; Nanoplasmonics for chemistry, *Chem. Soc. Rev.* **2014**, *43*, 3898-3907

12 Kale, M. J.; Avenesian, T.; Christopher, P. Direct photocatalysis by plasmonic nanostructures. *ACS Catal.* **2014**, *4*, 116-128.

13 Linic, S.; Aslam, U.; Boerigter, C.; Morabito, M.; Photochemical transformations on plasmonic metal nanoparticles. *Nat. Mater.* **2015**, *14*, 567-576.

14 Tatsuma, T.; Nishi, H.; Ishida, T. Plasmon-induced charge separation: chemistry and wide applications. *Chem. Sci.* **2017**, *8*, 3325-3337.

Chapter I

State of the Art

Table of content

While nanosciences and nanotechnologies appear as new concepts developed at the end of the 20th century, metallic nanoparticles have already been used since ancient times, in particular to colour glass and ceramics. Nowadays, nanomaterials and nanoparticles are used for many applications in our daily life, such as in the fields of electronics [1], catalysis [2], optics [3], biology [4], and medicine [5]. This first chapter will present a general context and background about metal nanoparticles and their physio-chemical properties.

I- Metal nanoparticles in history and nowadays

The properties of metal nanoparticles are different from the bulk and new properties emerge at the nanoscale. During the last fifty years, there has been a continuous development in understanding and controlling the optical and catalytic properties of noble metals at the nanoscale. A large number of different applications emerged during the previously mentioned development: catalysis, electrocatalysis, photocatalysis, sustainable energy, imaging, sensors, nanomedecine, and even artistic applications [1,6,7]. Our understanding of optical properties of bulk and metallic nanoparticles (NPs)(monometallic NPs and nanoalloys) has enhanced exponentially due to the innovative variety of microscopic characterization techniques and light sources such as pulse modulated fast lasers ranging from femtosecond laser pulses into continuous monochromatic lasers .

The main interest of choosing noble metals as a core of research and applications is a result of an ongoing research in the field of metallic objects and composites. Numerous publications report on the optical and catalytic properties of noble metals and their applications [7,8]. While nanoscience and nanotechnology appear as new concepts developed at the end of the 20th century, many studies showed the existence of metal nanoparticles in ancient art objects giving astonishing optical properties to vases, wine-cups, stained glass in churches, lusters, ceramics, plates, and even jewelry [1, 9].

While gold is known since long time for its golden color so appealing in jewelry, gold is also used since antiquity as red dye. For instance, Au NPs have been found in several red glasses or on porcelains decorated with red or pink enamels dating from ancient times. The most famous example of the use of metal nanoparticles concerns a piece of Roman glasswork, the Lycurgus Cup, dating from the fourth century CE, showing a mythological frieze depicting the legend of King Lycurgus and exposed in the British Museum in London. This

cup is made of bichromatic glass, which changes color when depending on how the light is shining on it (Figure I-1): The opaque green cup turns to a glowing translucent red when light is shined through it. These unusual optical properties are due to the presence of tiny amounts of gold, silver and copper nanoparticles (of about 50 nm) in the glass [1,8]. However, the inability to control the coloration process meant that relatively few glasses of this type were produced, and even fewer survived. The Lycurgus Cup is the outstanding example of this technology in every respect – its outstanding cut work and red-green dichroism render it a unique record [1].

Figure I-1. Lycurgus Cup (exhibited at the British Museum, London) showing two colors depending on how light is shined upon. It appears green when no light is inside (**left**), and red when light is shined inside (**right**) [1,8].

These "unexplained" (at that time) optical properties became handy, in terms of innovative decorations of churches windows during the renaissance age in Europe. Sainte-Chappelle in Paris-France is one of the many existing examples of where copper and silver nanoparticles were used to color stained glass (Figure I-2).

However, it is worth mentioning that these metallic amalgams were experimented repetitively for a long time. The craft of metallic alloys is handed from generation to generation. Hence, the practice in itself remained fascinating yet mysterious. Furthermore, one can depict from the historical timeline the overlap between the work of Alchemists and artisans led to formulate a sort of a protocol to synthesize colloidal solutions. Most references refer to the publication of Cassius: De Auro (1685) as a written protocol on synthesis of Cassius Purple [10]. Cassius purple was a colloidal solution used in the manufacturing of vases, cups, and windows. This is a colloidal solution of gold nanoparticles as we now know.

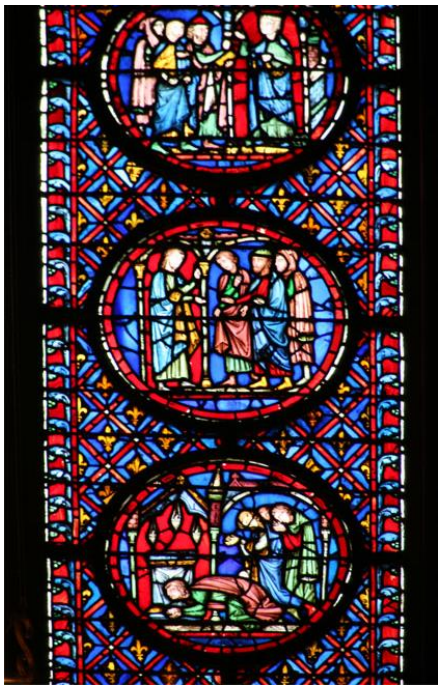

Figure I-2. Stained glass window from the Sainte-Chappelle in Paris.

Other interesting historical examples of unintentional presence of noble metal nanoparticles are porcelains and ceramics. For example, the recipe of the Purple of Cassius has reached China during the Qing Dynasty (eighteenth century), almost certainly conveyed by Jesuit missionaries, and has been successfully used for the production of the famous "Famille Rose" (Pink Family) porcelain [1].

Figure I-3. An example of "Famille Rose" (or "Pink family") porcelain: the "Mille Fleurs" vase, exposed in the Guimet Museum in Paris.

Later, in the 19th century, the properties of colloids attracted increasing attention. Michael Faraday was fascinated by the ruby color of colloidal gold and discovered that the optical properties of gold colloids differ from those of the bulk. In 1857, he reported the first synthesis of Au nanoparticles synthesized by the reduction of gold salts by white phosphorous in solution. This was the first reported observation of quantum size effects [11], and the birth of Nanoscience. Later, the specific properties of metal colloids were explained by Mie [12].

Noble metals had always been at the center of human activities. Copper, silver, and gold played a role in many social aspects of human development. Humans use silver and gold for jewelry as a manifestation of richness and of an upper social class. Gold and silver mines were a source of income and a motivation of dreamy workers during the industrial boost in Latin America and Central Asia.

Throughout the industrial revolution, the awareness of the importance of copper as a conductive metal led to the development of electronics, communication, and many more. Gold and silver kept their important value as the abundance of such noble metals is declining with time due to reservation and exhaustion of natural resources. Gold plays a key role not only in jewelry, decoration and esthetics, but also in finance and currency rates, and more recently in electronics and nanotechnology. This specific importance of noble metals encouraged researchers to understand their physical and chemical properties. In modern electronic devices, noble metals have a major role, although the full exploitation of their optical properties is at its beginnings.

Figure I-4 shows the world-wide production of gold according to the United States Geological Survey Center, and one can notice that China is a leader nowadays in the production of gold in metric tons.

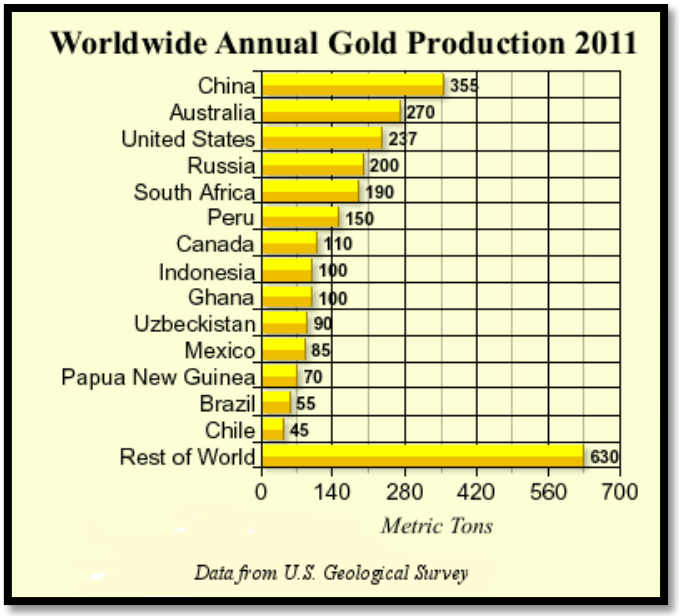

Figure I-4. Worldwide annual gold production according to United States Geological Survey Center.

II- Synthesis of metal nanoparticles

To understand nanoparticles' properties, which change with size and shape, and for applications of nanomaterials, it is important to develop protocols for controlled synthesis of nanoparticles. Various synthesis methods are developed to synthesize nanoparticles and nanomaterials of controlled size, shape, and composition. Thanks to the development of synthesis approaches, and technical tools to study nanomaterials, nanoscience and nanotechnology are showing a very fast development.

Nanoparticles can be prepared by two main approaches:

i. "Top-down" approach: by making the materials smaller, that is, by downscaling, using in general physical methods.

ii. Bottom-up" approach by constructing nanomaterials or nanoparticles from small building blocks, that is, by upscaling, using in general chemical or physico-chemical methods

In literature, there is a large abundance of innovative methods to synthesize gold nanoparticles (or other plasmonic nanostructures) with controlled size and shape in solutions or on supports. Herein, we will present some of these methods, with a particular focus on

synthesis of Au nanoparticles (NPs). Afterwards, we will focus on synthesis methods that were used during this research.

II-1- Physical methods for synthesis of metal nanoparticles

Generally, we refer to physical methods when a physical phenomenon is involved in the production of nanoparticles. It is in general a "top down" approach contrary to the chemical syntheses, which are "bottom up" methods. During this process, one can use a bulk solution of the noble metal and reduce the size by laser, grinding or other methods (not redox processes as used in general in chemical methods).

Recent advances in the fields of photochemistry and radiation chemistry allowed researchers to develop "green" synthesis protocols and alternative methods to synthesize nanostructures. Different light sources can be used to synthesize nanoparticles from "classical" UV-Visible light sources like Xenon lamps or LEDs to lasers. High energy radiations can be also used as a physio-chemical method to prepare nanoparticles and nanomaterials [13]. We describe here two physical methods for synthesis of metal nanoparticles: magnetron sputtering and laser ablation or vaporization.

II-1-1- Magnetron sputtering

Sputter deposition is a physical vapor deposition technique that ejects vapor of the material onto a substrate to synthesize nanoparticles on a solid support. The application of a potential difference between the target and the reactor walls in a rarefied atmosphere allows the creation of a cold plasma. In the presence of an electric field in the rarefied atmosphere, the cathode (the targeted support in this case) will attract the positive charges (the cations). Actually, an exchange between their momentums will cause sputtering of atoms in the form of neutral particles, which condense on the substrate. The sputtering gas is often an inert gas such as argon or nitrogen. This method has been used to synthesize various metal nanoparticles, including Au NPs (Figure I-5). Nevertheless, the control of the size by this method is limited [14].

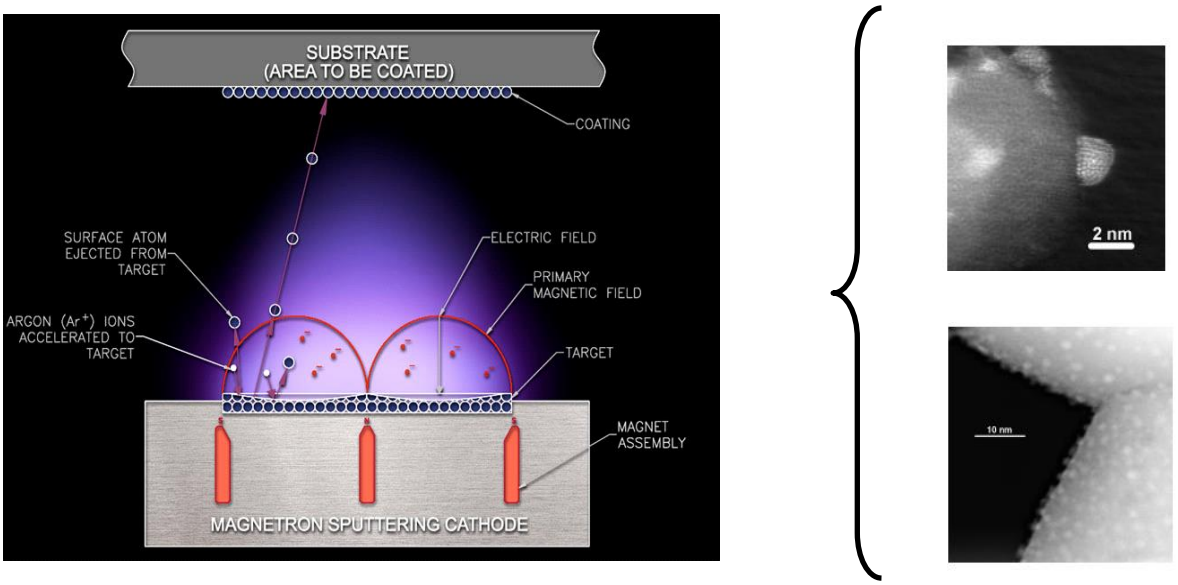

Figure I-5. A demonstrative scheme of magnetron sputtering technique and images of Au nanoparticles synthesized by this method [14].

II-1-2- Laser vaporization or ablation

Laser Vaporization or (Ablation) technique shares the same physical concept as the previous Magnetron Sputtering method. A laser vaporizes the target (for example Au high purity) to create neutral clusters deposited on the substrate (Figure I-6).

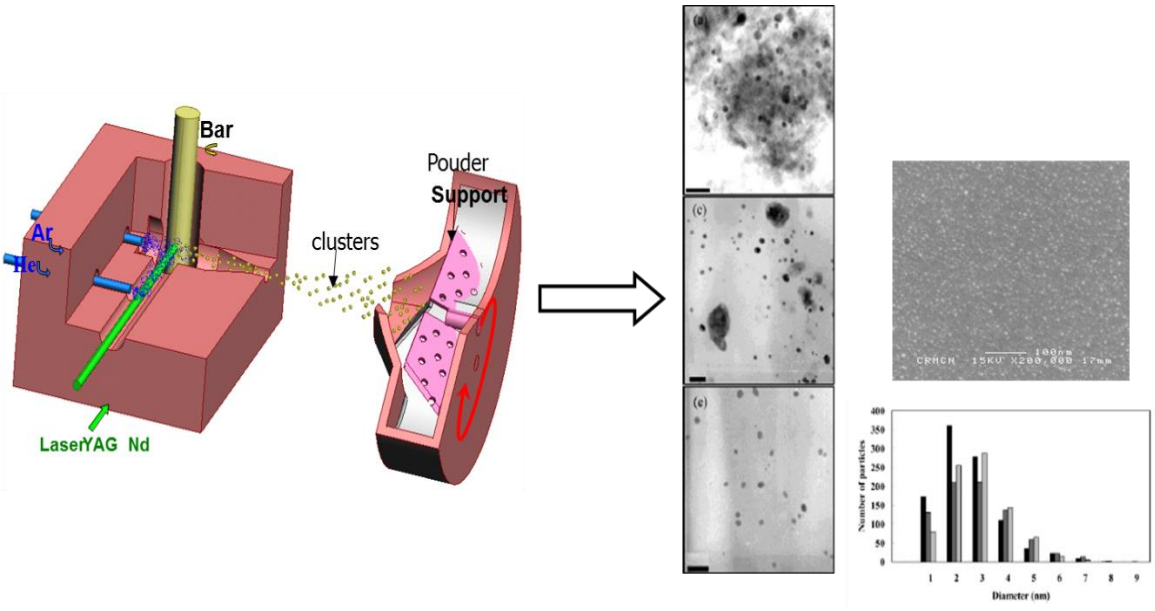

Figure I-6. A scheme representing laser vaporization technique to prepare nanoparticles, and an example TEM images of synthesized nanoparticles via this method along with their size historgram [15].

In other similar techniques, gold nanoparticles can also be synthesized by Laser Ablation in solution. At low laser flux, the material is heated by the absorbed laser energy and either evaporates or sublimates (Figure I-7). This method leads to the synthesis of well-dispersed and stable colloidal nanoparticles. Laser Ablation of solid targets in liquid environment allows the generation of nanoparticles (NPs) with high purity, easy surface functionability, metastable compositions, or complex structures, including doped nanocrystals, core−shells, hollow microspheres, nanotruffles, or nanocrescents [16].

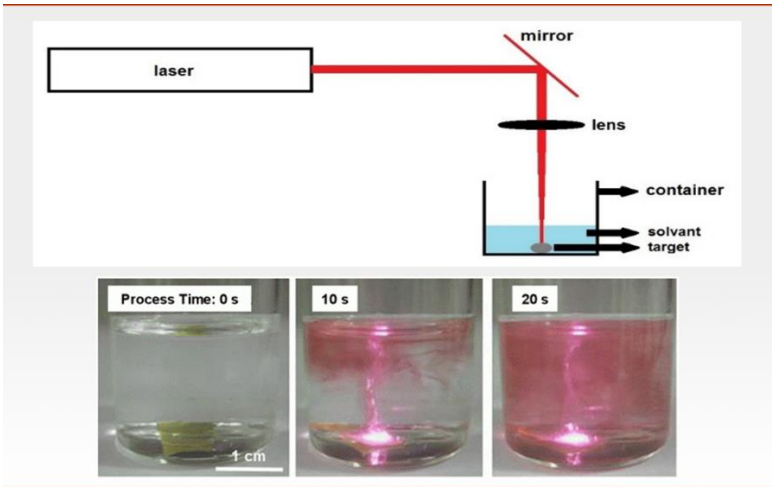

Figure I-7: Laser ablation technique used to synthesis gold nanoparticles in solution. Courtesy to Gregory Guisbiers.

II-2- Chemical methods for synthesis of metal nanoparticles

A metal salt or a metal complex is used as a precursor in solution or on supports (substrates) and is reduced by chemical agents or via radiation as we will explain later. In general, to obtain stable nanoparticles in solutions, synthesis proceeds in the presence of stabilizing agents (ligands, surfactants or polymers). Stability of colloidal solutions containing metal nanoparticles is either electrostatic or steric (Figure I-8). Electrostatic stability is due to a repulsive force generated by an electric double layer between charged nanoparticles in solution. Steric interactions with the stabilizing agents create a barrier that separates nanoparticles (polymer thiol chains can be an example) and can lead to stability of the colloidal solution.

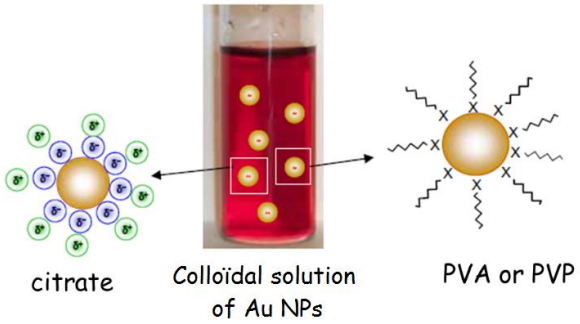

Figure I-8. Electrostatic (citrate) or steric (PVA or PVP polymer) of spherical gold nanoparticles.

Specific ligands such as calixarenes [17] or dendrimers can be used to control the size of Au NPs (Figure I-9). Few surfactants (such as cetyltrimethylammonium bromide (CTAB), because of their adsorption on specific nanoparticle faces, can lead to growth in 1 or 2 directions, and anisotropic nanoparticles can be formed.

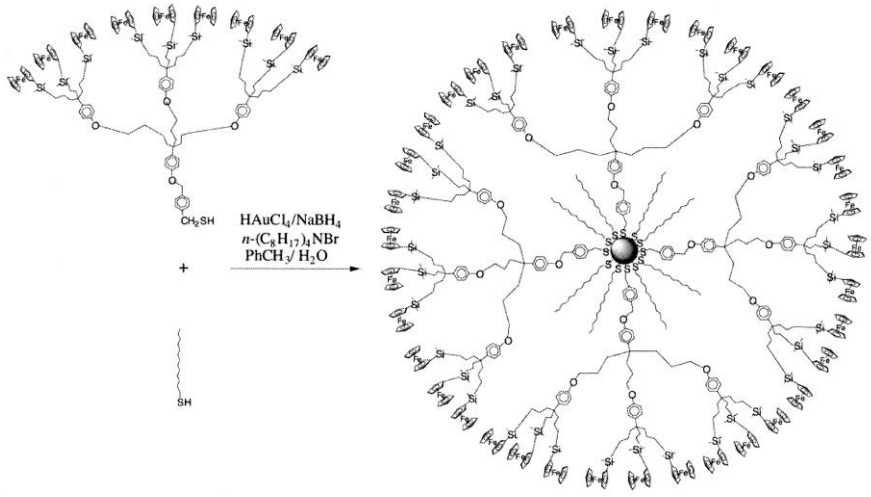

Figure I-9. Reduction and stabilization of gold nanoparticles with long chains of thiols and dendrimers [18].

In many chemical methods, gold nanoparticles are produced in solution by reduction of a gold complex (in general chloroauric acid $H[Au^{III}Cl_4]$ or potassium chloroauric $K[Au^{III}Cl_4]$). After dissolving $H[Au^{III}Cl_4]$, the solution is rapidly stirred while a reducing agent (a strong reducing agent such as $NaBH_4$ or NH_2-NH_2 or a weak reducing agent such as citrate) is added along with a stabilizing agent (ligand, surfactant or polymers) to limit the size of the nanoparticles and avoid aggregation [3,19,20]. In particular, citrate (a weak reducing agent) can play the double role of reducing and stabilizing agent [21].

II-2-1- Türkevich synthesis of gold nanoparticles

Türkevich method is probably one of the most basic and reproducible method for the synthesis of Au NPs. J. Turkevich *et al* [21] first published this method in 1951, and then G. Frens [22] studied this method extensively and developed it by adding the parameter of gold-to-reductant ratio to well control the nanoparticle size. Türkevich method is based on the reduction of an Au(III) salt ($HAuCl_4$ or $KAuCl_4$) in aqueous solution by trisodium citrate. Citrate plays a double role: reducing and stabilizing agent. Indeed, it will reduce Au^{III} into Au^0 and stabilize in the same time the formed Au nanoparticles. Because citrate is a weak reducing agent, the Au^{III} solutions are heated and generally boiled [9]. Türkevich-based methods can be also used for different precursors to form palladium, platinum, and bimetallic nanoparticles (NPs) such as silver-gold NPs.

In this study, we choose Türkevich-Frens method to synthesize Au nanoparticles in solutions because of the easiness and reproducibility of the method and the weak ligand character of citrate, which can be exchanged easily with other stronger ligands.

II-2-2- Deposition-Precipitation Method

Deposition-precipitation (DP) method is widely used by researchers to synthesize metal nanoparticles of controlled size on supports [4,23]. Typically, the supporting material, generally an oxide powder, is immersed into an aqueous solution of $HAuCl_4$ under stirring and fixed pH. Then, the catalyst precursor is recovered via centrifugation followed by washing steps with distilled water and sometimes ammonia to ensure maximum removal of Cl^- ions. The latter ions can affect the tuning of gold nanoparticles shape and morphology, as they tend to form undesired products during the thermal reduction of catalyst precursor. Afterwards, the remaining powder is calcinated (thermally treated under oxygen) in order to achieve certain size and morphology of gold nanoparticles.

Thermal reduction process consists in general in three steps:

(1) A slow rise in temperature until the desired calcination temperature is reached;

(2) A plateau of 2 hours at constant temperature should be maintained;

(3) A cooling-off at the same rate (in absolute value) as the initial temperature rise.

Any variation of temperature during the calcination plateau can affect the size of gold nanoparticles especially, when working on Au nanoparticles on TiO_2 [19,23].

Deposition method can also use other “reduction” methods to obtain gold nanoparticles. The replacement of calcination method can include photoreduction, radiolysis, and even chemical reduction and stabilization.

II-3- Synthesis of metal nanoparticles by radiolysis

Radiolysis is a powerful technique to synthesize metal nanoparticles of controlled size and shape in solutions and on supports [24-26]. This technique was largely developed in the Laboratoire de Chimie Physique (LCP, Université Paris-Sud). In this technique, solvated electrons and reducing radicals induced by solvent radiolysis are responsible of reducing the metal precursors [25]. Radiolysis presents the advantage of inducing a homogeneous reduction and nucleation in the whole volume of the sample leading to homogeneous nucleation and growth.

The primary effects of the interaction of high-energy radiation such as particle beams, X-rays or gamma photons with a solution of metal ions are the excitation and the ionization of the solvent molecules, which lead to the formation of primary species. In case of water, these primary species are:

$$H_2O \rightarrow e^-_{(aq)}, H_3O^+, H^{\cdot}, OH^{\cdot}, H_2, H_2O_2$$

The solvated electron $e^-_{(aq)}$ and the hydrogen atom are reducing species able to reduce metal ions to atoms, whereas the hydroxyl radical ˙OH is an oxidizing species:

$E^0(H_2O/e^-_{(aq)})$ = -2.87 V_{NHE}

$E^0\ (H^+/H^{\bullet})$ = -2.3 V_{NHE}

$E^0\ (OH^{\bullet}/H_2O)$ =1.8 V_{NHE} in pH=7 and 2.7 V_{NHE} pH<7

Consequently, 2-Propanol, for instance, is added to the solution (in general 0.1 M) to scavenge the $HO^{\cdot}$ radicals and generate reducing alcohol radicals, which can also reduce metal ions:

$$(CH_3)_2CHOH + OH^{\cdot} \rightarrow (CH_3)_2C^{\cdot}OH + H_2O$$

$$(CH_3)_2CHOH + H^{\cdot} \rightarrow (CH_3)_2C^{\cdot}OH + H_2$$

The reduction steps of $Au^{III}Cl_4$ into Au^0 in aqueous solution and the formation of gold nanoparticles have been studied by the LCP team [24,25]. Au^{III} is reduced to $Au^{0,}$ which will coalesce and aggregate to form nanoparticles, via the following pathways:

$$Au^{III} + e^-_{(aq)} \rightarrow Au^{II}$$

$$Au^{III} + (CH_3)_2C^{\bullet}OH \rightarrow Au^{II} + (CH_3)_2CO + H^+$$

$$2\ Au^{II} \rightarrow Au^{I} + Au^{III}$$

$$Au^{I} + e^{-}_{(aq)} \rightarrow Au^{0}$$

$$Au^{I} + (CH_3)_2C^{\bullet}OH \rightarrow Au^{0} \text{ or } + (CH_3)_2CO + H^{+}$$

$$Au^{I} + H^{\bullet} \rightarrow Au^{0} + H^{+}$$

Metal nanoparticles of controlled size can be obtained by controlling the precursor and stabilizer concentrations as well as the dose rates (which fix the reductions kinetics) and the dose (which control the reduction rate).

Anisotropic nanoparticles, such as Au nanorods [13] or palladium nanosheets and nanoflowers [27-30] can be obtained using surfactants or ligands, which promote 1D- or 2D-growth. In case of bimetallic nanoparticles, the structure (core-shell structures or alloys) can be easily tuned by controlling the dose rate: At low dose rate, core-shell nanoparticles are generally obtained, while nanoalloys are obtained at high dose rate [31].

III-Properties of metal nanoparticles and applications

III-1- Catalytic properties

Chemists have long neglected gold because of its inertness. In 1987, M. Haruta has demonstrated that very small Au nanoparticles (with diameters less than 5 nm) can catalyze the oxidation of CO (which is a very toxic gas) into CO_2, even at room temperature [28,30,32]. Compared to platinum catalyst used for the CO oxidation reaction in the catalytic convertors of cars, the reactivity is not only multiplied by a factor close to 10, but it also occurs at much lower temperature (even at room temperature). Since this discovery, gold NPs are attracting a huge attention from the scientific community [28,29].

Usually, these Au nanoparticles are supported on support oxides such as titania or alumina for application in heterogeneous catalysis. Au NPs displayed catalytic properties for many other chemical reactions, such as oxidation of alcohols to acids or aldehydes, the formation of hydrogen peroxide, and selective hydrogenation of C-C bonds and NO [33,34].

III-2- Optical properties

Light and matter interaction has received extensive attention in recent years [29]. Noble metals specifically, exhibit interesting optical properties at the nanoscale. Optical properties of plasmonic nanostructures have been a very interesting subject for physicists and chemists,

especially since Mie solution to Maxwell-Garnette equation was published in early 1900 [12]. The ability of acting as nanoscale heat sources under light irradiation is also considered equally puzzling and interesting for many applications.

Plasmonic nanostructures are mainly characterized by their excellent absorption of visible light through localized surface plasmon resonance (LSPR). This resonance can be described as coherent oscillations of the confined surface electrons gas excited by incident electromagnetic radiation, when the excitation frequency matches the characteristic frequency of metal nanostructures. Furthermore, the definition of a Plasmon can be presented as following "a plasmon is a quantum of plasma oscillation" (Figure I-10). In other words, a plasmon is the quantization of the collective longitudinal and/or transversal excitation of a conductive electron gas in a metal. Narayanan *et al.* published a very interesting review that discusses the physical origin of surface plasmon resonance in gold nanoparticles while focusing on Mie and Maxwell-Garnette theory and reviews the effects of particle size and shape on the resonance conditions [35]. Furthermore, it is known that reducing the size of a nanoparticle has a pronounced effect on the energy level spacing as the system becomes more confined [16,36]. The plasmon resonance phenomenon, which arises from the dipolar nature of the wave-driven collective electron excitation allowed by the small nanoparticle size, is essentially a coherent set of in-phase intraband transitions.

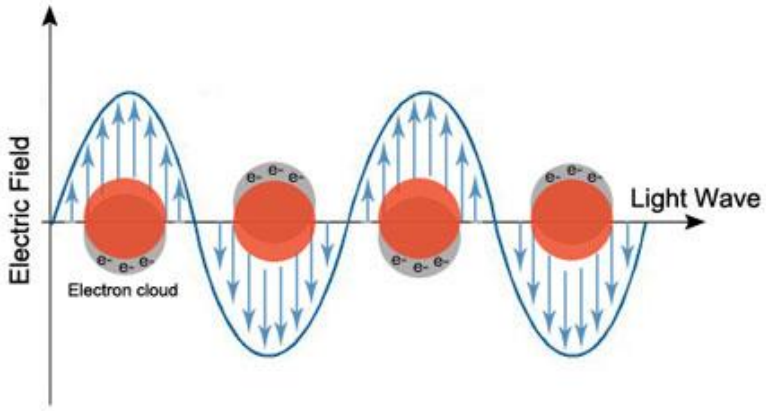

Figure I-10. Schematic presentation of polarization of a spherical plasmonic nanoparticle and the continuous oscillation due to dielectric function interactions.

These collective oscillations of the electrons is constrained by the reduced dimensions of the NP in which they are confined, leading to a significant absorption of the wavelengths around 520 nm (green) in case of spherical AuNPs with a diameter in the range of 10 nm in

water (Figure I-11). Then, NPs appear within the complementary colour, which is red. In case of silver the plasmon is around 420 nm (for the same size) leading to a yellow colour (Figure I-11). Moreover, as the size of gold and silver nanospheres increases, there is a red-shift in the LSPR due to a low frequency for the collective oscillation of electrons, which causes electromagnetic retardation in larger particles. The LSPR absorption is also tuned by the surrounding dielectric environment that is influenced by the solvent effect and substrate effect [37].

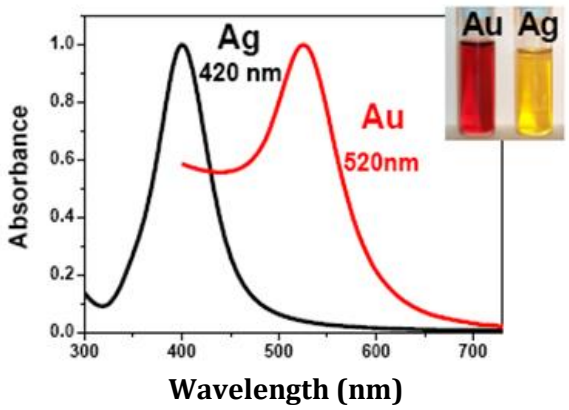

Figure I-11. Plasmon spectra of spherical Au and Ag nanoparticles in water and the corresponding vials containing these nanoparticles.

Gold nanorods (NRs) have recently attracted a lot of attention because of their exceptional optical properties and their potential applications in nanomedicine and the field of sensors [38-40]. Indeed, they present two surface plasmon resonance (SPR) absorption bands corresponding to the electromagnetic wave-driven oscillation of the quasi-free electrons along (longitudinal SPR, LgSPR) and perpendicular (transverse SPR, TrSPR) to the rod long axis (Figure I-12). The selective excitation of one or the other depends on the electric field polarization. Whereas the TrSPR is almost insensitive to the NR morphology, the spectral location of the longitudinal one (LgSPR) can be easily tuned from green to near-infrared by modifying the NR aspect ratio (the aspect ratio being the ratio of the largest axis to the shortest one): The longer the rod is, the smaller the LgSPR frequency. On the basis of these properties, noble metal NRs are thought to be good candidates for different applications, such as nanoparticle mediated hyperthermal therapy against cancer and optical data storage [41].

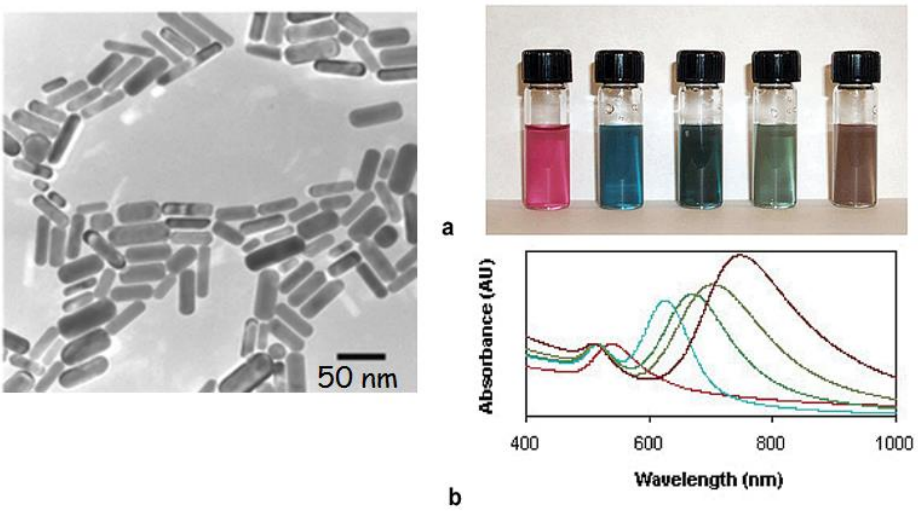

Figure I-12: Transmission electron microscopy image showing Au nanorods (**right**), and vials containing Au nanorods of different aspect ratios (**a-left**) and the corresponding absorption spectra (exhibiting longitudinal and transverse plasmon bands) (**b-left**) [42].

It is also worth mentioning that noble metals at a nanoscale could act as sources of electrons and heat under illumination. The localized Surface Plasmon Resonance (LSPR) phenomenon could become a very effective way of disposing energy into nanoobjects, especially in the case of noble metals.

When the incident light excites the confined surface electrons, the nanoparticle itself tend to experience a depolarization of the electron gas. The vibrational modes of conductive electrons will vibrate in a coherent manner that will be followed by either an ejection of a hot-electron, or a localized thermal change due to energy input and dissipation in the surrounding medium. Hot electrons originate from the relaxation pattern in which excited electrons relax by electron-electron (e-e) scattering (heat dissipation) [43].

Moreover, LSPR is an efficient way to input energy in a small metallic objects, which will enhance the yield of nano-scale light to heat conversion. Thus, a new door in applied sciences is open for investigation. The applications of LSPR can range from bio-sensors and medical application in cancer therapy, to plasmonic catalysis and solar light harvesting. Plasmonic solar-cells are for example being developed to enhance light-harvesting mechanisms, thus raising the efficiency of solar cells in terms of photo conversion efficiency (PCE) [44].

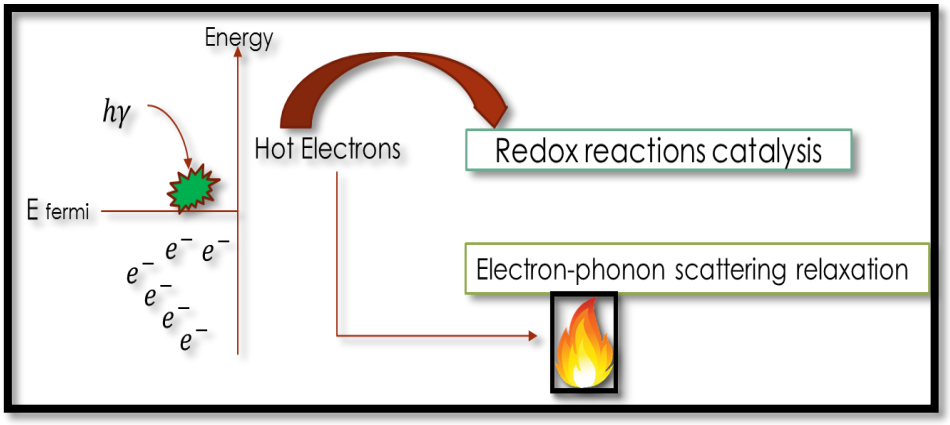

Figure I-13: Schematic presentation of the two main possible pathways for hot electrons to interact with the surrounding medium [45].

III-3- Biological applications

Cancer therapy by hyperthermia can treat tumors by heating, for example using lasers. This is the principle of the "thermal therapy". NPs allow to heat cancer cells very locally and to kill them. Plasmonic NPs absorb light rapidly and the excitation is converted into heat, increasing hyperthermia locally generated by the laser [46].

The absorption band of the NPs has to be located in the near-infrared region "biological window" from 650 to 900 nm (the wavelength range penetrating living tissues). Because of their optical properties, stability and their biocompatibility, gold nanoparticles are the candidate of choice for this application. Therefore, it is important to optimize the size and shape of gold nanoparticles: Au nanorods, Au bipyramides and Si_{core}-Au_{shell} NPs are developed for thermal therapy [47-50]. Au nanoparticles can be used in imaging and therapy in the same time (theranostics) using their optical properties. Drug-delivery using photochemical properties of metal nano-objects is also widely studied [51,52]. Photothermal imaging is also being developed as the understanding of the fundamental physics of LSPR is continuing to expand. Individual detection of single-nanometer sized particles in liquid by photothermal microscope was proposed [53]. Single metallic nanoparticles imaging for protein detection in cells was proposed using antibodies carrying gold nanoparticles (10 nm) and heated by a laser at 514 nm [48].

Au NPs can be easily functionalized and used as sensors to detect biological molecules [54-56]. They are for example used in the pregnancy tests, where they are functionalized with anti-bodies — anti-β-HCG hormones — for detection of β-HCG hormones characteristic of pregnancy. Au NPs can also be used for detection of malignant cells or infectious agents such

as bacterial agents or viruses (for example Mycobacterium tuberculosis, which causes tuberculosis, or viral agents such as the AIDS virus or Hepatitis B). In these cases, Au NPs are functionalized with a DNA sequence complementary to a gene or a portion of gene specific of these infectious agents. They can be also used for the diagnosis of Alzheimer's disease [1].

IV- Catalysis assisted by plasmon of metal nanoparticles

In the following paragraphs, we will try to go over the latest developments in the field of catalysis assisted by plasmonic nanostructures. Since most of the work introduced in this manuscript is focused on gold nanoparticles, we will emphasis on that particular aspect. In addition to photophysical processes, optically excited plasmonic nanoparticles can also activate and induce chemical transformations directly on their surfaces. This phenomenon is called plasmonic catalysis and offers opportunities in reduction or oxidation reactions and in the field of selective chemical synthesis [57].

In the last decade, application of plasmonic nanoparticles for solar to electrical energy and solar to chemical fuel conversions attracted a lot of interest. In a review, Linic *et al.* summarized recent progress in the field of photochemical catalysis on plasmonic metallic nanostructures [44]. The use of LSPR excitation to drive photocatalysis is called plasmonic photocatalysis and falls into two categories: (a) indirect photocatalysis, where excitation of LSPR is used to transfer photon energy to nearby semi-conductors, molecular photocatalysts, and other metals to drive chemical reaction, and (b) direct photocatalysis, where excited metal nanoparticles act as direct catalytic active sites. In the present work we will focus on direct photocatalysis (where the metal nanoparticles are not supported). By precise control of the size, shape, and environment of a plasmonic metal nanostructure, it is possible to design efficient plasmonic photocatalysts for applications.

IV-1- Plasmon assisted catalysis with non-supported metal nanoparticles:

Surface plasmon excitation of colloidal gold nanoparticles with visible light in the presence of H_2O_2 led to rapid and selective oxidation of sec-phenethyl and benzyl alcohols to acetophenone and benzaldehyde, respectively (Figure I-14**)**. Au NPs were excited by light (through both 532 nm laser and 530 nm LED techniques) or via microwave irradiation [58].

The authors proposed electron transfer with the nanoparticle surface, as well as the participation of peroxyl and ketyl free radicals as fundamental steps in the reaction pathway.

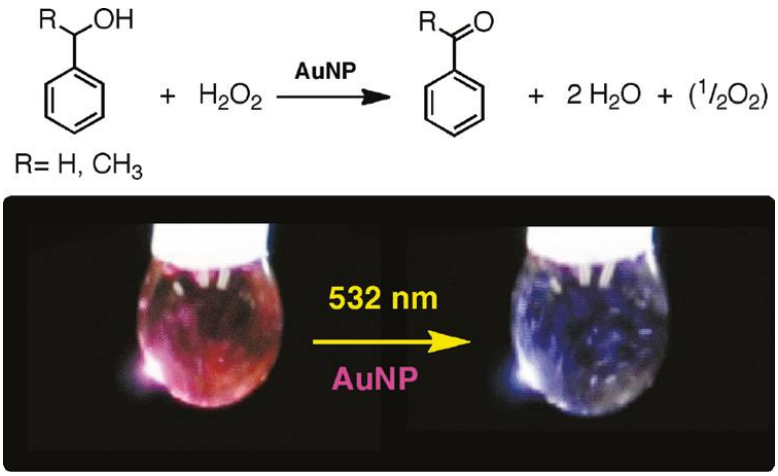

Figure 1-14. Plasmon mediated selective oxidation of sec-phenethyl and benzyl alcohols. to acetophenone and benzaldehyde obtained by irradiation of colloidal Au NPs by LED at 532 nm Aggregation of Au NPs is observed after photocatalytic process (inducing a blue colour because of plasmon coupling) [59].

This study was one of the first examples of colloidal Au NPs employed in plasmon-mediated organic reactions, specifically for alcohol oxidations. These results showed that plasmonic photocatalysis allows the use of more environmentally friendly precursors, such as water and H_2O_2, rather than the more current and toxic alternatives in oxidation reactions used in organic chemistry. Interestingly, the authors studied and discussed the mechanism. The authors proposed that hydroxyl radicals can be induced by electron transfer to H_2O_2 or by thermal decomposition of H_2O_2 and that HO· and ·OOH (formed by the reaction of HO· with H_2O_2) radicals induce oxidation of the alcohols. After exposure to light, the nanoparticles aggregated, which led to a change in color (from red to blue).

The intermediate polarization of the NP surface electrons via plasmon excitation can induce rapid localized heating of the NP surface allowing for harvesting of thermal energy. The important increase in temperature around the NPs allows chemical reactions requiring high temperatures to be carried out in the microenvironment surrounding the AuNPs at ambient conditions. The induced electromagnetic field generated upon plasmonic excitation can also be used to exploit the photochemical activity of metal nanoparticles. The use of plasmon excitation can amplify the efficiency of many photochemical processes by excitation in the visible region of the electromagnetic spectrum. More importantly, direct excitation of metal nanoparticles can also favor ejection of electrons, and this can be applied in a variety of

photo-initiated electron transfer reactions. Figure I-15 outlines the possible dominant pathways following plasmon excitation of metal nanoparticles in the presence of organic molecules in the plasmon-mediated catalytic processes.

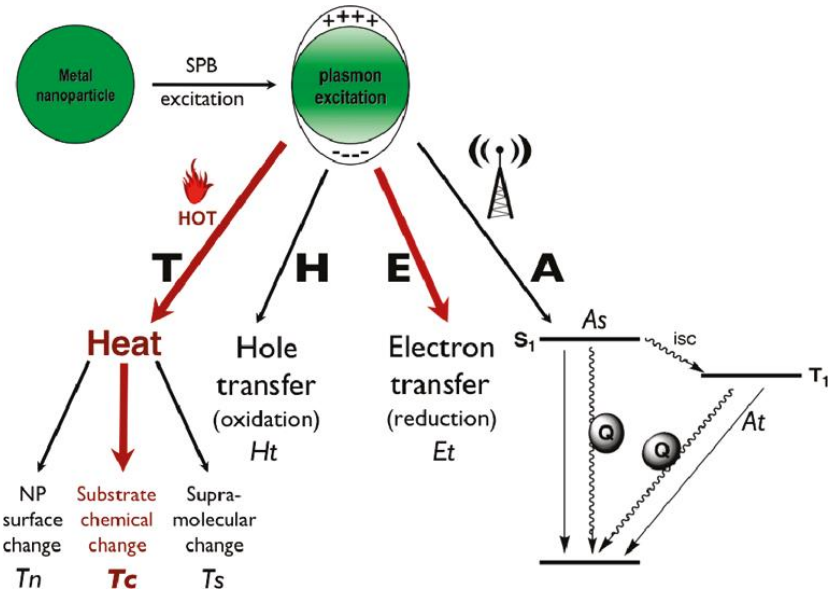

Figure 1-15. Possible reaction pathways following plasmon excitation of metal nanoparticles in the presence of organic molecules. In the presence of a suitable receiver, antenna effects (A) can result in excited state processes (As and At). Plasmon relaxation can lead to thermal effects (T) that can themselves induce supramolecular changes in guest molecules (Ts), chemical change (Tc) sometimes referred as photocatalysis, or changes in the nanoparticle itself (Tn) of either a physical or chemical nature (e.g., oxidation). Under plasmon excitation the nanoparticle can act as an electron donor (Et) or as an electron acceptor (Ht). Red arrows are used to highlight the mechanisms to be discussed in this contribution [43].

Bimetallic nanoparticles have attracted increasing attention for applications in different fields such as catalysis, electrocatalysis, sensing, magnetic storage, etc. In particular, bimetallic nanoparticles based on gold have are attracting a lot of interest because of their optical properties and their application in catalysis and electrocatalysis [58-61]. Development of metal nanostructures that exhibit both unique plasmonic and unique catalytic features is critical for application in plasmonic catalysis. Bimetallic AuPd nanowheels (Au core surrounded by metallic Pd) with tunable SPR have been synthesized by Huang *et al* [62]. These AuPd nanowheels can utilize solar energy to drive catalytic reactions, such as the oxidation of benzyl alcohol and Suzuki coupling reactions, at lower temperatures, and with much higher performance compared to conventional heating processes.

However, in catalysis, for practical applications, to prevent NPs from aggregation or sintering and to recover the catalysts after reactions, metal nanoparticles are in general supported on solid substrates. Different studies report on plasmonic catalysis conducted by metal nanoparticles on different supports [63].

IV-2- Plasmon assisted catalysis via supported metal nanoparticles

Different inert supports are commonly used to deposit metal nanoparticles for application in catalysis such as: alumina (Al_2O_3), Silica (SiO_2), ceria (CeO_2), zirconia (ZrO_2), zeolites, hydrotalcite ($Mg_6Al_2(CO_3)(OH)_{16}$) [4]. The first example of plasmonic catalysis by metal NPs on inert supports was reported by Hallet-Tapley *et al.* who showed the conversion of benzyl alcohol in benzaldehyde and 1-phenylethanol in acetophenone by Au NPs deposited on hydrotalcyte, alumina or zeolites (1% in mass) and excited by LED at 530 nm (Figure I-16) [58].

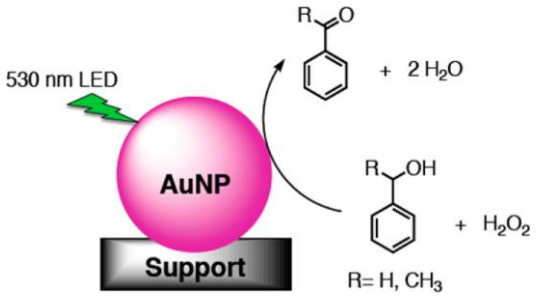

Figure I-16. A scheme showing conversion of benzyl alcohol in benzaldehyde and 1-phenylethanol in acetophenone by Au NPs deposited on a support and excited by LED at 530 nm [58].

NaY zeolites decorated with Au NPs were used to catalyze the acetalization of aromatic aldehydes with methanol [61]. Interestingly, Zhang et al. reported that enhanced catalytic performance of zeolites via the plasmonic effect of gold nanoparticles is closely correlated with the molecular polarity of reactants. The intensified polarized electrostatic field of Na^+ in NaY zeolites plays a critical role in stretching the C=O bond of aldehydes to improve the reaction rate. The catalysts could be recycled and reused after five runs, but a small decay in catalytic activity was observed.

The AuNPs also exhibit significant ultraviolet (UV) absorption because of interband transitions of electrons from 5d to 6sp. Visible light and UV irradiation constitute around 43

% and 4 % of the solar energy emitted by the sun, respectively. The sun spectrum is summarized in Figure I-17.

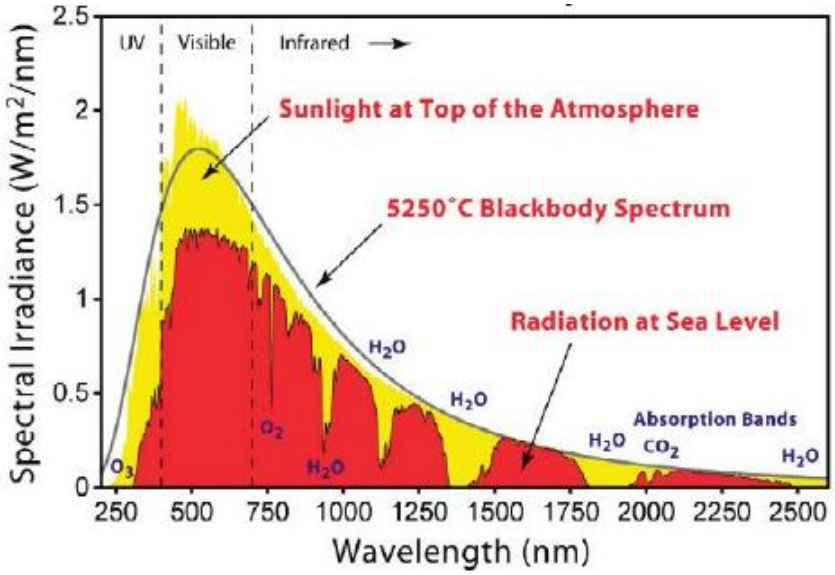

Figure I-18- Solar spectrum at the top of the atmosphere and at sea level [64].

AuNPs have also the potential to use sunlight to efficiently drive chemical reactions and induce photocatalytic processes. These catalytic processes induced by light can be used for synthesis of azo-dyes, which are widely used in the production of dyes, pharmaceutical products, and food additives. Currently azo-dues are synthesized under high pressures and at high temperatures using transition-metal reducing agents and the formed by-products are harmful to the environment [65]. It has been shown for example that Au NPs (of about 6 nm) supported on ZrO_2 can drive reduction of nitro-aromatic compounds (in particular nitrobenzene into azobenzene in the presence of isopropanol (which will be converted into acetone) when excited under solar light [66]. Isopropanol plays the role of sacrificial donor of protons and electrons. Pineda *et al.* reported that Au/SiO_2 nanoparticles irradiated by a laser at 532 nm catalyze amidation reactions: The production of 4-benzoylmorpholine from benzaldehyde and morpholine via amide formation was obtained with higher conversion rate and higher selectivity when the nanoparticles were irradiated [2].

Plasmonic catalysis can also be used for water treatment. Excitation of 5 nm-Au NPs deposited on SiO_2 leads to decomposition of methyl orange dye (used as model pollutant) and trichloroethylene (selected as an example of a real water pollutant) [67]. These oxidative processes are induced by oxidative radicals ($O_2^{\cdot-}$ can be formed by reaction of hot electrons with O_2), as well as $HO^{\cdot}$ formed by the reactions:

$O_2^{\bullet-} + H^+ \rightarrow HO_2^{\bullet}$ (1)

$2\ HO_2^{\bullet} \rightarrow H_2O_2 + O_2$ (2)

$H_2O_2 + O_2^{\bullet-} \rightarrow {}^{\bullet}OH + O_2 + OH^-$ (3)

$H_2O_2 + h\nu \rightarrow 2\ {}^{\bullet}OH$ (4)

Plasmon excitation can also be used for functionalization of Au NPs. Reactivity of aryl diazonium salts is commonly used to graft them on surfaces by electro-reduction. Aryl diazonium can also be grafted using UV or visible light (photo-grafting), but with this process the grafting slow or weak, photosensitizers can then be used to enhance its efficiency. Controlling the surface grafting of species at the nanoscale remains a major challenge for different applications. Nguyen *et al.* reported plasmon-mediated grafting of aryl films derived from diazonium salts on regular arrays of gold nanostripes. This grafting occurs specifically in the regions of maximum of field enhancement [68]. The thickness of the aryl film can be monitored by the LSP wavelength and the incident light energy.

IV-3- Plasmonic NPs supported on photocatalytic substrates

TiO_2 is a very efficient photocatalyst due to its strong oxidation capacity, high photochemical and biological stability and low cost. Since the discovery of photoinduced decomposition of water on a TiO_2 electrode, TiO_2-based photocatalysts have attracted wide attention [69]. The limitation in TiO_2 application, results from low quantum yield due to fast charge carriers (electron/hole e-/h+) recombination and its activation only under UV irradiation because of the value of its band gap (3.2 eV for anatase and 3.0 eV for rutile). UV light constitutes only about 3-4 % of the solar spectrum impinging on the Earth's surface, therefore modification of titania to extent its absorption to visible domain and to enhance its activity is a very active area of research. Surface modification with noble metal (platinum, palladium, silver, gold) nanoparticles (NPs) can result in enhancement of the photo-conversion quantum yield and may allow the extension of the light absorption of wide band-gap semiconductors to the visible light. In particular, plasmonic photocatalysts have appeared as a very promising way to induce a photocatalytic activity of TiO_2 in the visible range [7,44].

Different studies report on modification of TiO_2 with metal nanoparticles for photocatalytic applications: water depollution and hydrogen production.

In the plasmonic photocatalytic Au/TiO_2 system, the presence of Au is essential, due to their localized surface plasmon resonance (LSPR). These plasmonic properties can be used to induce photocatalytic activity of the semiconductor material under visible light. However, the support presents also important effects on the photocatalytic processes, *i.e.*, *(i)* the electron-hole recombination for anatase and rutile particles has been studied and was found to be higher for rutile than anatase; *(ii)* the higher Fermi level of anatase results in stronger electronic interaction with Au-NPs, which can inhibit the growth and aggregation of metal nanoparticle; *(iii)* the difference in energy band gap of anatase (3.2 eV) and rutile (3.0 eV) could result in activation of TiO_2 at longer wavelengths for rutile and finally, *(iv)* the dielectric constant of the support could shift the LSPR of metal nanoparticles toward the red spectral region. For example, it was shown that crystalline composition and surface properties of Au/TiO_2 photocatalysts, prepared by photodeposition of gold on fifteen commercial titania, influenced significantly the resultant photocatalytic activities in a different manner under UV and visible light irradiation [70]. Small gold nanoparticles (Au-NPs) around 2-3 nm on the surface of titanium dioxide work as visible-light absorbers and thermal redox active centers. Au-NPs were synthesized on commercial TiO_2 by reduction with tetrakis(hydroxymethyl)-phosphonium chloride [71]. The photocatalytic activity of Au/ TiO_2 was evaluated for degradation of phenol, 2-propanol, acetic acid and for H_2 production from aqueous methanol solution. This photocatalytic activity was much higher for the plasmonic TiO_2 compared to the activity of bare titania. Time resolved microwave conductivity (TRMC) signals showed injection of electrons from Au-NPs to the conduction band of TiO_2 under visible-light excitation, due to the activation of localized surface plasmon resonance (LSPR) of the Au-NPs [71]. Action spectra (AS) correlated with the absorption spectra proving that decomposition of model pollutants is carried out by a photocatalytic mechanism. Au- TiO_2 were also active for hydrogen evolution under visible light. It has been also shown that these photocatalysts can be reused several times without appreciable loss of activity.

V- Conclusion

Nanoscience and Nanotechnology show an increasing interest and a huge development. The fields of potential applications of nanoparticles and nanomaterials are large: chemistry, plasmonics, catalysis, optics, electronics, nanomedicine…

Gold has fascinated humans from the ancient time because of its colour and nobelty. Today Au NPs are attracting increasing attention because of their plasmonic and catalytic properties and their potential applications in different fields. These plasmonic properties can be used to assist catalytic processes using solar light, and with lower energy consumption. The use of plasmonic photocatalysts to catalyze chemical reactions is a new field, and its applications are challenging. In the next chapters, examples of catalysis assisted by plasmon with Au nanoparticles and Pd nanostructures will be presented.

References

1. Shaming, D.; Remita, H. Nanotechnology: from the Ancient Time to Nowadays. *Found. Chem.* **2015**, *17*, 187-205.
2. Pineda, A.; Gomez, L.; Balu, A.M.; Sebastian, V.; Ojeda, M.; Arruebo, M.; Romero, A.A.; Santamaria, J.; Luque, R. Laser-driven heterogeneous catalysis: efficient amide formation catalysed by Au/SiO2 systems. *Green Chemistry* **2013**, *15*, 2043.
3. Baffou, G.; Rigneault, H. Femtosecond-pulsed optical heating of gold nanoparticles. *Physical Review B* **2011**, *84*.
4. Louis, C.; Pluchery, O. *Gold nanoparticles for physics, biology and chemistry*; 2012.
5. Huang, X.; Neretina, S.; El-Sayed, M. Gold Nanorods: From Synthesis and Properties to Biological and Biomedical Applications. *Adv. Mater.* **2009**, *21*, 4880-4910.
6. Corma, A.; Garcia, H. Supported gold nanoparticles as catalysts for organic reactions. *Chem Soc Rev* **2008**, *37*, 2096-2126.
7. Hou, W.; Cronin, S.B. A Review of Surface Plasmon Resonance-Enhanced Photocatalysis. *Advanced Functional Materials* **2013**, *23*, 1612-1619.
8. Vincenzo; Amendola, e.a. Surface plasmon resonance in gold nanoparticles: a review. . *J Phys Condens Matter.* **2017**, *29*.
9. Schaming D., P., O., Remita, H. Descriptive experiments with Gold nanoparticles and gold nano-films: an introduction to nanoscience. *Gold Bulletin* **2013**, *46*, 49708-49718.
10. Hunt, L.B. The true story of Purple of Cassius. *Gold Bulletin* **1976**, *9*, 134-139.
11. Michael, F.X. The Bakerian Lecture: Experimental relations of gold (and other metals) to light. *Philosophical Transactions of the Royal Society of London* **1857**, *147*, 145-181.
12. Mie, G. Beiträge zur Optik trüber Medien, speziell kolloidaler Metallösungen. *Annalen der Physik* **1908**, *330*, 377-445.
13. W. Abidi, H.R. Gold based nanoparticles generated by the radiolytic and photolytic methods. *Recent Pat Eng* **2010**, *4*, 170–188.
14. Gabriel M. Veith, A.R.L., Stephen J. Pennycook, Gary W. Ownby, Nancy J. Dudney. Nanoparticles of gold on γ -Al2O3 produced by dc magnetron sputtering. *Journal of Catalysis* **2015**, *231*, 151-158.
15. Arrii, F.M.; Renouprez., A.J.; Rousset., J.L. Oxidation of CO on Gold Supported Catalysts Prepared by Laser Vaporization: Direct Evidence of Support Contribution. *J. Am. Chem. Soc.* **2004**, 1199-1205.
16. Scaramuzza, S.; Zerbetto, M.; Amendola, V. Synthesis of Gold Nanoparticles in Liquid Environment by Laser Ablation with Geometrically Confined Configurations: Insights To Improve Size Control and Productivity. *The Journal of Physical Chemistry C* **2016**, *120*, 9453-9463.
17. Priyanka Ray, M.C., Cyril Martini, Ibrahim Abdellah, Patricia Beaunier, José-Luis Rodriguez-Lopez, Vincent Huc, Hynd Remita, Isabelle Lampre. Stabilisation of small mono- and bimetallic gold–silver nanoparticles using calix[8]arene derivatives. *New Journal of Chemistry* **2018**, *42*, 14128-14137
18. Woehrle, G.H.; Brown, L.O.; Hutchison, J.E. Thiol-functionalized, 1.5-nm gold nanoparticles through ligand exchange reactions: scope and mechanism of ligand exchange. *Journal of the American Chemical Society* **2005**, *127*, 2172-2183.
19. Hugon, A.; Kolli, N.E.; Louis, C. Advances in the preparation of supported gold catalysts: Mechanism of deposition, simplification of the procedures and relevance of the elimination of chlorine. *Journal of Catalysis* **2010**, *274*, 239-250.

20. Turkevich, J.; Stevenson, P.; Hillier, J. A study of the nucleation and growth processes in the synthesis of colloidal gold. *Discuss Faraday Soc.* **1951**, *11*, 55-57.
21. Turkevich J, S.P., Hillier J A study of the nucleation and growth processes in the synthesis of colloidal gold. *Discuss Faraday Soc* **1951**, *11*, 55-57.
22. Frens, G. Controlled Nucleation for the Regulation of the Particle Size in Monodisperse Gold Suspensions. *Nature Physical Science* **1973**, *241*, 20-22.
23. Zanella, R.; Giorgio, S.; Shin, C.; Henry, C.; Louis, C. Characterization and reactivity in CO oxidation of gold nanoparticles supported on TiO2 prepared by deposition-precipitation with NaOH and urea. *J. Catal.* **2004**, *222*, 357-367.
24. Gachard, E.; Remita, H.; Khatouri, J.; Keita, B.; Nadjo, L.; Belloni, J. Radiation-induced and chemical formation of gold clusters. *New J Chem* **1998**, *22*, 1257–1265.
25. J. Belloni, M.M., H. Remita, J.-L. Marignier, Marie-Odile Delcourt. Radiation-induced synthesis of mono- and multi-metallic clusters and nanocolloids. *New Journal of Chemistry* **1998**, *22*, 49708-49718.
26. Remita, S.; Remita, H.; Wishart, J.F. *Recent Trends in Radiation Chemistry.*; Word Scientific 2010; pp. 347-383.
27. I.Sarhid; I.Abdellah; Lampre, I.; Huc, V.; Martini, C.; Remita, H. Plasmonic catalysis for the Suzuki–Miyaura cross-coupling reaction using palladium nanoflowers. *New J. Chem* **2019**, *43*, 4349-4355
28. Zanella, R.; Giorgio, S.; Henry, C.R.; Louis, C. Alternative Methods for the Preparation of Gold Nanoparticles Supported on TiO2. *The Journal of Physical Chemistry B* **2002**, *106*, 7634-7642.
29. Hashmi, A.S.K.; Hutchings, G.J. Gold Catalysis. *Angewandte Chemie International Edition* **2006**, *45*, 7896-7936.
30. Wang, C.; Astruc, D. Nanogold plasmonic photocatalysis for organic synthesis and clean energy conversion. *Chem. Soc. Rev.* **2014**, *43*, 7188-7216.
31. Treguer, M.; de Cointet, C.; Remita, H.; Khatouri, J.; Mostafavi, M.; Amblard, J.; Belloni, J.; de Keyzer, R. Dose Rate Effects on Radiolytic Synthesis of Gold−Silver Bimetallic Clusters in Solution. *The Journal of Physical Chemistry B* **1998**, *102*, 4310-4321.
32. Haruta, M.; Kobayashi, T.; Sano, H.; Yamada, N. Novel Gold Catalysts for the Oxidation of Carbon Monoxide at a Temperature Far Below 0 °C. *Chem. Lett* **1987**, *37*, 1290 - 1291.
33. Zheng, Z.; Tachikawa, T.; Majima, T. Plasmon-enhanced formic acid dehydrogenation using anisotropic Pd-Au nanorods studied at the single-particle level. *Journal of the American Chemical Society* **2015**, *137*, 948-957.
34. Abad, A.; Concepcion, P.; Corma, A.; Garcia, H. A collaborative effect between gold and a support induces the selective oxidation of alcohols. *Angew Chem Int Ed Engl* **2005**, *44*, 4066-4069.
35. Narayanan, R.; Tabor, C.; El-Sayed, M.A. Can the Observed Changes in the Size or Shape of a Colloidal Nanocatalyst Reveal the Nanocatalysis Mechanism Type: Homogeneous or Heterogeneous? *Top. Catal.* **2008**, *48*, 60-74.
36. Link, S.; El-Sayed, M.A. Shape and size dependence of radiative, non-radiative and photothermal properties of gold nanocrystals. *International Reviews in Physical Chemistry* **2000**, *19*, 409-453.
37. Kelly, K.L.; Coronado, E.; Zhao, L.L.; Schatz, G.C. The Optical Properties of Metal Nanoparticles: The Influence of Size, Shape, and Dielectric Environment. *The Journal of Physical Chemistry B* **2003**, *107*, 668-677.
38. Jana, N.R.; Gearheart, L.; Murphy, C.J. Wet Chemical Synthesis of High Aspect Ratio Cylindrical Gold Nanorods. *J. Phys. Chem.* **2001**, *105*, 4065-4067.

39. Nikoobakht, B.; El-Sayed, M.A. Preparation and Growth Mechanism of Gold Nanorods (NRs) Using Seed-Mediated Growth Method. *Chemistry of Materials* **2003**, *15*, 1957-1962.
40. Ahmed, W.; Bhatti, A.S.; van Ruitenbeek, J.M. Efficient seed-mediated method for the large-scale synthesis of Au nanorods. *Journal of nanoparticle research : an interdisciplinary forum for nanoscale science and technology* **2017**, *19*, 115-115.
41. Jain, P.K.; El-Sayed, I.H.; El-Sayed, M.A. Au nanoparticles target cancer. *Nano Today* **2007**, *2*, 18-29.
42. Kim, F.; Song, J.H.; Yang, P. Photochemical Synthesis of Gold Nanorods. *Journal of the American Chemical Society* **2002**, *124*, 14316-14317.
43. Rashidi-Hueyh, M. Influence des effets thermique sur la reponse optique de materiaux nanocomposites metal-dielectrique *PhD thesis University Pierre and Marie Curie* **2006**.
44. Linic, S.; Christopher, P.; Ingram, D.B. Plasmonic-Metal Nanostructures for Efficient Conversion of Solar to Chemical Energy. *Nat. Mater.* **2011**, *10*, 911-921.
45. Linic, P.; Christopher, D.B.I. Plasmonic-Metal Nanostructures for Efficient Conversion of Solar to Chemical Energy. *Nat. Mater.* **2011**, *10*, 911–921.
46. Loo, C.; Lin, A.; Hirsch, L.; Lee, M.H.; Barton, J.; Halas, N.; West, J.; Drezek, R. Technology in Cancer Research & Treatment. *ISSN* **2004**, *1533-0346*, 33-40.
47. Hirsch, L.R.; Stafford, R.J.; Bankson, J.A.; Sershen, S.R.; Rivera, B.; Price, R.E.; Hazle, J.D.; Halas, N.J.; West, J.L. Nanoshell-mediated near-infrared thermal therapy of tumors under magnetic resonance guidance. *Proceedings of the National Academy of Sciences* **2003**, *100*, 13549-13554.
48. Huang, X.; El-Sayed, M.A.; El-Sayed, I.H.; Qian, W. Cancer cell imaging and photothermal therapy in the near-infrared region by using gold nanorods. . *J. Am. Chem. Soc.* **2006**, *128*, 2115-2120.
49. Jain, S.; Coulter, J.A.; Hounsell, A.R.; Butterworth, K.T.; McMahon, S.J.; Hyland, W.B.; Muir, M.F.; Dickson, G.R.; Prise, K.M.; Currell, F.J., et al. Cell-Specific Radiosensitization by Gold Nanoparticles at Megavoltage Radiation Energies. *International Journal of Radiation Oncology • Biology • Physics* **2011**, *79*, 531-539.
50. Niidome, T. Development of functional gold nanorods for bioimaging and photothermal therapy. *Journal of Physics: Conference Series* **2010**, *232*, 012011.
51. Farokhzad, O.C.; Langer, R. Impact of Nanotechnology on Drug Delivery. *ACS Nano* **2009**, *3*, 16-20.
52. Andreu, I.; Natividad, E.; Solozábal, L.; Roubeau, O. Nano-objects for Addressing the Control of Nanoparticle Arrangement and Performance in Magnetic Hyperthermia. *ACS Nano* **2015**, *9*, 1408-1419.
53. Xiaohua, H.; Ivan, H., El-Sayed. ; Qian., W.; El-Sayed, M.A. Cancer Cell Imaging and Photothermal Therapy in the Near-Infrared Region by Using Gold Nanorods. *J. Am. Chem. Soc.* **2006**, *128*, 2115.
54. Bedford, E.; Boujday, S.; Pradier, C.-M.; Gu, F. *Spiky gold shells on magnetic particles for DNA Biosensors*; 2018; Vol. 182.
55. Loiseau, A.; Asila; Boitel-Aullen; Lam; Salmain; Boujday, S. *Silver-Based Plasmonic Nanoparticles for and Their Use in Biosensing*; 2019; Vol. 9, pp. 78.
56. Ben Haddada, M.; Huebner, M.; Casale, S.; Knopp, D.; Niessner, R.; Salmain, M.; Boujday, S. Gold Nanoparticles Assembly on Silicon and Gold Surfaces: Mechanism, Stability, and Efficiency in Diclofenac Biosensing. *The Journal of Physical Chemistry C* **2016**, *120*, 29302-29311.
57. Wang, C.; Astruc, D. Photocatalysis for Organic Synthesis and Clean Energy Conversion. *Chem. Soc. Rev* **2014**, *43*, 7188–7216.

58. Hallett-Tapley, G.L.; Silvero, M.J.; González-Béjar, M.; Grenier, M.; Netto-Ferreira, J.C.; Scaiano, J.C. Plasmon-Mediated Catalytic Oxidation of sec-Phenethyl and Benzyl Alcohols. *The Journal of Physical Chemistry C* **2011**, *115*, 10784-10790.

59. Sandoval, A.; Aguilar, A.; Louis, C.; Traverse, A.; Zanella, R. Bimetallic Au–Ag/TiO2 catalyst prepared by deposition–precipitation: High activity and stability in CO oxidation. *Journal of Catalysis* **2011**, *281*, 40-49.

60. Li, D.; Wang, H.; Shi, C.; Xu, X. Improved activity and stability of dealloyed bimodal nanoporous PtCo catalysts for CO oxidation. *RSC Advances* **2016**, *6*, 35340-35347.

61. Zhang, X.; Du, A.; Zhu, H.; Jia, J.; Wang, J.; Ke, X. Surface plasmon-enhanced zeolite catalysis under light irradiation and its correlation with molecular polarity of reactants. *Chemical Communications* **2014**, *50*, 13893-13895.

62. Huang, X.; Li, Y.; Chen, Y.; Zhou, H.; Duan, X.; Huang, Y. Plasmonic and Catalytic AuPd Nanowheels for the Efficient Conversion of Light into Chemical Energy. *Angewandte Chemie International Edition* **2013**, *52*, 6063-6067.

63. Zhang, J.; Wang, L.; Ali, S.; Wang, C.; Wang, L.; Meng, X.; Li, B.; Su, D.; Xiao, F. Wet-Chemistry Strong Metal-Support Interactions in Titania-Supported Au Catalysts. *ACS* **2019**, *141*, 2975-2983.

64. Wu, H.W.; Emadi, A.; Graaf, G.; Leijtens, J.; Wolffenbuttel, R.F. *Design and Fabrication of an Albedo Insensitive Analog Sun Sensor*; 2011; Vol. 25, pp. 527-530.

65. Grirrane, A.; Corma, A.; García, H. Gold-Catalyzed Synthesis of Aromatic Azo Compounds from Anilines and Nitroaromatics. *Science* **2008**, *322*, 1661-1664.

66. Zhu, H.; Ke, X.; Yang, X.; Sarina, S.; Liu, H. Reduction of Nitroaromatic Compounds on Supported Gold Nanoparticles by Visible and Ultraviolet Light. *Angewandte Chemie International Edition* **2010**, *49*, 9657-9661.

67. Gomez, L.; Sebastian, V.; Arruebo, M.; Santamaria, J.; Cronin, S.B. Plasmon-enhanced photocatalytic water purification. *Physical Chemistry Chemical Physics* **2014**, *16*, 15111-15116.

68. Nguyen, M.; Lamouri, A.; Salameh, C.; Lévi, G.; Grand, J.; Boubekeur-Lecaque, L.; Mangeney, C.; Félidj, N. Plasmon-mediated chemical surface functionalization at the nanoscale. *Nanoscale* **2016**, *8*, 8633-8640.

69. Fujishima, A.; Honda, K. Electrochemical Photolysis of Water at a Semiconductor Electrode. *Nature* **1972**, *238*, 37-38.

70. Kowalska, E.; Mahaney, O.O.; Abe, R.; Ohtani, B. Visible-light-induced photocatalysis through surface plasmon excitation of gold on titania surfaces. *Phys. Chem. Chem. Phys.* **2010**, *12*, 2344-2355.

71. Méndez-Medrano, M.G.K., E; Lehoux, A; Herissan, A; Ohtani, B; Bahena, D; Briois, V; Colbeau-Justin, C; Rodríguez-López, J.L; Remita, H. Surface Modification of TiO2 with Ag Nanoparticles and CuO Nanoclusters for Application in Photocatalysis. *J. Phys. Chem. C* **2016**, *120*, 5143-5154.

Chapter II

Experimental setups, materials and methods

Table of content

This chapter describes the synthesis and characterization techniques of plasmonic gold nanoparticles and palladium nanoflowers performed in this research as well as the illumination setups and the analytical methods used to follow the chemical reactions.

I- Synthesis of metal nanoparticles and nanostructures

I-1- Türkevich synthesis of spherical gold nanoparticles in solution

Spherical gold nanoparticles can be prepared by several methods (chemical, photochemical and radiolytic, and physical methods (cf. Chapter I).

We have chosen the Türkevich method for gold nanoparticles synthesis, as it allows us to work in an aqueous medium with controlled pH at room temperature. This method is based on the reduction of Au^{III} complexes $[AuCl_4]^-$ by citrate ions, which act as reducing and stabilizing agents.

Türkevich method is probably one of the most basic and reproducible method for synthesis of Au NPs. J. Türkevich et al. [1] first published this method in 1951, and then G. Frens [2] developed this method, and added the parameter of gold-to-reductant ratio to well control the nanoparticle size. Indeed, citrate ions reduce Au^{III} into Au^0 (Figure II-1) and simultaneously stabilize the formed Au nanoparticles via electrostatic weak-bonds. Because citrate is a weak reducing agent, the gold salt solution is heated and generally boiled [3]. The synthesis of Au-NPs@Citrate starts by boiling a gold salt aqueous solution, then sodium citrate (a solution containing 1% in mass) is added as a reducing and stabilizing agent (Figure II-2).

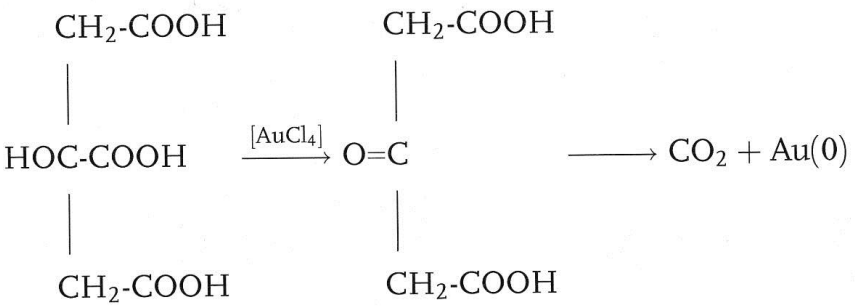

Figure II-1. Reduction of Au^{III} complexes by citrate ions.

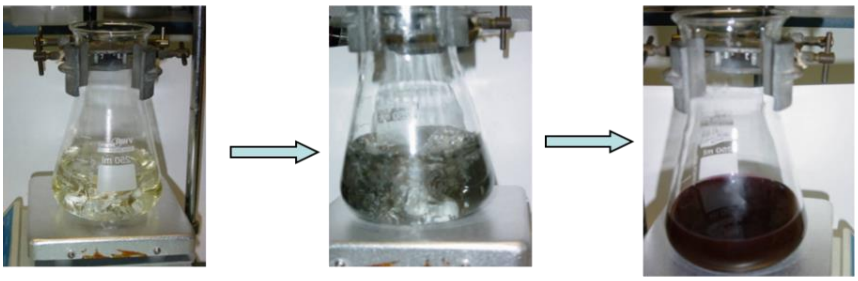

Figure II-2. Synthesis of Au nanoparticles (NPs) by Türkevich method: The light yellow solution containing $AuCl_4^-$ is boiled and a solution containing citrate ions is added, the mixture turns to grey and then to a red solution, the red color attests the formation of Au nanoparticles.

Table II-1 provides the concentrations and the citrate/gold ratios used to synthesize well-dispersed quasi-spherical gold nanoparticles with a mean diameter of 15 or 30 nm.

Gold salt solution [$KAuCl_4$]	Sodium citrate solution	Ratio of citrate to gold	Au NPs' mean diameter determined by TEM (nm)
20 mL at 0.25 mM	1 mL at 34 mM	6.8	15
20 mL at 1 mM	0.8 mL at 34 mM	1.0	30

Table II-1. Experimental conditions of concentrations and ratios [citrate]/[Au^{III}] for AuNPs@Citrate of 15 and 30 nm.

I-2- Synthesis of Palladium Nanoflowers

Ultrathin palladium hexagonal nanosheets were synthesized in emulsions constituted of droplets of toluene containing Pd complexes in water and stabilized by CTAB as surfactant and in quaternary mesophases formed by water, toluene containing Pd complexes, CTAB, and a co-surfactant (pentanol) [4,5]. In this work, we synthesize palladium nanoflowers by radiolysis [5,6]:

20 mL of ethanol solution containing $Pd(acac)_2$ (10^{-3} M) were transferred in a small pyrex bottle, which was then sealed with a rubber septum. The solution was flushed by flowing argon, and then CO (1 atm) was carefully passed through the sample at a very low flow rate for 15 min.

Caution: CO is highly toxic gas. Hence, bubbling was done with extreme caution in a very well ventilated hood with external evacuation.

The resulting solution has a light-yellow color. Immediately after CO bubbling, the samples were exposed to gamma irradiation with a ^{60}Co panoramic source for 1 hour at a dose rate of 3 kGy/h to complete the full reduction of Pd^{II} into Pd^0. The light yellow solution turned to dark blue after irradiation. The radiolytic reduction of Pd $(acac)_2$ at 10^{-3} mol L^{-1} in ethanol under CO atmosphere leads to Pd nanostructures [5].

It has to be noted that $Pd^{II}(acac)_2$ solutions are stable under CO for many hours: There is no evolution of the absorption spectrum and black large Pd particles (which precipitate) are formed only after few days. Indeed, CO reduces Pd(II) very slowly and the direct reduction by CO is negligible at the scale of hours.

The Pd nanostructures are stable in ethanol solution for few days in the dark and for few hours under light irradiation.

II- Characterization techniques of the metal nanostructures

Different characterization techniques were used to characterize the Au nanoparticles and the Pd nanoflowers synthesized in this thesis, before and after catalytic reactions.

II-1- UV–Visible absorption spectroscopy

The optical properties of the metal nanoparticles in solution were studied by UV-visible absorption spectroscopy. A beam with a wavelength varying between 180 and 1100 nm passes through a solution in a cuvette. The sample in the cuvette absorbs this UV or visible radiation. The absorbance $A(\lambda)$ at a certain wavelength λ is governed by the Beer-Lambert law:

$$A(\lambda) = log\left(\frac{I_0}{I}\right) = \varepsilon l c$$

I_0 and I are the intensities of the incident and transmitted light, respectively. The amount of light that is absorbed by the solution depends on the concentration *c* of the solute, the path length *l* of the light through the cuvette and the absorption coefficient ε of the solute, *i.e.* how well the solute absorbs the light at the wavelength λ. If there is no absorption of the light passing through the solution, the absorbance is 0 and the transmittance is 100% (neglecting the scattering by the cell windows).

For metal nanoparticles the characteristic surface plasmon resonance band is observed by absorbance spectroscopy. The spectra of spherical nanoparticles of gold present a SPR located around 520 nm. As the SPR depends on the size and shape of nanoparticles, this observation

also gives us an idea about the size of nanoparticles formed. From the absorbance spectroscopy we can also observe scattering, which is due to the size of the particles, their dispersion and also agglomeration in the medium.

UV–vis absorption spectra of the solutions were recorded on either a Carry 5000 (Agilent) spectrophotometer or a HP8435 diode array spectrophotometer.

II-2- Transmission Electron Microscopy (TEM)

Transmission Electron Microscopy (TEM) is a powerful imaging tool for the characterization of morphology, lattice coordinates, and distribution of nanostructures. TEM is used to observe the size, shape and morphology of nanoparticles. It probes the internal structure of solids in order to give us an idea about the morphology of the material. When the accelerating electrons are focused on the grid containing the sample, part of the electrons is transmitted by the sample while a part of them are scattered. The electromagnetic lenses in the TEM machine focuses the transmitted electrons into an image or a diffraction pattern and provides us with insight about the sample under observation. The electron diffraction, observed by TEM provides us with the Fourier transform reconstruction. In TEM apparatus, the sample is illuminated using multiple electron beams confined in a high vacuum space, and the transmitted beam makes the image magnified from about fifty to over one million times (Figure II-3). In principle, contrast of the TEM image arises because of the differences in electron density of the elements constituting the sample under investigation.

Transmission electronic microscopy (TEM) observations were performed with a JEOL JEM 100 CXII TEM instrument operated at an accelerating voltage of 100 kV and a JEOL JEM 2011 operated at 200 kV. Prior to observations, a few droplets of the metal nanostructure solution were deposited and dried on carbon-coated copper TEM grids under N_2 flow. The images were collected using a CCD camera. These characterizations were done in collaboration with Patricia Beaunier, LRS (Sorbonne Université).

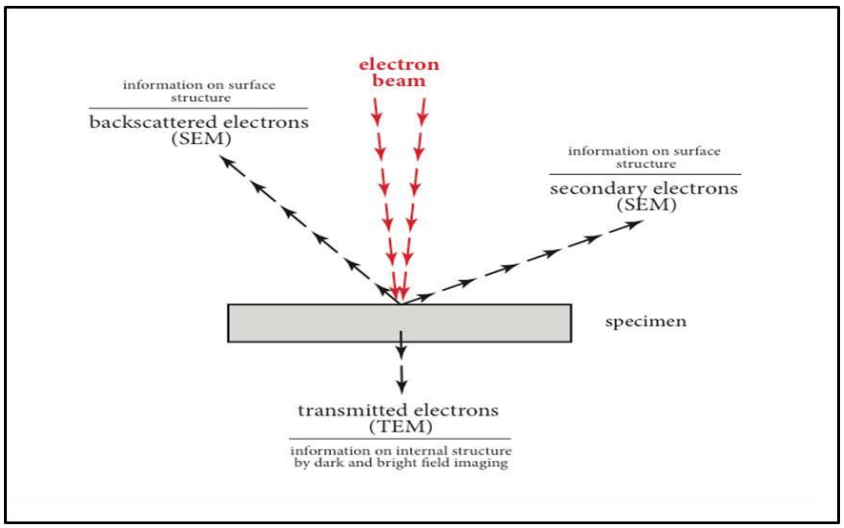

Figure II-3. Interaction between matter and the electron beam for TEM imaging (*https://bsp.med.harvard.edu/node/221*)

II-3- X-Ray Photoelectron Spectroscopy (XPS)

X-ray photoelectron spectroscopy (XPS) is a surface-sensitive spectroscopic technique providing information concerning the elemental composition as well as the chemical state of the elements present at the surface. XPS spectra are obtained by irradiating a material with a beam of X-rays (the X-ray sources usually employed consist of an Al / K_α = 1486.6 eV or Mg / K_α = 1253.6 eV anodes) in vacuum while simultaneously measuring the kinetic energy and number of electrons that escape from roughly the first 5 to 10 nm of the material being analyzed. The measured kinetic energy (E_k) can be converted into the atomic core level binding energy (E_B), relative to the Fermi level of the sample using the formula:

$$E_B = E_{source} - E_k$$

The various core level binding energies observed in a spectrum can be used to identify all the elements of the periodic table except for hydrogen and helium. Chemical state information can also be extracted because binding energies are sensitive to the chemical environment of the atom.

XPS measurements were performed on a K-Alpha X-Ray Photoelectron Spectrometer (Thermo Fisher Scientific) under ultrahigh vacuum (base pressure in the low 10^{-9} mbar), equipped with a monochromatic Al source ($Al_{K\alpha}$ = 1486.7 eV) using a spot size of 400 µm corresponding to an irradiated area of approximately 1 mm^2. The hemispherical analyzer was operated at 0° take off angle in the Constant Analyzer Energy (CAE) mode, with a pass

energy of 200 eV and a step of 1 eV for the acquisition of survey scans and a pass energy of 50 eV and a step of 0.1 eV for the acquisition of narrow scan spectra. Charge compensation was accomplished by means of a “dual beam” flood gun. Drops of a suspension were deposited on silica plates and allowed to dry in the Load Lock prior to transfer in the analysis chamber in order to minimize the contact with air. The recorded XPS spectra were analyzed by means of Avantage software provided by the manufacturer. The C 1s signal 284.8 eV was used as reference for the bonding energy scale. The XPS characterization experiments were done in collaboration with Diana Dragoe (ICMMO, Université Paris-Saclay).

III-Analytical methods

III-1-Electrospray Ionization Mass Spectrometry

Mass spectrometry is an analytical technique that can provide both qualitative (structure) and quantitative (molecular mass or concentration) information on analyte molecules after their conversion to ions. The molecules of interest are first introduced into the ionisation source of the mass spectrometer, where they are first ionized to acquire positive or negative charges. The ions then travel through the mass analyzer and arrive at different parts of the detector according to their mass/charge (m/z) ratio. Electrospray Ionization -mass spectrometer (ESI-MS) is composed of three basic components: ion source, mass analyzer, and detector. The intact molecular ions are produced in the ionization chamber where the ion source is kept, and then they are transferred in the mass analyzer region via several optics [7]. The mass analyzer sorts and separates the ions according to their mass to charge ratio (m/z value). The separated ions are then passed to the detector systems to measure their concentration,

In the ESI unit (figure II-4), a dilute (less than mM in polar volatile solvent) analyte solution is injected by a mechanical syringe pump through a hypodermic needle or stainless steel capillary at low flow rate (typically 1–20 μL/min). A very high voltage (2–6 kV) is applied to the tip of the metal capillary relative to the surrounding source-sampling cone or heated capillary (typically located at 1–3 cm from the spray needle tip) [7].

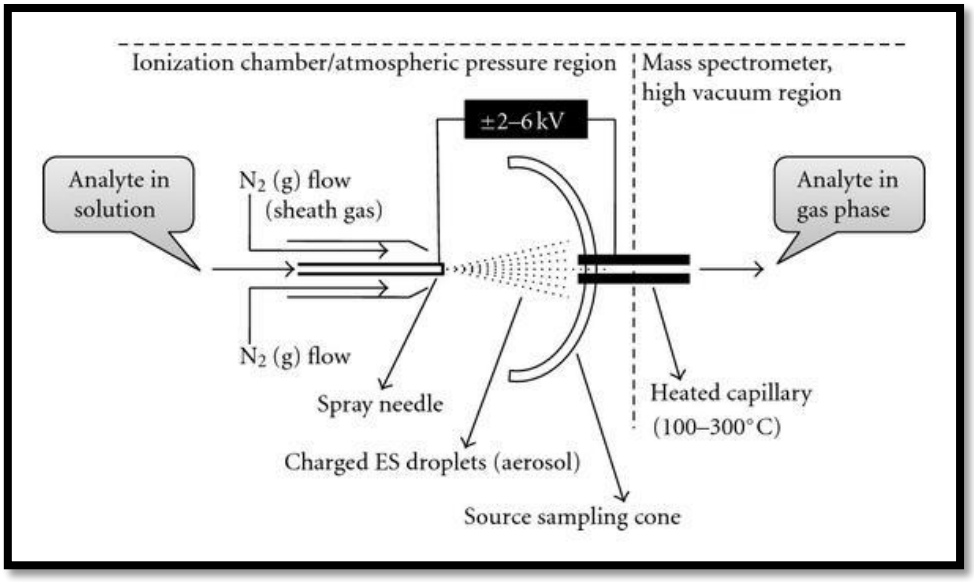

Figure II-4. A schematic representation of the ESI-ion source.

The interpretation of ESI-MS results can be complex as peaks can become noisy and overlapping. Further fragmentation of interesting peaks to dissect detected mass and verify possible masses corresponding to a certain molecule.

ESI-MS experiments were carried out on a TSQ Quantum Ultra equipped with an electrospray ion source. Data acquisition and processing were performed using Xcalibur data system.The mass spectrometer was operated in negative mode; the spray voltage was 3 kV. The experiments were done in collaboration with Marine de Person (IUT d'Orsay).

III-2-Gas Chromatography coupled with Mass Spectroscopy

Gas Chromatography coupled with mass spectroscopy (GC-MS) is considered as an important analytical tool for natural products analysis, volatile organic compounds, active medical materials and pollutants. GC-MS offers an in-depth knowledge of the sample components as it allows to detect their masses along with their chemical structure.

For example, when analyzing volatile organic compounds (VOC), target analytes are extracted by mixing the sample with water and purge with inert gas (Argon gas in our studies) into an airtight chamber, this is known as purging. Purge-Trap technic is widely used in many petrochemical industries [8]. The trap is a column of adsorbent material at ambient temperature that holds the compounds by returning them to the liquid phase. The trap is then heated and the sample compounds are introduced to the GC-MS column via a volatiles interface, which is a split inlet system. Purge and trap gas chromatography-mass spectrometry system (P&T GC-MS) is particularly suited to volatile organic compounds (VOCs).

Gas chromatography (GC) analyses were performed on a Varian 430-GC gas chromatograph and GC coupled to mass spectrometry (GC-MS) analyses were performed on a Thermo Scientific DSQ apparatus.

III-3-Surface Raman Enhanced Spectroscopy (SERS)

Surface Raman Enhanced Spectroscopy (SERS) was first observed in 1974. It is an extension of normal Raman spectroscopy that relies on electronic and chemical interactions between the excitation laser, analyte of interest, and SERS substrate [9]. Raman signal enhancements as high as 1014 can occur for resonant molecules found in "hot spots" on a SERS substrate because of combined electromagnetic (EM), charge transfer (CT), and resonance signal enhancement mechanisms ,[9].

After the centrifugation of sample dispersed in solution at different times of the reaction, the samples were separated into a supernatant and a residue. The resulting residue is a fairly dense aggregation of spherical gold nanoparticles at the bottom of the Eppendorf. The medium of the reaction is aqueous, which raises an issue regarding the resolution of Infra-Red preliminary characterization. Hence, it was necessary to ensure evaporation of water residue in the droplet. This could not be conducted via localized thermal evaporation because of a possible degradation of several organic reagents/pollutants, which is a limitation for the inspection. However, the droplets were left to dry at room temperature, while reserved in dark to avoid possible excitation under visible light.

There were other limitations related to the usage of Infra-Red based techniques. One limitation was the vibrational modes of the ensemble of molecules that cover a wide range of wavenumbers, hence, a limiting overlap between initial and final products. Other obstacle was maintaining a considerable final concentration of reagents remaining in the droplet. The latter can be overcome by preparing series of samples ranging from 10^{-3} to 10^{-6} M of final concentrations and by enhancing the spectral resolution. Nevertheless, the enhancement of spectral resolution will extend the acquisition time.

Raman and Surface-Enhanced Raman Spectroscopy (SERS) measurements were carried out with a Raman spectrometer (Labram HR evolution (Horiba Sicentific, France SAS Villeneuve d'Ascq). The excitation source was a 633 nm He-Ne laser. The spectral region studied was 400–2000 cm^{-1} with a spectral resolution of 4 cm^{-1}. Acquisition time of each spectrum was 1 to 5 seconds. SERS experiments were done in collaboration with Ali Tfayli (Lip(Sys)², EA7357, Faculté de Pharmacie, Châtenay Malabry, Université Paris-Saclay)..

IV- Irradiation setups

In order to carry out a catalytic reaction induced by plasmon, we used visible light (200 to 800 nm) as a source of excitation.

Several parameters were taken into consideration when choosing the light source. Intensity of light source is an important factor. Intensity refers to the number of photons emitted by a light source with a sufficient energy to excite the confined surface electrons. This number can differ depending on optical properties of catalysts, light-exposure geometry, reaction medium, and reflection/absorption characteristics of the catalytic setup [10].

IV-1- Xenon Lamp equipped with a longpass filter

Xenon lamps had been widely used in laboratory experiments, mainly for photocatalysis application. Irradiation was performed using a 300 W Xe arc lamp equipped with a water cell filter (15 cm) to absorb the near-IR radiation (Figure II-5) and a longpass filter to avoid the direct photoactivation of chemical reagents during irradiation.

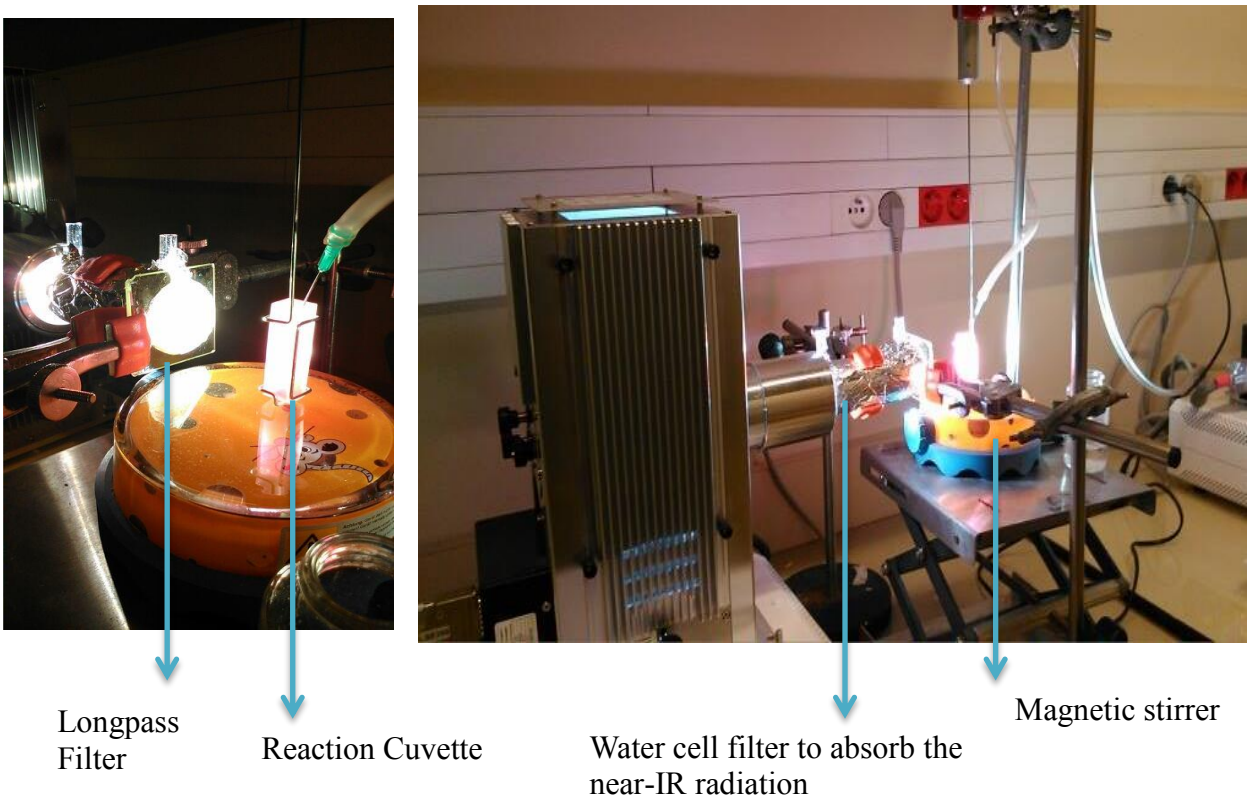

Figure II-5. Xe lamp installation for photocatalytic reactions under UV-Vis selected wavelengths via a cut-off filter.

The cell is placed at 3 cm of the water filter. The reaction cuvette is exposed to incident light from one side only, and a small magnetic stirrer is used to insure homogeneous light

absorption by the metal nanoparticles. Since most of our experiments are done in water-based solutions, viscosity will not be a barrier for energy dissipation. A thermal couple is introduced inside the cuvette to measure temperature fluctuation inside the solution during irradiation.

IV-2- Homemade LED-based cylindrical photochemical reactor

In order to achieve a panoramic and homogenous irradiation, we designed a cylindrical photochemical reactor equipped with 6 arrays of light emitting diodes (LEDs). The reactor was built by Raymong Herren (Technician at LCP). We can use different LEDs emitting at different wavelengths; 470, 525 and 605 nm. In our case, we used green LEDs at 525 nm. The light power was tunable up to 18 Watts. The reaction cell is placed at the center of the reactor (Figure II-6). Hence, irradiation is well distributed over the total volume inside the cylinder. The tunable intensity with a maximum of 18 W will allow us to compare reaction rates when using different light sources.

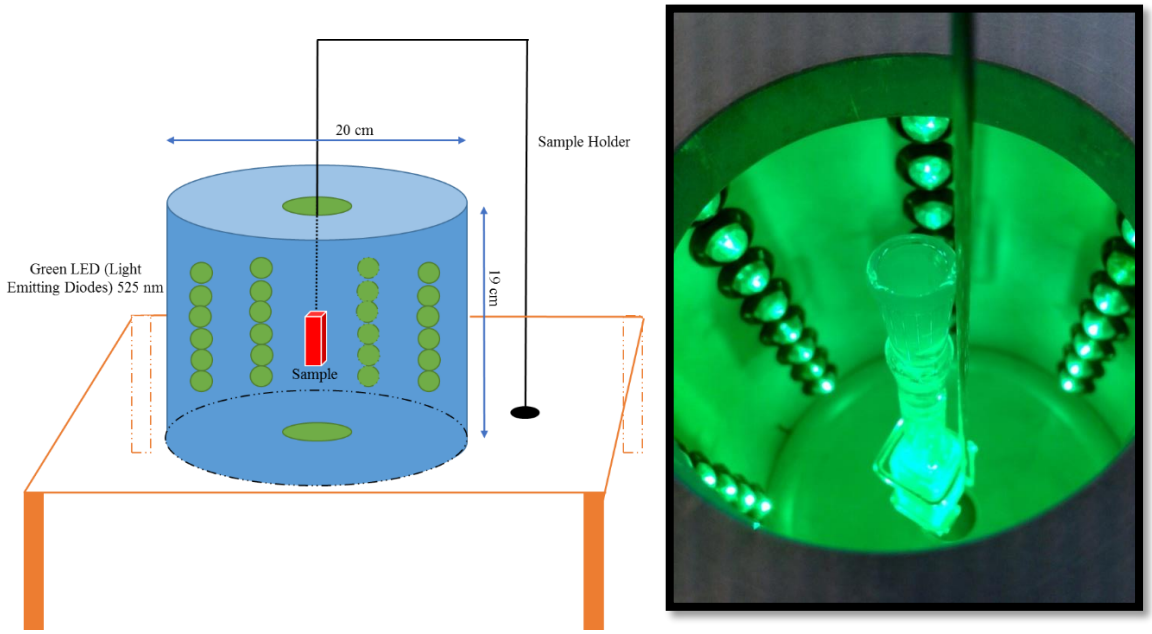

Figure II-6. Illustration of LED home-made reactor (left); a photograph of the inside of the reactor and cuvette sample held at the center (right).

IV-3- Continuous green laser excitation

The third set-up we used was developed by Bruno Palpant (LPQM, CentraleSupelec) and it is based on a continuous green laser at 532 nm. The laser beam with a defined intensity passes through a sample quartz cuvette. Another light source is used to record the absorption

spectra with a specific interval between each reading, hence, the cross-section between laser and light passing through the sample, the absorption spectra is being recorded (Figure II-7).

The intensity of the laser is tunable, and we managed to optimize it at 20 mW per 10% of exposed sample carrier. In addition, a continuous stirring of the sample is arranged to homogenize the irradiated volume to the green light laser irradiation.

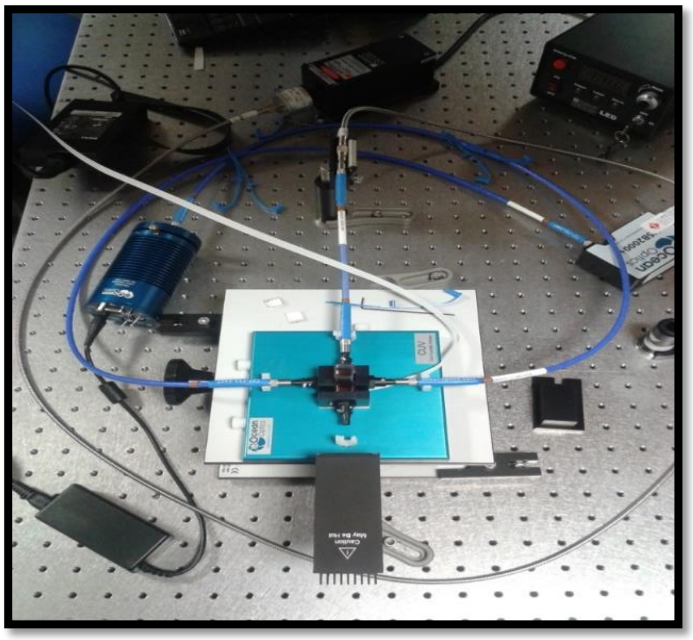

Figure II-7. Laser experimental setup where the cross-section of the two fibers connected to the visible lamp and green laser.

With this laser excitation, we were able to achieve a visual imprint of spatial distribution of heat dissipating in the solution of gold nanoparticles (Figure II-8).

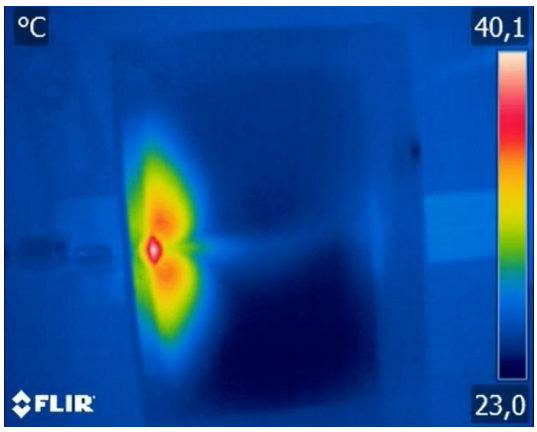

Figure II-8. Screen shot of the video recorded via CCD camera. One can notice that the temperature rises to its maximum at the point of entry of the continuous green

laser beam. As long the irradiation is on, fluctuations in heat dissipated can be observed.

V- Chemicals

Most common laboratory chemicals were reagent grade, purchased from commercial sources (Sigma-Aldrich mainly or ACROS) and used without further purification:

Tetrachloroauric acid trihydrate: $HAuCl_4$, $3H_2O$

Palladium acetylacetonate ($Pd(acac)_2$): $Pd(C_5H_7O_2)_2$

Potassium ferricyanide or potassium hexacyanoferrate (III) (HC-FeIII): $K_3Fe(CN)_6$

Trisodium citrate dehydrate: $Na_3C_6H_5O_7$

para-nitrothiophenol (pNTP) or 4-nitrothiophenol: $O_2NC_6H_4SH$

para-aminothiophenol (pATP) or 4-aminothiophenol: $H_2NC_6H_4SH$

Sodium thiosulfate (ST): $Na_2S_2O_3$

Phenylboronic acid : $C_6H_5B(OH)_2$

Iodobenzene: C_6H_5I

4-nitrobromobenzene: $O_2NCC_6H_4Br$

4-nitroiodobenzene: $O_2NCC_6H_4I$

Iodotoluene: $H_3CC_6H_4I$

Potassium carbonate: K_2CO_3

Potassium phosphate: K_3PO_4

Cesium carbonate: Cs_2CO_3

Potassium hydroxide: KOH

Ethanol: C_2H_5OH

Water used as solvent was obtained by passing through a Millipore Q water purification set (18.2 MΩ cm).

When indicated, the solutions were deaerated by bubbling with nitrogen (N_2, purity > 99,995%, from Air Liquide) or saturated with carbon monoxide (CO, purity 99.99 % from Air Liquide).

References

1. Turkevich, J.; Stevenson, P.; Hillier, J. A study of the nucleation and growth processes in the synthesis of colloidal gold. *Discuss Faraday Soc.* **1951**, *11*, 55-57.
2. Turkevich J, S.P., Hillier J A study of the nucleation and growth processes in the synthesis of colloidal gold. *Discuss Faraday Soc* **1951**, *11*, 55-57.
3. Schaming D., P., O., Remita, H. Descriptive experiments with Gold nanoparticles and gold nano-films: an introduction to nanoscience. *Gold Bulletin* **2013**, *46*, 49708-49718.
4. Siril, P.F.; Ramos, L.; Beaunier, P.; Archirel, P.; Etcheberry, A.; Remita, H. Synthesis of Ultrathin Hexagonal Palladium Nanosheets. *Chemistry of Materials* **2009**, *21*, 5170-5175.
5. Redjala, T.; Apostolecu, G.; Beaunier, P.; Mostafavi, M.; Etcheberry, A.; Uzio, D.; Thomazeau, C.; Remita, H. Palladium nanostructures synthesized by radiolysis or by photoreduction. *New Journal of Chemistry* **2008**, *32*, 1403-1408.
6. Remita, H.; Ibrahim, A.; Sarhid, I.; al., E. Plasmonic catalysis for the Suzuki–Miyaura cross-coupling reaction using palladium nanoflowers. *New J. Chem* **2019**, *43*, 4349-4355
7. Banerjee, S.; Mazumdar, S. Electrospray Ionization Mass Spectrometry: A Technique to Access the Information beyond the Molecular Weight of the Analyte. *International Journal of Analytical Chemistry* **2012**, *2012*, 40.
8. Sparkman, O.D.; Penton, Z.; Kitson, F.G. *Gas Chromatography and Mass Spectrometry: A Practical Guide*; Elsevier Science: 2011.
9. Moskovits, M. Surface-enhanced Raman spectroscopy: a brief retrospective. *Journal of Raman Spectroscopy* **2005**, *36*, 485-496.
10. Linic, S.; Christopher, P.; Ingram, D.B. Plasmonic-Metal Nanostructures for Efficient Conversion of Solar to Chemical Energy. *Nat. Mater.* **2011**, *10*, 911-921.

Chapter III

Degradation of *para*-nitrothiophenol by plasmon excitation of gold nanoparticles

Table of Content

I- Introduction

For the past decades, nanoscience has become a growing field of interest. In particular, metal nanoparticles (MNPs) have been the subject of numerous research studies because of their unique properties that differ from their bulk counterparts and find applications in various domains, such as optics, electronics, catalysis or biology [1-5]. Among the MNPs, silver (Ag) and gold (Au) nanoparticles present a strong absorption band in the visible spectral region due to a localized surface plasmon resonance (LSPR) [6]. This resonance corresponds to a coherent oscillation of the free electron gas of the MNPs for which the frequency matches the incident light frequency [1,7-9]. LSPR depends on the metal, the size, the shape and the environment of the NPs and induces several effects i.e. electromagnetic-field enhancement, heat generation, "hot" electrons production, which have been exploited, for instance, in biosensing, photothermal therapy, photovoltaics or (photo-) catalysis [7,10-14].

Lately, applications of plasmonics in chemistry has arouse with the main objectives to trigger, select chemical reactions and control their yield. Several reviews have already been published describing the optical and thermal properties of the nanoparticles and their main possible effects in chemical reactions [15-18]. According to the role played by the plasmonic nanoparticles, two classes of reactions are distinguished: plasmon-assisted surface catalysis and plasmon-driven photocatalysis However, the involved mechanisms are not always well understood and sometimes still under debate [13,19,20].

Among the chemical reactions studied, many papers deal with the reactivity of nitroarenes in the presence of nanoparticles [20-22]. Indeed, the photo-induced reduction of nitroarenes is often chosen to test the catalytic properties of metal nanoparticles, Para-nitrophenol (pNP, 4-nitrophenol) and para-nitrothiophenol (pNTP, 4-nitrobenzenethiol) being used as model pollutants [8,20,23-27]. The metal nanoparticles serve as catalyst, the reductant being usually $NaBH_4$ (Scheme III-1).

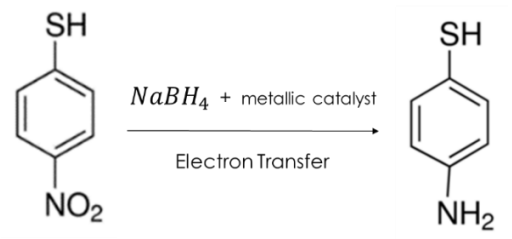

Scheme III-I. Illustration of reduction of pNTP via a metallic catalyst.

However, in the case of plasmonic nanoparticles under light illumination, it has been shown that nitroarenes react on the surface and may form different products depending on the environment [8,20,25].

Within this context, we have undertaken to study the degradation of *para*-nitrothiophenol (pNTP) in aqueous solution in the presence of plasmonic gold nanoparticles (AuNP) under visible light irradiation. UV-visible absorption spectroscopy, electrospray-mass spectrometry and surface-enhanced Raman spectroscopy were used to follow the disappearance of pNTP, to analyze the formed products and to get information on the involved mechanisms [28-35].

II- Sample preparations and irradiation

Para-nitrothiophenol ($C_6H_5NO_2S$) is a highly toxic compound resulting from pesticides treatment of soil and many manufacturing processes. It is a yellow crystalline powder that is partly soluble in water and chloroform; the storage temperature is around 4° C as it has a fusion point of 72-77° C.

Aqueous solutions of pNTP (6×10^{-4} M) were prepared and the pH was adjusted to 11 by addition of 0.1 M NaOH solution in order to form the phenolate anion (pKa = 4.4 [36,37]) which has a characteristic UV-visible electronic absorption band peaking at 405 nm (Figure III.-1).

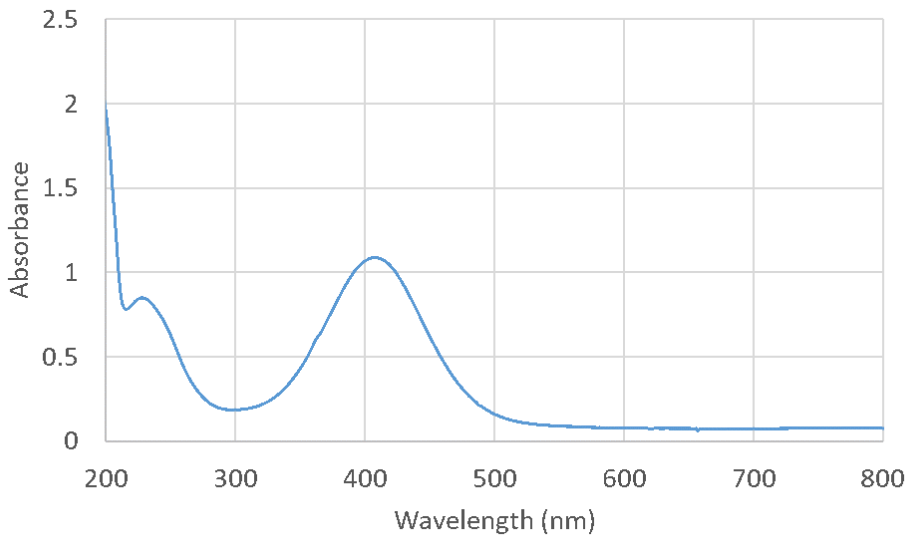

Figure III-1. Absorption spectrum of a 1.64×10^{-4} M pNTP aqueous solution. Optical path: 1 cm

Spherical gold nanoparticles (AuNPs) were synthesized using the Turkevitch method based on the reduction of auric salt (Au^{III}) by citrate, as described in the previous chapter II according published methods [38] [39].

750 µL of alkaline pNTP solution were added to 2 mL of AuNPs solutions contained in a 1 cm square cuvette with four clear quartz windows. The final pH of the solutions was around 9 resulting from the mixture of a highly alkaline pNTP solution and a mildly acidic AuNPs solution. A small magnetic stirrer is placed in the cuvette. The solutions were let under stirring in darkness (cuvette covered with aluminum foil) for 40 minutes before any illumination to allow exchange of ligands (Scheme III-2) and during all the time of light irradiation to ensure continuous and homogeneous light exposure of the solution. It is to be noted that in the case of laser irradiation due to the size of the laser beam, only half of the volume of the prepared solution was used.

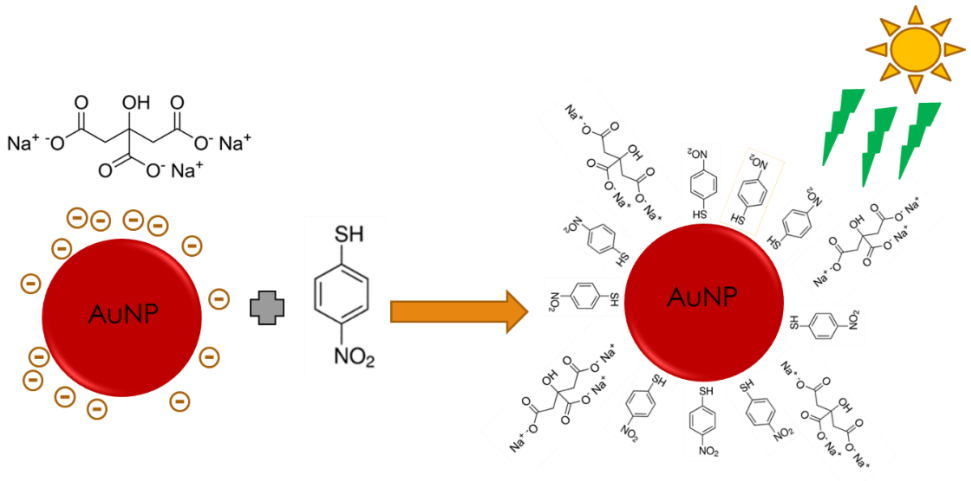

Scheme III-2. An illustration of the reagents and functionalization of spherical gold nanoparticles at the beginning of the photo-induced reaction.

It is worth noticing that, in the present study, whatever the set-up used for irradiation, in order to avoid possible two-photon absorption phenomena leading to the direct photodecomposition of pNTP, the light power was limited, i.e. 9 W for the LED reactor, 20 mW for the laser and 150 W for the lamp. Moreover, for the Xe lamp irradiations, a 520 nm longpass filter was used to avoid the direct photoactivation of pNTP.

Otherwise specified, all experiments were performed under ambient atmosphere (i.e. in the presence of dioxygen). Experiments were also carried out at room temperature (23 ± 2 °C) and the temperature of the solution did not increase by more than 5 degrees during light illumination.

III- Degradation of pNTP followed by UV-visible spectroscopy

The degradation of pNTP is followed by UV-visible spectroscopy as pNTP in aqueous alkaline solution exhibits characteristic absorption bands at 225 and 405 nm. The formed AuNPs also present absorption in the same spectral domain, but the main characteristic LSPR band is shifted towards the visible area, around 530 nm and 520 nm for 30 nm and 15 nm AuNPs, respectively.

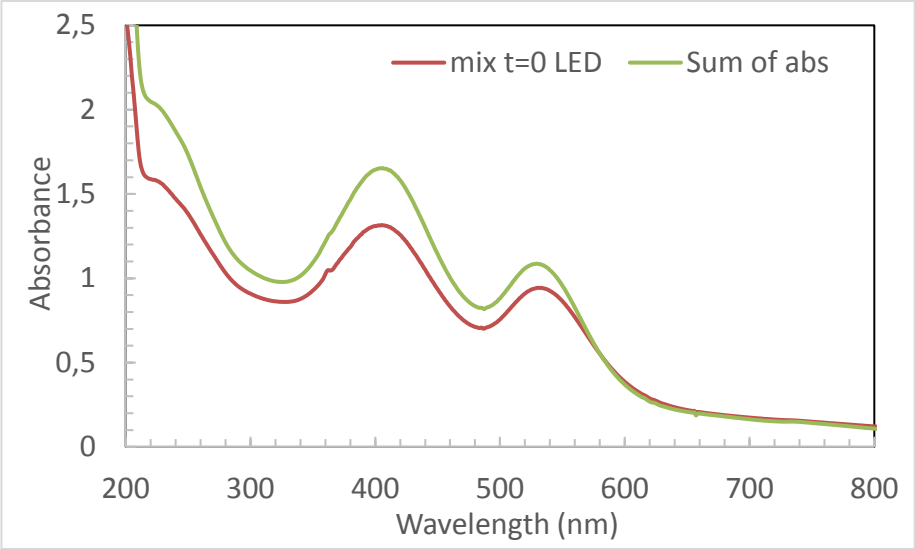

Figure III-2. UV-visible absorption spectrum of an aqueous solutions containing both 1.64×10^{-4} M pNTP, 30 nm AuNP ($[Au^0] = 1.74 \times 10^{-4}$ M), after 40 minutes stirring under darkness, and the sum of the absorption spectra of the aqueous solutions containing either 1.64×10^{-4} M pNTP or 30 nm AuNP ($[Au^0] = 1.74 \times 10^{-4}$ M). Optical path: 1 cm.

Figure III-2 presents the UV-visible absorption spectrum of an aqueous solution containing pNTP, and 30 nm AuNPs after 40 minutes of stirring in the dark, as well as the sum of the absorption spectra of the aqueous solution of each compound at the same concentration. It is to note that the absorption spectrum of the mixture of pNTP and Au NPs differs slightly from the expected spectrum obtained from the sum of the spectra of the two compounds. That indicates that, upon mixing, interactions between pNTP and AuNP occur modifying the absorption properties. Moreover, if the mixture is let under stirring in the dark for several hours, a decrease in the absorbance is observed (Figure III-3) This decrease can be explained either by a low degradation of pNTP or by a small change in the absorption properties of pNTP related to adsorption and replacement of citrate on the Au NPs surface. Indeed, due to the presence of thiol group, adsorption of pNTP on Au NPs is favourable and expected as already reported in the literature.

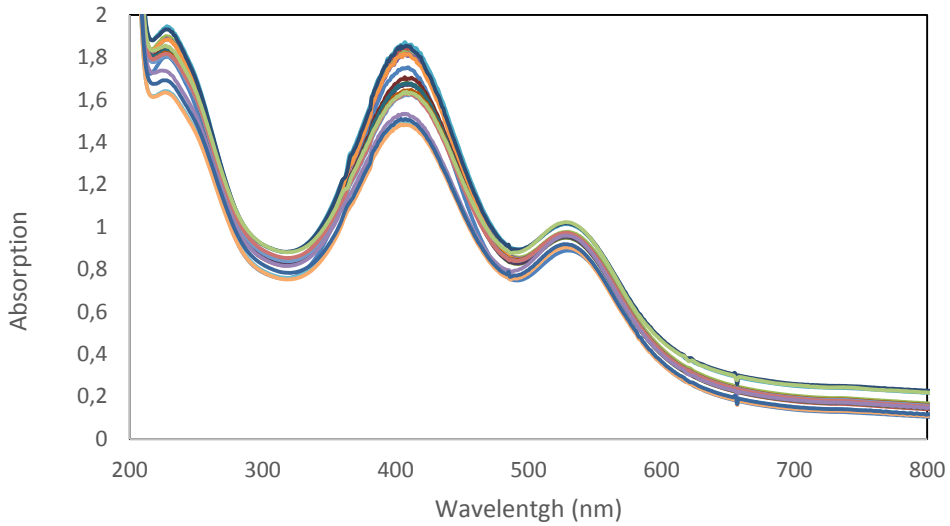

Figure III-3. Temporal evolution of the absorption spectra of an aqueous solution containing 1.64×10^{-4} M pNTP and 30 nm AuNP ($[Au^0] = 1.74 \times 10^{-4}$ M) under stirring in darkness for 900 minutes.

In contrast, if the mixture is put under light irradiation, its absorption spectrum changes significantly. Figure III-4 shows the evolution of the UV-visible absorption spectra of the aqueous solution containing pNTP and 30 nm AuNPs under excitation at 525 nm in the **LED** photochemical reactor. Under illumination, while the AuNPs LPSR band at 525 nm remains stable, the absorption bands at 225 and 405 nm corresponding to pNTP decrease strongly showing the degradation of pNTP. For the first 8 hours of light excitation (Figure III-4 top), this decrease is associated with the appearance of a new weak absorption band around 280 nm and the presence of two isobestic points at 272 and 310 nm. That suggests that the degradation of pNTP corresponds to a unique reaction and the formation of a unique species. The new absorption band could be attributed to the formation of para-aminothiophenol (pATP). For illumination over 8 hours (Figure III-4 bottom), the decrease in the absorption bands at 225 and 405 nm goes on showing the degradation of pNTP, but the isobestic points are no longer present suggesting the formation of other products than pATP.

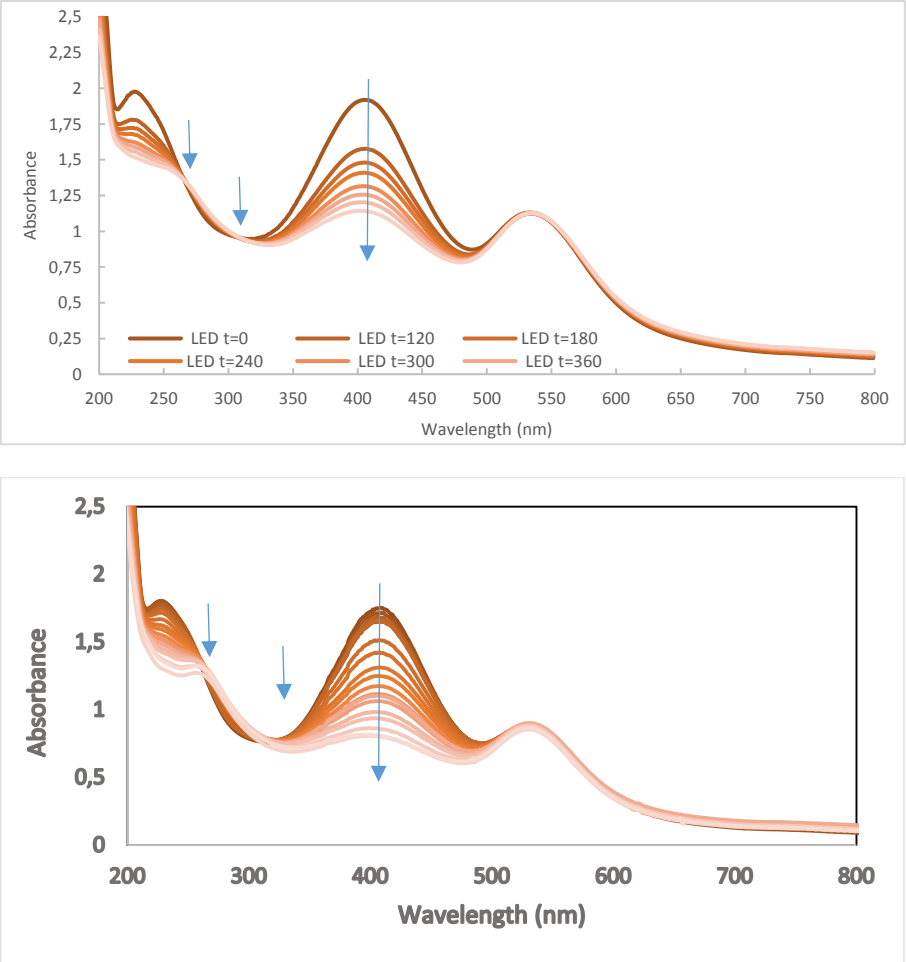

Figure III-4. Temporal evolution of the absorption spectra of an aqueous solution containing 1.64×10^{-4} M pNTP and 30 nm AuNPs ($[Au^0] = 1.74 \times 10^{-4}$ M) under stirring and illumination at 525 nm in the LEDs photochemical reactor **(top)** for 8 hours and **(bottom)** for 14 hours. Spectra taken after every hour of illumination.

The light irradiation of the solutions was performed using the LEDs reactor (Figure III-4), but also using a green continuous laser and a Xe lamp (Figure III-5). In all cases, similar results were obtained. The degradation of pNTP is observed via the decrease in the absorbance at 405 nm, and the rates are very close (Figure III.6).

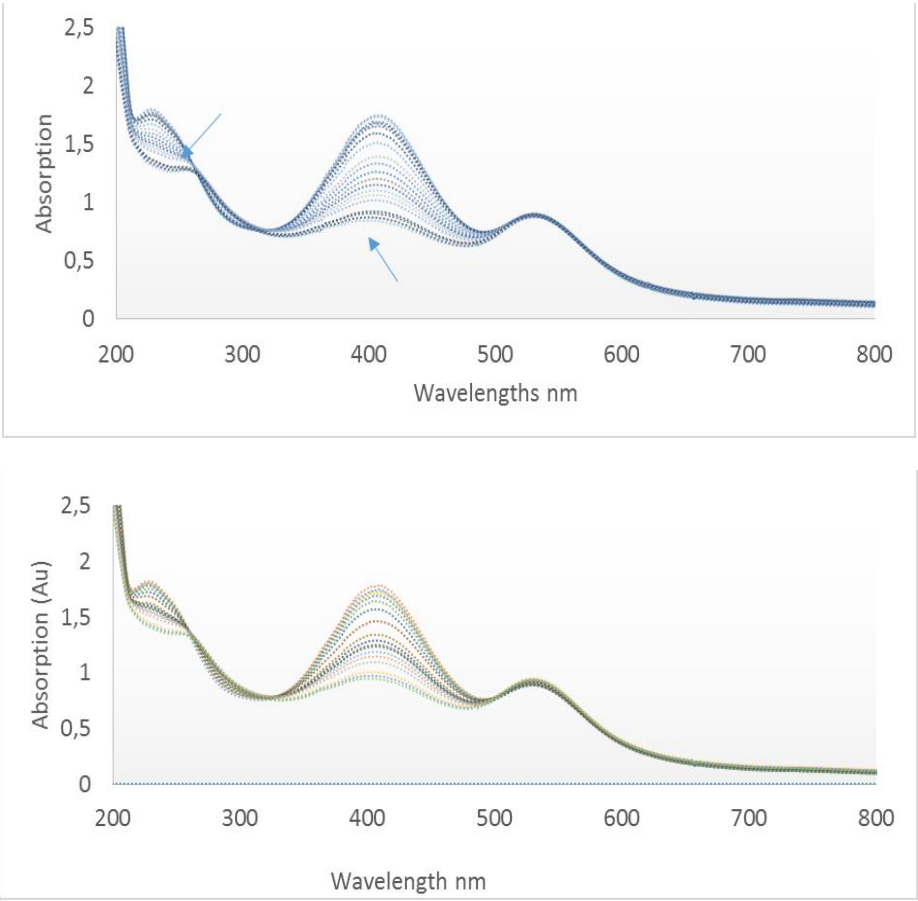

Figure III-5. Temporal evolution of the absorption spectra of an aqueous solution containing 1.64×10^{-4} M pNTP and 30 nm AuNP ($[Au^0] = 1.74 \times 10^{-4}$ M) under stirring and (top) laser excitation at 532 nm for 15 hours, (bottom) illumination by a Xe lamp ($\lambda > 520$ nm) for 15 hours. Spectra taken after every hour of illumination.

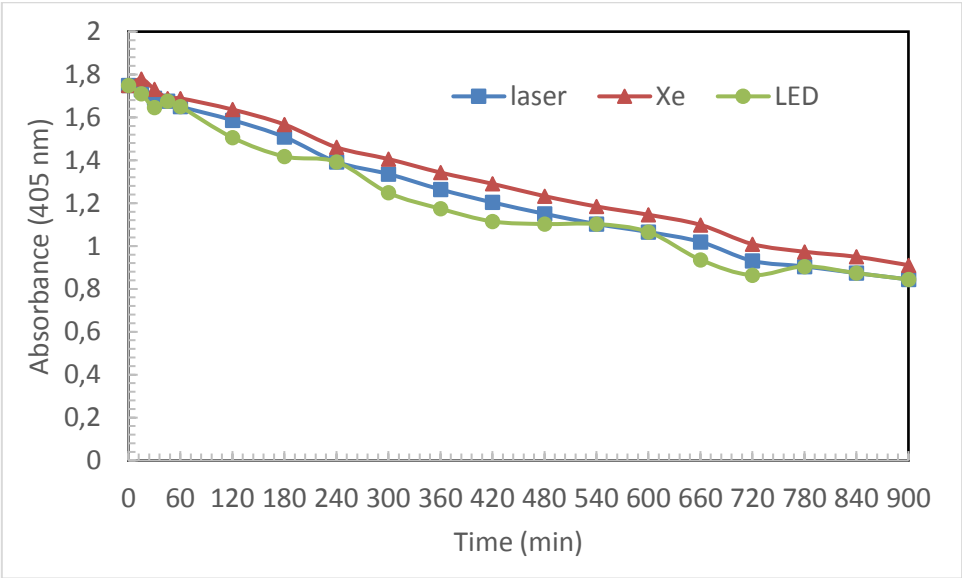

Figure III-6. Absorbance at 405 nm as a function of time for aqueous solutions containing 1.64×10^{-4} M pNTP and 30 nm AuNPs under illumination with 525 nm LEDs photoreactor, 532 nm laser beam, **or** Xe lamp ($\lambda > 500$ nm).

The described experiments were conducted under ambient atmosphere, *i.e.*, in the presence of dioxygen. However, the formation of pATP corresponds to a reduction reaction. In consequence, O_2 may play a role as an oxidizing agent. So, experiments were also performed under nitrogen atmosphere; for that, the mixture solutions (containing pNTP and 30nm Au NPs) were deaerated by nitrogen bubbling during the initial 40 min of stirring in darkness. Then, upon LED irradiation, the degradation of pNTP is observed by the disappearance of the absorption band at 405 nm (Figure III.7). The decrease at 405 nm is similar compared to that registered under air atmosphere (Figure III.8). But in contrast to what was reported under air atmosphere, the AuNPs LSPR band is not stable but decreases and broadens slightly, which suggests modifications of the AuNps in size, shape and/or concentration.

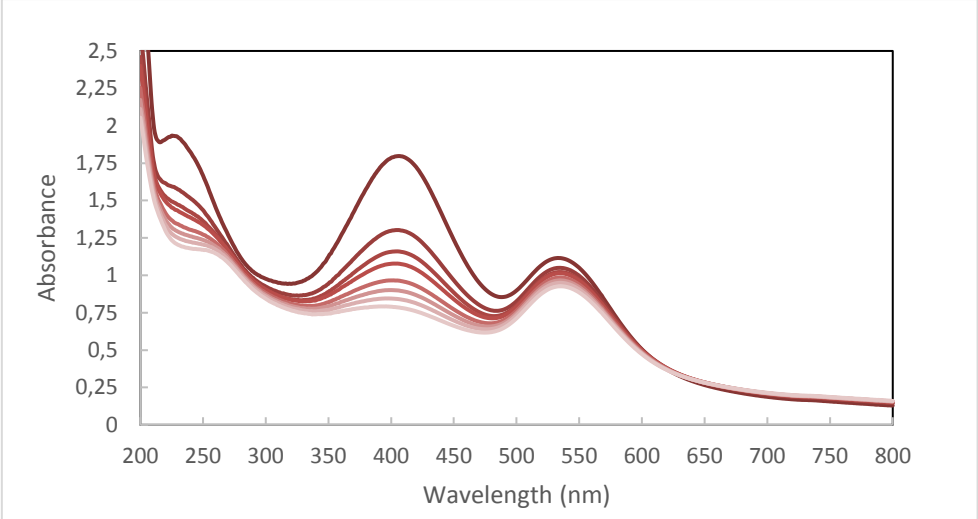

Figure III-7. Temporal evolution of the absorption spectra of an aqueous solution containing 1.64×10^{-4} M pNTP and 30 nm AuNPs ($[Au^0] = 1.74 \times 10^{-4}$ M) under stirring, N_2 atmosphere and illumination at 525 nm in the LED photochemical reactor for 480 minutes.

In order to study the influence of the size of the AuNPs, experiments were also carried out using smaller NPs with a diameter of 15 nm. The evolution of the absorption spectra (Figure III-9) looks similar as those obtained with 30 nm NPS but under N_2 atmosphere and not under air as, in addition to the degradation of pNTP, a change in the LSPR band is observed. That indicates that the smaller NPs are not as stable as the larger ones. However, the rate of the pNTP degradation is faster, at least at the beginning, compared to that determined for 30 nm NPs. That can be related to a larger surface area and a greater number of pNTP molecules adsorbed on 15 nm NPs than on 30 nm AuNPs.

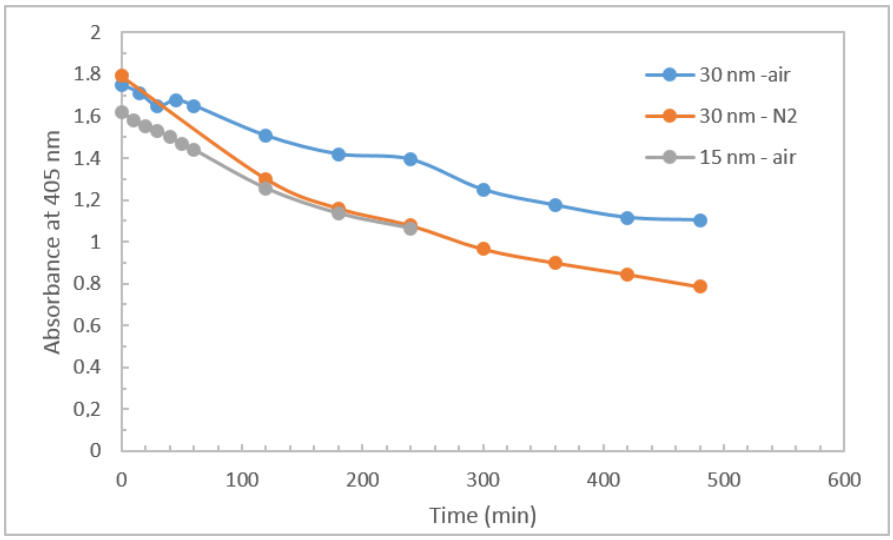

Figure III-8. Absorbance at 405 nm as a function of time for aqueous solutions containing 1.64×10^{-4} M pNTP and 30 nm AuNPs under illumination with 525 nm LEDs photoreactor, 532 nm laser beam, **or** Xe lamp ($\lambda > 500$ nm).

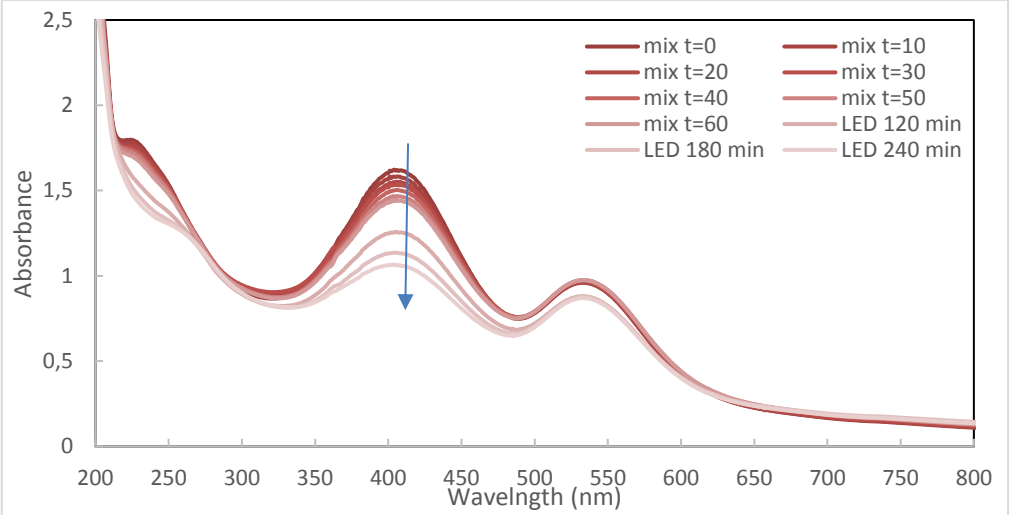

Figure III-9 Temporal evolution of the absorption spectra of an aqueous solution containing 1.64×10^{-4} M pNTP and 15 nm AuNP ($[Au^0] = 1.74 \times 10^{-4}$ M) under stirring and LED illumination 525 nm.

It has to be noted that light irradiation at 525 nm of alkaline pNTP solution in the absence of AuNPs induces no change in the absorption spectrum, indicating no degradation of pNTP.

Additionally, the degradation of para-nitrophenol, instead of pNTP, was also studied under similar conditions. But, in that case no degradation was observed. That suggests that the thiol group, known to have a good affinity to Au surface, may play a role by favoring the interactions between the molecules and the AuNPs.

IV-Characterizations of the formed products

The monitoring of the degradation of pNTP by UV-visible absorption spectroscopy suggests the formation of pATP and other products. For chemical analysis, centrifugations of the irradiated solutions were performed at room temperature in darkness for 15 minutes with a velocity of 10.000 rpm. Samples were then separated into supernatant solutions and residues. The residues containing the AuNPs were left to dry at room temperature in darkness to remove water molecules as much as possible. In order to determine the compounds generated under illumination, the supernatant solutions and the AuNPs surfaces were analyzed by ESI and SERS, respectively (Scheme III.3)

.

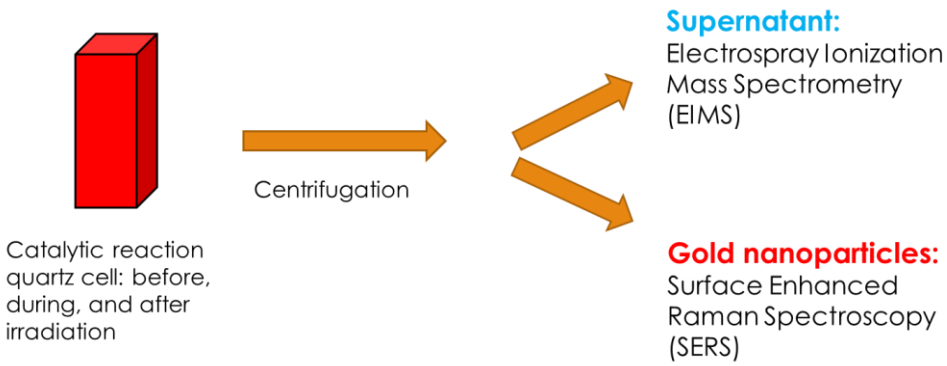

Scheme III-3. Representation of products characterization frame-work**.**

IV-1-Analysis of the supernatant

IV-1-1- ESI-MS spectra of known compounds

In order to help the identification of the formed products, first the ESI spectra of the pNTP and trisodium citrate initial compounds, as well as the spectra of pNP were recorded (Figure III.10).

The ESI-MS spectrum of pNTP alone in alkaline solution (Figure III.10a) is dominated by a peak at 153.9 m/z as expected for thiolate ion $C_6H_4NO_2S^-$, but the presence of peaks at 170, 186 and 202 m/z with differences of m/z between the peaks equal to 16 suggest partial oxidation of the thiol function into sulfenenic, sulfinic and sulfonic acids (or more exactly their ions).

The second spectrum (Figure III.10b) of the trisodium citrate solution shows a main peak at 190.95 m/z which corresponds to $[C_6H_5O_7+2H]^-$. Three peaks with relative abundancies

higher than 10% are observed at 111, 213 and 281 m/z; taking into account the theoretical mass of sodium, the last values of m/z may correspond to $[C_6H_5O_7+H+Na]^-$ and $[C_6H_5O_7+4Na]^+$.The small peak at 259 m/z may also be related to addition of Na $[C_6H_5O_7+H+3Na]^+$.

The spectrum of para-nitrophenol (Figure III-10c) displays a significant peak at 138 m/z corresponding to the nitrophenolate ion and another small peak at 255 m/z.

In Table III-1 are also listed possible products with their formula and mass.

Chemical entity	**Formula**	**Monoisotopic Mass**	**Isotopes**
4-NTP	$C_6H_5NO_2S$	155.0041	M+1 (6.6%) M+2 (4.4%)
Nitrophenol	$C_6H_5NO_3$	139.0269	M+1 (6.7%)
DMAB Dimer (4,4'-[-1,2-Diazenediyl] dibenzenethiol)	$C_{12}H_{10}N_2S_2$	246.0285	M+1 (13%) M+2 (9%)
3-[4-(1,3-benzothiazol-2-yl)-3-oxo-8-[2-(2-thienyl)vinyl]-1-thia-4,6,7-triazaspiro[4.4]non-7-en-6-yl] benzenesulfonic acid	$C_{24}H_{18}N_4O_4S_4$	554.0211	M+1 (17%) M+2 (24%)

Table III-1. Possible products (name, formula and mass) obtained by the degradation of pNTP

IV-1-1- ESI-MS spectra of the irradiated solutions

Figure III-11 presents the ESI-MS full scan spectra of the supernatant solutions corresponding to pNTP and AuNP mixture solutions before illumination (i.e. after 40 minutes of mixing under darkness) and after 6 hours and 12 hours of illumination by the 525 nm LEDs photoreactor.

In the spectrum before illumination (Figure III-11a), the two main peaks observed at 153.9 and 190.9 m/z correspond to pNTP ions and citrate molecules, respectively. However, the spectrum is complex with many peaks.

After 6 hours of illumination (Figure III-11b), these two peaks are still present, but the peak at 153. 9 m/z is highly diminished and a new dominant peak has appeared at 185.8 m/z.

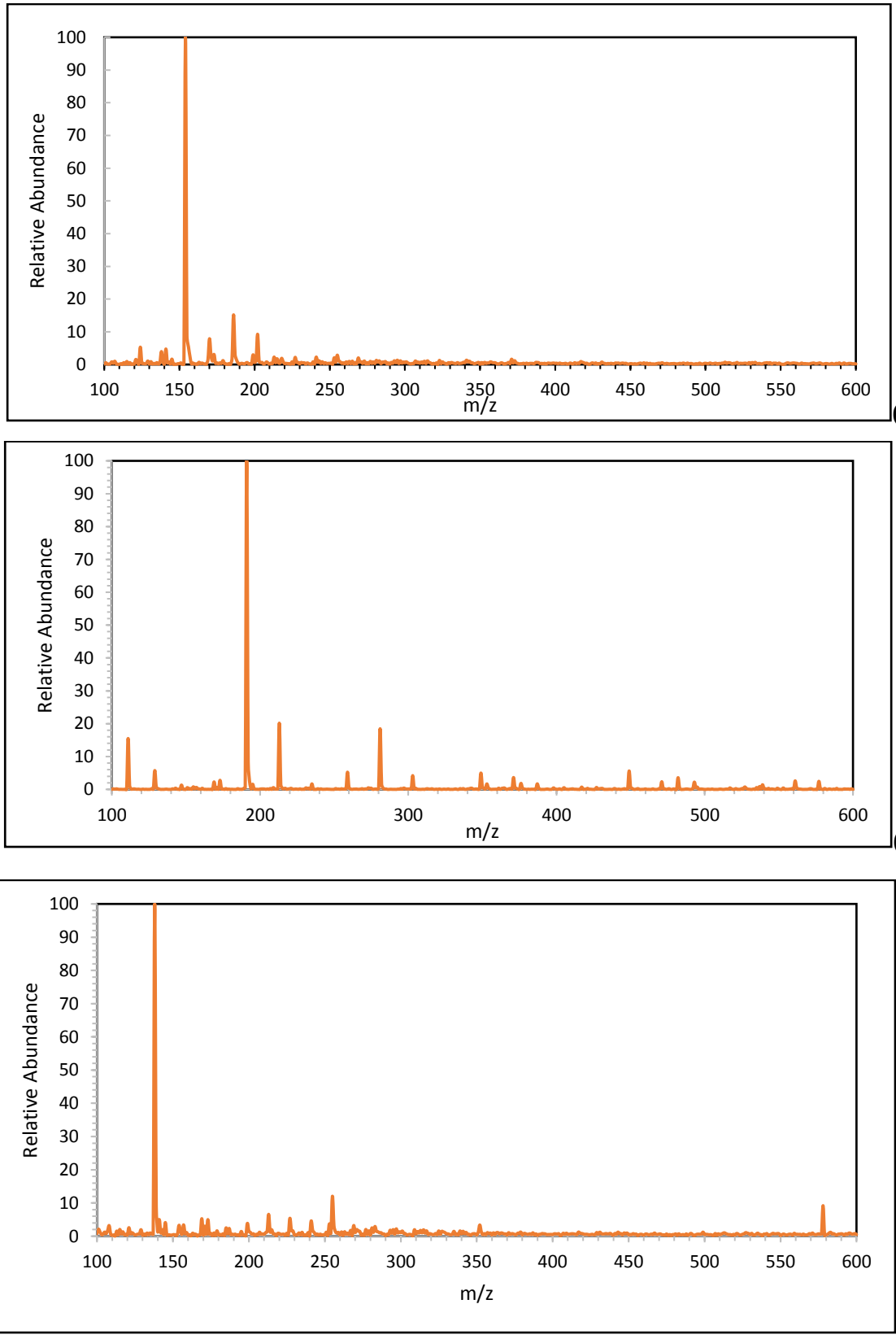

Figure III-10. ESI spectra of solutions containing only the initial compounds: **(a)** pNTP, **(b)** trisodium citrate; or **(c)** para-nitrophenol (pNP)

Other peaks with significant abundance (> 10%) are located at 202, 213, 218 and 259 m/z. 202 m/z peak is already present in the spectrum of pNTP while 213 and 259 m/z are observed in trisodium citrate spectrum.

After 6 hours of illumination (Figure III-11b), these two peaks are still present, but the peak at 153. 9 m/z is highly diminished and a new dominant peak has appeared at 185.8 m/z. Other peaks with significant abundance (> 10%) are located at 202, 213, 218 and 259 m/z. 202 m/z peak is already present in the spectrum of pNTP while 213 and 259 m/z are observed in trisodium citrate spectrum.

After 12 hours of illumination, the ESI-MS spectrum of the supernatant (Figure III.11c) is dominated by the peak of citrate at 190.9 m/z; the peak at 153.9 m/z associated to pNTP has disappeared and the peak at 186 m/z has dropped. Three other peaks with an abundance higher than 15% are observed at 110.9, 202 and 212.9 m/z; two of them (110.9 and 212.9 m/z) can be related to citrate (Figure III.10). Hence, it appears that after 12 hours of illumination, there is no more pNTP in solution.

By comparison, the ESI-MS spectrum of the supernatant solution obtained from the mixture solution maintained in darkness during 12 hours (Figure III-11d) is much simpler with three dominant peaks at 153.9, 190.9 and 212.9 m/z. The peaks at 190.9 and 212.9 m/z are associated to citrate; the peak at 153.9 m/z is related to pNTP and has decreased compared to the initial spectrum (Figure III-11a) indicating degradation of the compound.

For some specific peaks in order to confirm their attribution, product ion scan (PIS) spectra were recorded to detect fragmentation occurring in the ionic source.

The PIS spectrum obtained from the peak at 185.8 m/z (dominant in Figure III-11b) reveals two peaks at 121.9 and 138.0 m/z (Figure III. 12a) that can be associated to para-nitrobenzene ion and para-nitrophenolate (Figure III-10c). As the $\Delta m/z = 185.8 - 153.9 = 31.9 \cong 32$, i.e. the mass of two oxygen atoms, the peak at 185.8 m/z might be attributed to 4-nitrobenzenesulfinate, corresponding to a partial oxidation reaction of the thiolate group. It is to note that the ESI spectrum of pNTP alone in alkaline solution (Figure III-10a) is dominated by a peak at 153.9 m/z as expected for thiolate ion $C_6H_4NO_2S^-$, but presents also small peaks at 170, 186 and 202 m/z; the differences of m/z between the peaks equal to 16 suggest partial oxidation of the thiol function into sulfenenic, sulfinic and sulfonic acids (or more exactly their ions). Consequently, the peak at 202 m/z in Figure III-11b could be related to 4-nitrobenzene sulfonate.

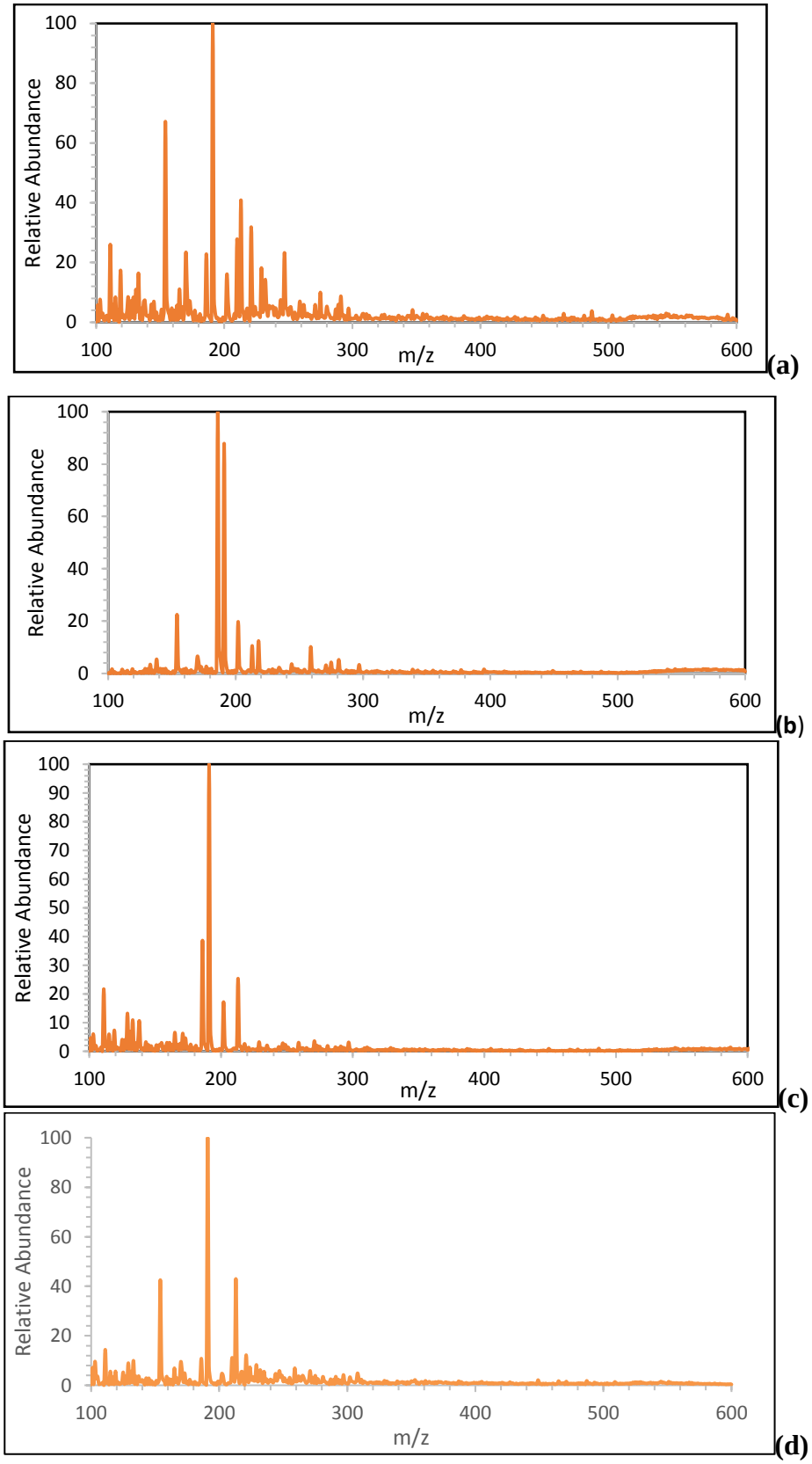

Figure III-11. ESI spectra of the supernantant solutions obtained after centrifugation of pNTP and AuNPs mixture solutions **(a)** before illumination (i.e. after 40 minutes of mixing under darkness), **(b)** after 6 hours and **(c)** 12 hours of illumination by the LEDs photoreactor, and (d) after 12 hours in dark.

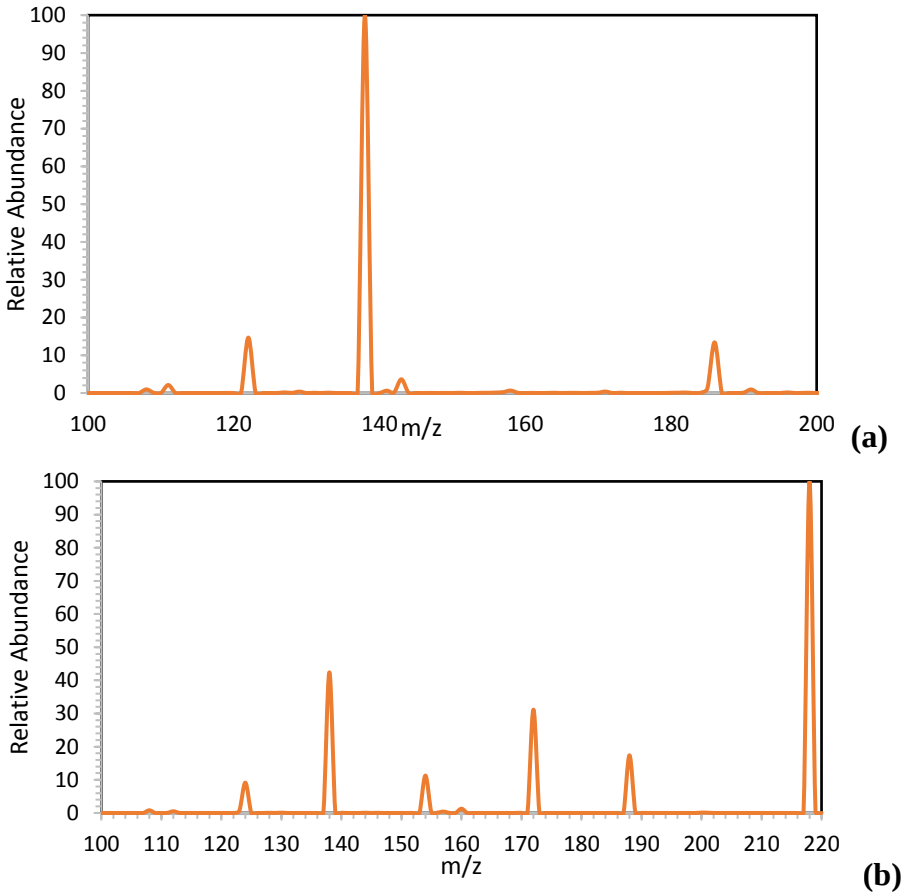

Figure III-12 EI-MS spectra obtained by fragmentation of the peak at **(a)** 185.75 m/z and **(b)** 218 m/z for the pNTP and AuNPs mixture solution after 6 hours illumination with the LEDs photoreactor 185.75 m/z

For the attribution of the peak at 218 m/z, PIS was performed (Figure III-12b). Affiliated peaks are observed at 124, 137.9, 153.8, 171.9, 187.9 m/z. Peaks at 137.9 and 153.9 m/z can be attributed to pNP and pNTP anions, respectively. The interpretation of the other peaks could be 124 para-aminobenzenethiolate, 171.9 [pNTP+H_2O] or para-aminobenzene sulfonate, 187.9 [para-nitrobenzenesulfenate+H_2O].

IV-2- SERS analysis of the AuNPs surface

Information on the AuNPs surfaces was obtained by SERS measurements. Figure III.13 shows the SERS spectra of the AuNPs extracted by centrifugation from pNTP and AuNPs mixture solutions before illumination (i.e. after 40 minutes of mixing under darkness) and after 12 hours of illumination by the LEDs photoreactor. After 40 min of mixing in darkness with pNTP, the SERS spectrum of the AuNPs (Figure III-13a) reveals new peaks at 1077, 1332 and 1568 cm^{-1}. As already reported in the literature, theses peaks are characteristic of

pNTP molecule (Figure III-15a), with in particular the Raman intensity at 1332 cm^{-1} related to $\nu(NO_2)$. That gives evidence of the presence of pNTP at the surface of the AuNPs and so, a co-adsorption with citrate. After 12 hours of illumination (Figure III-13b), the Raman intensity of $\nu(NO_2)$ disappears and new intensities emerge at 1135, 1388 and 1432 cm^{-1}. These peaks are in accordance with the SERS spectrum of ATP reported in the literature. Consequently, photoreduction of pNTP to ATP has occurred on the AuNPs surface.

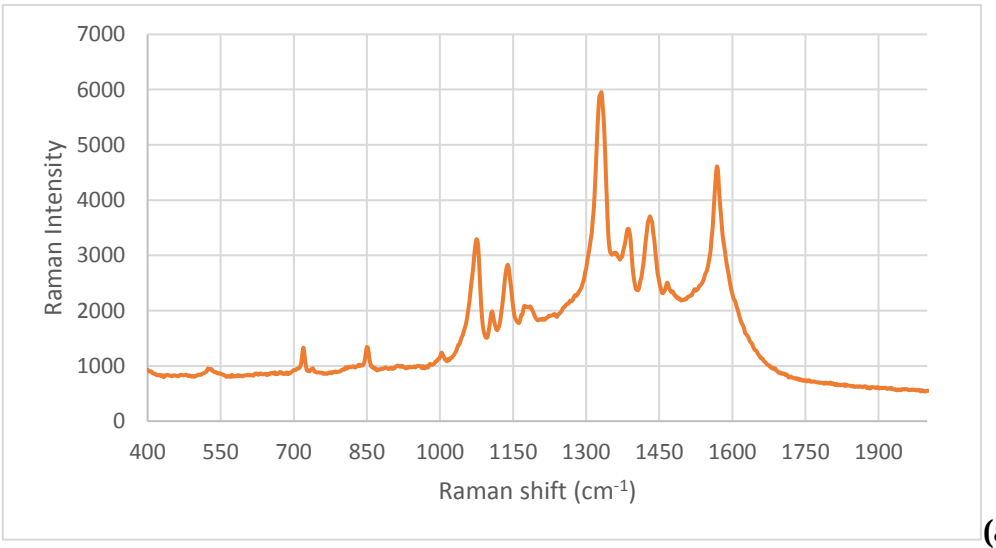

(a)

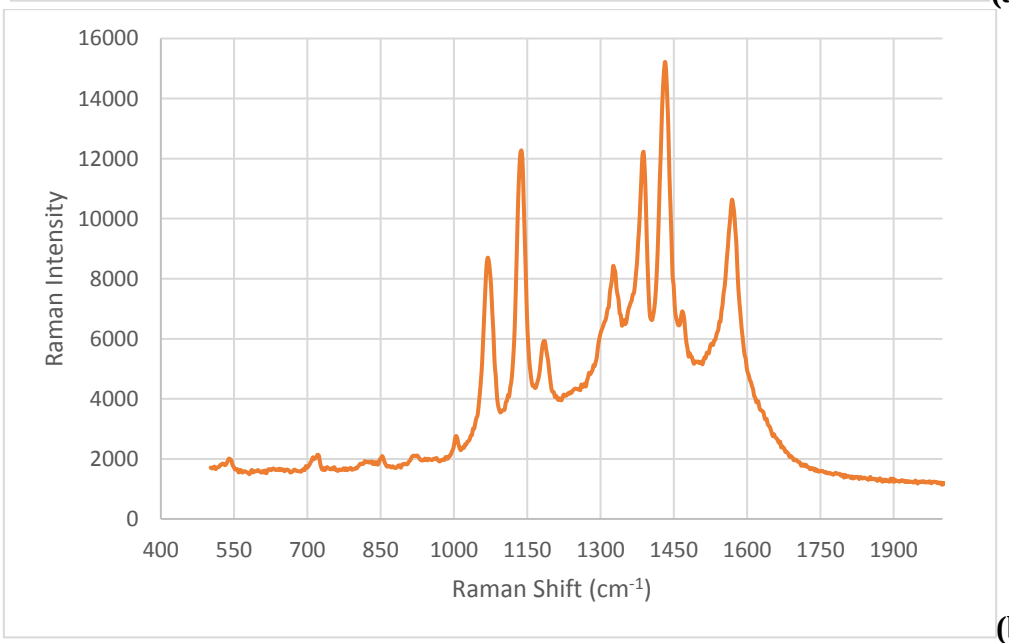

(b)

Figure III-13. Neat SERS spectra of 30 nm AuNPs obtained after centrifugation from pNTP and AuNPs mixture solutions before illumination (i.e. after 40 minutes of mixing under darkness) **(a)** and after 12 hours of illumination by the LEDs photoreactor **(b).**

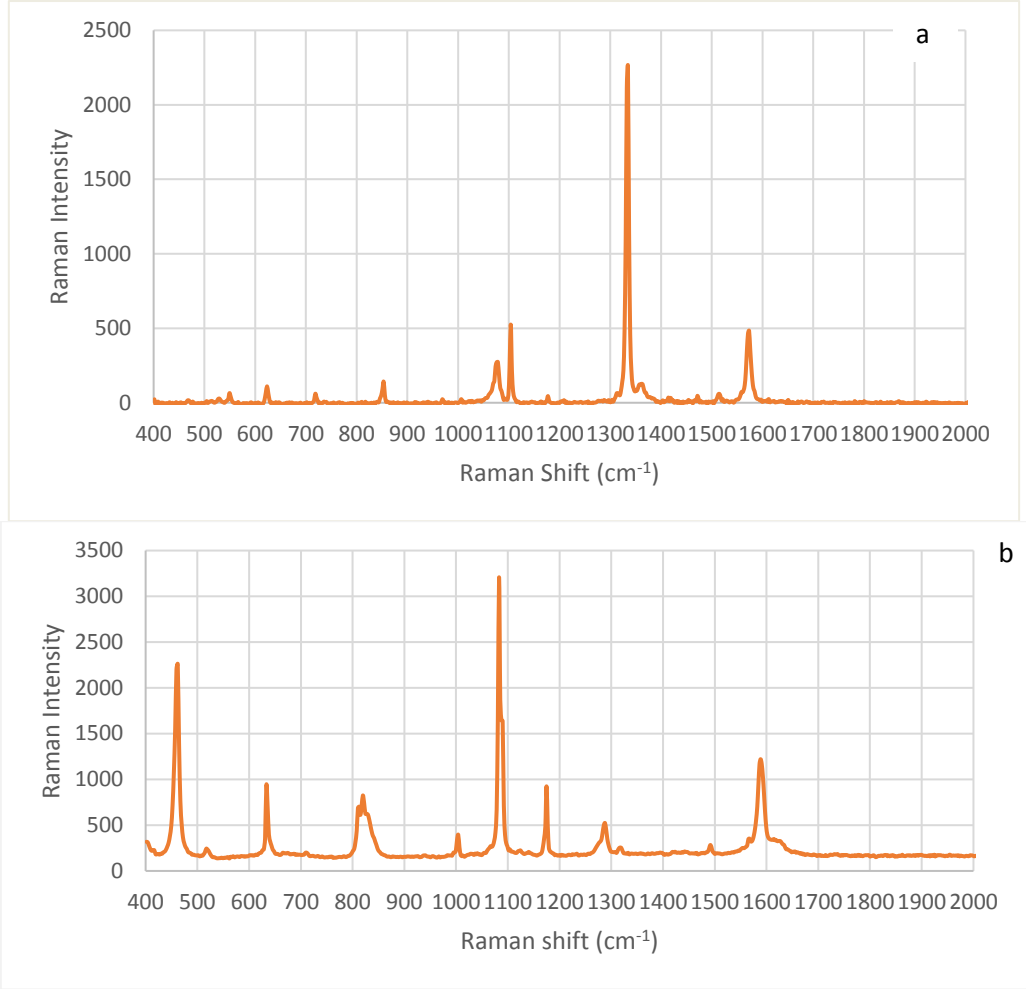

Figure III-15. Raman spectra of **(a)** pNTP **(b)** pATP.

V- Discussion

According to the above results, the disappearance of pNTP requires both the presence of AuNPs and the excitation of their plasmon band, since almost no degradation is observed either in the absence of AuNPs under light irradiation, or in the presence of AuNPs without light. That indicates that reactions leading to degradation of pNTP are induced by plasmon excitation. Moreover, the absence of degradation of para-nitrophenol in the presence of AuNPs under irradiation, and the detection of pNTP on the surface of the AuNPs show that adsorption of the molecules on the NPs is an important factor, too. UV-visible spectroscopy and SERS measurements show the formation of pATP. This compound is present at the surface of the AuNPs, but not in the solution. That suggests that the reduction reaction of pNTP takes place on the surface and involves “hot” electrons produced by plasmon excitation. Moreover, the formed pATP seems to remain on the AuNPs surface as it is hardly

detected in the supernatant solution by ESI. Besides, when the reaction is nearly finished after 12 hours of illumination, there is no more pNTP in solution, and only small amounts of nitro-benzene derivatives bearing oxidized thiol group are detected (Figure III.11c). However, these oxidized compounds are in much higher quantity during the illumination (after 6 hours of illumination, Figure III.11b) while they correspond to traces before illumination. That indicates that these species are produced and then disappear during the illumination time.

Taking into account these observations, we may propose the following mechanism. Plasmon-excitation of AuNPs generates "hot" electrons and "holes"; the formers are responsible of the reduction, while the latters induce oxidation. So, in a first step, reduction of pNTP adsorbed on the AuNPs surface takes place in parallel to oxidation of the thiol group of pNTP molecules in solution (thiol groups are not very stable and easily oxidized). In a second step, the oxidized nitrobenzene are also reduced to form pATP, once they are in close interaction with the AuNP surface, i.e. when they have replaced citrate ions as ligands.

It is to note that, when experiments are carried out under air atmosphere, the electrons may react with the dioxygen and generate $O_2^{\bullet -}$, which is an oxidizing radical. Such reaction favors the oxidation of pNTP of the detriment of its reduction. That may explain why no pNTP is detected in the supernatant.

VI- Conclusion

We have shown that the excitation of the plasmon band of AuNPs is responsible for the disappearance of pNTP indicating that reactions are induced by plasmon excitation, and hot electrons are involved in these reactions. However, adsorption of the molecules on the NPs seems to be an important factor. To validate our proposed mechanism, further experiments are needed. In particular, the above experiments where performed under air atmosphere, i.e. with dioxygen. To unravel the role of dioxygen in the formed products, chemical analysis of the products generated with irradiation experiments carried out under inert atmosphere should be done.

Anyway, these results demonstrate that plasmon-driven chemical reactions are very promising for environmental applications and depollution since pNTP is considered as a model pollutant and can be degraded. Yet the mechanism involving plasmonic nanomaterials, especially in solution, needs further examination.

References

1. Hou, W.; Cronin, S.B. A Review of Surface Plasmon Resonance-Enhanced Photocatalysis. *Advanced Functional Materials* **2013**, *23*, 1612-1619.
2. Hirsch, L.R.; Stafford, R.J.; Bankson, J.A.; Sershen, S.R.; Rivera, B.; Price, R.E.; Hazle, J.D.; Halas, N.J.; West, J.L. Nanoshell-mediated near-infrared thermal therapy of tumors under magnetic resonance guidance. *Proceedings of the National Academy of Sciences* **2003**, *100*, 13549-13554.
3. Kelly, K.L.; Coronado, E.; Zhao, L.L.; Schatz, G.C. The Optical Properties of Metal Nanoparticles: The Influence of Size, Shape, and Dielectric Environment. *The Journal of Physical Chemistry B* **2003**, *107*, 668-677.
4. Huang, X.; El-Sayed, M.A. Gold nanoparticles: Optical properties and implementations in cancer diagnosis and photothermal therapy. *Journal of Advanced Research* **2010**, *1*, 13-28.
5. Wang, C.; Astruc, D. Photocatalysis for Organic Synthesis and Clean Energy Conversion. *Chem. Soc. Rev* **2014**, *43*, 7188–7216.
6. Linic, S.; Christopher, P.; Ingram, D.B. Plasmonic-Metal Nanostructures for Efficient Conversion of Solar to Chemical Energy. *Nat. Mater.* **2011**, *10*, 911-921.
7. Vincenzo; Amendola, e.a. Surface plasmon resonance in gold nanoparticles: a review. . *J Phys Condens Matter.* **2017**, *29*.
8. Lin, T.W.; Tasi, T.T.; Chang, P.L.; Cheng, H.Y. Reversible Association of Nitro Compounds with p-Nitrothiophenol Modified on Ag Nanoparticles/Graphene Oxide Nanocomposites through Plasmon Mediated Photochemical Reaction. *ACS applied materials & interfaces* **2016**, *8*, 8315-8322.
9. Baffou, G.; Rigneault, H. Femtosecond-pulsed optical heating of gold nanoparticles. *Physical Review B* **2011**, *84*.
10. Linic, P.; Christopher, D.B.I. Plasmonic-Metal Nanostructures for Efficient Conversion of Solar to Chemical Energy. *Nat. Mater.* **2011**, *10*, 911–921.
11. Loiseau, A.; Asila; Boitel-Aullen; Lam; Salmain; Boujday, S. *Silver-Based Plasmonic Nanoparticles for and Their Use in Biosensing*; 2019; Vol. 9, pp. 78.
12. Bedford, E.; Boujday, S.; Pradier, C.-M.; Gu, F. *Spiky gold shells on magnetic particles for DNA Biosensors*; 2018; Vol. 182.
13. Golubev, A.A.; Khlebtsov, B.N.; Rodriguez, R.D.; Chen, Y.; Zahn, D.R.T. Plasmonic Heating Plays a Dominant Role in the Plasmon-Induced Photocatalytic Reduction of 4-Nitrobenzenethiol. *The Journal of Physical Chemistry C* **2018**, *122*, 5657-5663.
14. Kim, K.; Lee, I.; Lee, S.J. Photolytic reduction of 4-nitrobenzenethiol on Au mediated via Ag nanoparticles. *Chemical Physics Letters* **2003**, *377*, 201-204.
15. Link, S.; El-Sayed, M.A. Shape and size dependence of radiative, non-radiative and photothermal properties of gold nanocrystals. *International Reviews in Physical Chemistry* **2000**, *19*, 409-453.
16. Huang, X.; Neretina, S.; El-Sayed, M. Gold Nanorods: From Synthesis and Properties to Biological and Biomedical Applications. *Adv. Mater.* **2009**, *21*, 4880-4910.
17. Narayanan, R.; Tabor, C.; El-Sayed, M.A. Can the Observed Changes in the Size or Shape of a Colloidal Nanocatalyst Reveal the Nanocatalysis Mechanism Type: Homogeneous or Heterogeneous? *Top. Catal.* **2008**, *48*, 60-74.
18. Burda, C.; Chen, X.; Narayanan, R.; El-Sayed, M.A. Chemistry and Properties of Nanocrystals of Different Shapes. *Chemical reviews* **2005**, *105*, 1025-1102.

19. Zhao, L.-B.; Chen, J.-L.; Zhang, M.; Wu, D.-Y.; Tian, Z.-Q. Theoretical Study on Electroreduction of p-Nitrothiophenol on Silver and Gold Electrode Surfaces. *The Journal of Physical Chemistry C* **2015**, *119*, 4949-4958.
20. Zhao, L.B.; Zhang, M.; Huang, Y.F.; Williams, C.T.; Wu, D.Y.; Ren, B.; Tian, Z.Q. Theoretical Study of Plasmon-Enhanced Surface Catalytic Coupling Reactions of Aromatic Amines and Nitro Compounds. *J. Phys. Chem. Lett.* **2014**, *5*, 1259-1266.
21. Dong, B.; Fang, Y.; Chen, X.; Xu, H.; Sun, M. Substrate-, wavelength-, and time-dependent plasmon-assisted surface catalysis reaction of 4-nitrobenzenethiol dimerizing to p,p'-dimercaptoazobenzene on Au, Ag, and Cu films. *Langmuir : the ACS journal of surfaces and colloids* **2011**, *27*, 10677-10682.
22. Kim, K.; Lee, I.; Lee, S.J. Photocatalytic reduction of 4-nitrobenzenthiol on Au mediated via Ag nanoparticles. . *Chem. Phys. Lett.* **2003**, *377*, 201-204.
23. Zhu, H.; Ke, X.; Yang, X.; Sarina, S.; Liu, H. Reduction of Nitroaromatic Compounds on Supported Gold Nanoparticles by Visible and Ultraviolet Light. *Angewandte Chemie International Edition* **2010**, *49*, 9657-9661.
24. Grirrane, A.; Corma, A.; García, H. Gold-Catalyzed Synthesis of Aromatic Azo Compounds from Anilines and Nitroaromatics. *Science* **2008**, *322*, 1661-1664.
25. Kim, K.; Choi, J.-Y.; Shin, K.S. Surface-Enhanced Raman Scattering of 4-Nitrobenzenethiol and 4-Aminobenzenethiol on Silver in Icy Environments at Liquid Nitrogen Temperature. *The Journal of Physical Chemistry C* **2014**, *118*, 11397-11403.
26. Cui, Q.; Yashchenok, A.; Li, L.; Möhwald, H.; Bargheer, M. Mechanistic study on reduction reaction of nitro compounds catalyzed by gold nanoparticles using in situ SERS monitoring. *Colloids and Surfaces A: Physicochemical and Engineering Aspects* **2015**, *470*, 108-113.
27. Aditya, T.; Pal, A.; Pal, T. Nitroarene reduction: a trusted model reaction to test nanoparticle catalysts. *Chemical Communications* **2015**, *51*, 9410-9431.
28. Pozun, Z.D.; Rodenbusch, S.E.; Keller, E.; Tran, K.; Tang, W.; Stevenson, K.J.; Henkelman, G. A Systematic Investigation of p-Nitrophenol Reduction by Bimetallic Dendrimer Encapsulated Nanoparticles. *The journal of physical chemistry. C, Nanomaterials and interfaces* **2013**, *117*, 7598-7604.
29. Dong, B.; Fang, Y.; Xia, L.; Xu, H.; Sun, M. Is 4-nitrobenzenethiol converted to p,p′ -dimercaptoazobenzene or 4-aminothiophenol by surface photochemistry reaction? *Journal of Raman Spectroscopy* **2011**, *42*, 1205-1206.
30. Sun, M.; Huang, Y.; Xia, L.; Chen, X.; Xu, H. The pH-Controlled Plasmon-Assisted Surface Photocatalysis Reaction of 4-Aminothiophenol to p,p′ -Dimercaptoazobenzene on Au, Ag, and Cu Colloids. *The Journal of Physical Chemistry C* **2011**, *115*, 9629-9636.
31. Park, J.-W.; Shumaker-Parry, J.S. Strong Resistance of Citrate Anions on Metal Nanoparticles to Desorption under Thiol Functionalization. *ACS Nano* **2015**, *9*, 1665-1682.
32. Hong, S.; Li, X. Optimal Size of Gold Nanoparticles for Surface-Enhanced Raman Spectroscopy under Different Conditions. *Journal of Nanomaterials* **2013**, *2013*, 1-9.
33. Zheng, Z.; Tachikawa, T.; Majima, T. Plasmon-Enhanced Formic Acid Dehydrogenation Using Anisotropic Pd–Au Nanorods Studied at the Single-Particle Level. *Journal of the American Chemical Society* **2015**, *137*, 948-957.
34. Zhang, Z.; Deckert-Gaudig, T.; Singh, P.; Deckert, V. Single molecule level plasmonic catalysis – a dilution study of p-nitrothiophenol on gold dimers. *Chemical Communications* **2015**, *51*, 3069-3072.
35. Ciganda, R.; Li, N.; Deraedt, C.; Gatard, S.; Zhao, P.; Salmon, L.; Hernández, R.; Ruiz Aranzaes, J.; Astruc, D. *Gold nanoparticles as electron reservoir redox catalysts for 4-nitrophenol reduction: A strong stereoelectronic ligand influence*; 2014; Vol. 50.

36. N. Dalby, K.; P. Jencks, W. General acid catalysis of the reversible addition of thiolate anions to cyanamide. *Journal of the Chemical Society, Perkin Transactions 2* **1997**, 1555-1564.

37. Jencks, W.P.; Salvesen, K. Equilibrium deuterium isotope effects on the ionization of thiol acids. *Journal of the American Chemical Society* **1971**, *93*, 4433-4436.

38. Turkevich, J.; Stevenson, P.; Hillier, J. A study of the nucleation and growth processes in the synthesis of colloidal gold. *Discuss Faraday Soc.* **1951**, *11*, 55-57.

39. Pluchery, O.; Remita, H.; Schaming, D. Demonstrative experiments about gold nanoparticles and nanofilms: an introduction to nanoscience. *Gold Bulletin* **2013**, *46*, 319-327.

Chapter IV

Hexacyanoferrate (III) reduction by electron transfer induced by plasmonic catalysis on gold nanoparticles

Table of Content

I- Introduction

Redox reactions are of great importance in environmental catalysis as, for example, reduction of nitrogen oxides (deNOx), CO_2 or heavy metals, and generation of hydrogen from water or oxidation of CO or organic pollutants [1]. Platinum, palladium and rhodium are the most used metal catalysts in hydrogenation reactions or in catalytic convertors for deNOx and CO reduction [2]. Catalysis by gold is a domain of increased interest since the discovery by Haruta [3] that small gold nanoparticles (Au-NPs) can catalyze CO reduction at room temperature [4-8].

Au-NPs have also attracted much attention due to their localized surface plasmon resonance (LSPR), *i.e.*, the oscillations of metal free electrons driven by the electric field of the incident light [6, 9-11]. There are many applications utilizing the SPR of gold nanoparticles, including subwavelength electromagnetic energy transport, chemical and biological sensors [1,10], surface enhanced Raman scattering (SERS) [12,13], plasmonic photocatalysis [14-16], and photothermal cancer therapy [17-20], where the plasmonic energy is converted locally into heat that raises the surrounding medium temperature, leading to cancer cell killing. In thermal therapy, hot electrons induced by surface plasmon excitation, lead (after reaction with oxygen or water) to formation of reactive oxygen species (ROS) ($HO^{\cdot}$, $O_2^{\cdot -}$ and singlet oxygen), which are also responsible in cancer cell killing [21].

Metal nanoparticles such as gold and platinum NPs are efficient catalysts in different reactions with environment applications. These catalytic reactions often involve electron transfers [22,23]. Reduction of ferrocyanate (III) has been taken as a model reaction to study catalysis by metal NPs [22-24].

Mulvaney, *et al* [24] studied redox catalysis by colloidal gold for the reduction of ferricyanide (III) ions by borohydride ions in alkaline aqueous solution. They found that Au-NPs dramatically increase the reaction rate and that Au-NPs also change the mechanism: The reaction is zero order in hexacyanoferrate (III) concentration for the non-catalyzed reaction to first order for the catalyzed reaction. In the latter reaction, Au-NPs act as a reservoir for the electrons and become cathodically polarized. In a first step, borohydride can inject electrons onto Au-NPs, then ferricyanide ions diffuse to the nanoparticle surface and are reduced by excess surface electrons. These nanoparticles serve as a relay for electrons.

El Sayed‘s group reported on catalysis by metal nanoparticles for the reduction of ferricyanide ion by thiosulfate to ferrocyanide [23,25,26]:

$$2Fe(CN)_6^{3-} + 2S_2O_3^{2-} \rightarrow 2Fe(CN)_6^{4-} + S_4O_6^{2-}.$$

This model reaction has been used to compare the catalytic activity of different nanoparticles [24,27]. Size and shape dependent catalytic activity of platinum nanoparticles for this reaction has been demonstrated [23,28]. The study conducted on tetrahedral, cubic and spherical Pt nanoparticles has demonstrated that the kinetic parameters correlate with the fraction of surface atoms located on the corners and edges in each size and shape [28]. It has been also demonstrated that Au-NPs are very efficient catalysts for the reduction of ferricyanide (III) ion to ferrocyanide. El-Sayed *et al*. reported that catalysis of this reaction by gold nanoparticles was enhanced when the latter were irradiated at their plasmon wavelength [23]. The value of the activation energy of this electron transfer reaction for two different shapes of Au-NPs (nanospheres and nanocages) was measured. This activation energy was found to be similar when using a thermostatic water bath or by using a plasmonic photothermal reactor. This result supported the conclusion that the role of the surface plasmon field on the electron dynamics during the reaction was negligible, and that the main effect was due to temperature increase after plasmon excitation [7,15,16].

Recently, the LSPR effect of plasmonic nanostructures has been successfully applied to photocatalysis under visible light irradiation and proved to be very promising [15,29,30].

In the present study, we investigated in details the reduction of ferricyanide (III) ion into ferrocyanide (II) ion catalyzed by spherical Au-NPs and excited at their LSPR band. Experiments were conducted in the presence (or not) of sodium thiosulfate. This catalysis is enhanced in the presence of Au-NPs with light excitation. We show for the first time that this reduction takes place even without sodium thiosulfate demonstrating the implication of hot electrons in this reduction.

II- Experimental details

Spherical Au-NPs were synthesized by Türkevich method [31-33]. Two well-defined sizes of Au-NPs (Au-NPs@citrate) with a mean diameter of 15 and 30 nm, respectively, were obtained by changing the experimental conditions (cf. chapter II). The 30 nm-Au-NPs@citrate solutions were diluted by a factor of four to get the same concentration of Au atoms as in the 15 nm-Au-NPs@citrate solutions. Figure. IV-1 shows the UV-visible spectra and TEM images of the synthesized and used Au-NPs@citrate The maximum of the LSPR band is located at 515 and 525 nm for the solutions containing Au-NPs of a mean size of 15 and 30 nm respectively.

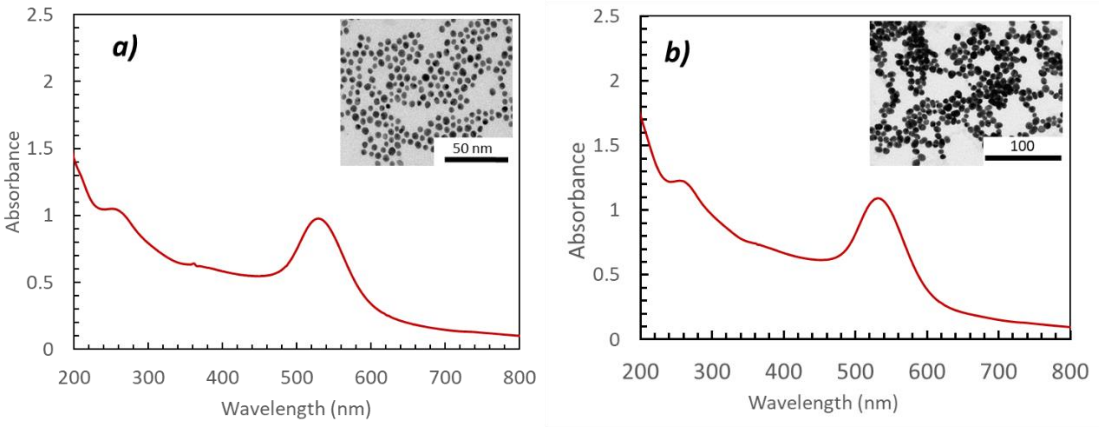

Figure IV-1. UV-Visible spectra and inset TEM images of the spherical gold nanoparticles synthesized by citrate reduction: (**a**) 15 nm-AuNPs@citrate and (**b**) 30 nm-AuNPs@citrate. Optical path length: 1 cm.

Change of ligands was performed by replacing citrate by *para*-nitrothiophenol (pNTP). For that, 750 µL of an alkaline solution of pNTP (6×10^{-4} M)were added to 2 mL of AuNP solutions contained in a 1 cm square cuvette. Following that, the solutions were left under continuous stirring in the dark for 40 minutes to ensure the adsorption of pNTP and replacement of citrate on the surface of Au-NPs.

For the catalytic reactions under irradiation, sodium thiosulfate and hexacyanoferrate (III) were added to a solution containing Au-NPs. The final concentrations for each reagent were usually: 5×10^{-4} M sodium thiosulfate, 5×10^{-4} M hexacyanoferrate (III), 0.25×10^{-3} M Au-NPs: (concentration in Au atoms). 2 mL of the mixture were introduced in a quartz cell with an optical path of 1 cm (and containing a small magnetic rod). The cell was properly sealed, bubbled with N_2 for 20 minutes to get rid of O_2, and then irradiated under stirring either with LEDs at ƛ = 520 nm (homemade reactor, cf. chapter II) or with an Oriel 300 W Xenon lamp equipped with an infrared water filter and an optical cutoff filter (longpass filter GG450, ƛ > 450 nm). The cutoff filter allows to avoid the direct excitation of ferrocyanide (III) ion, which absorbs in the range 350-400 nm (Figure. IV-2**)**.

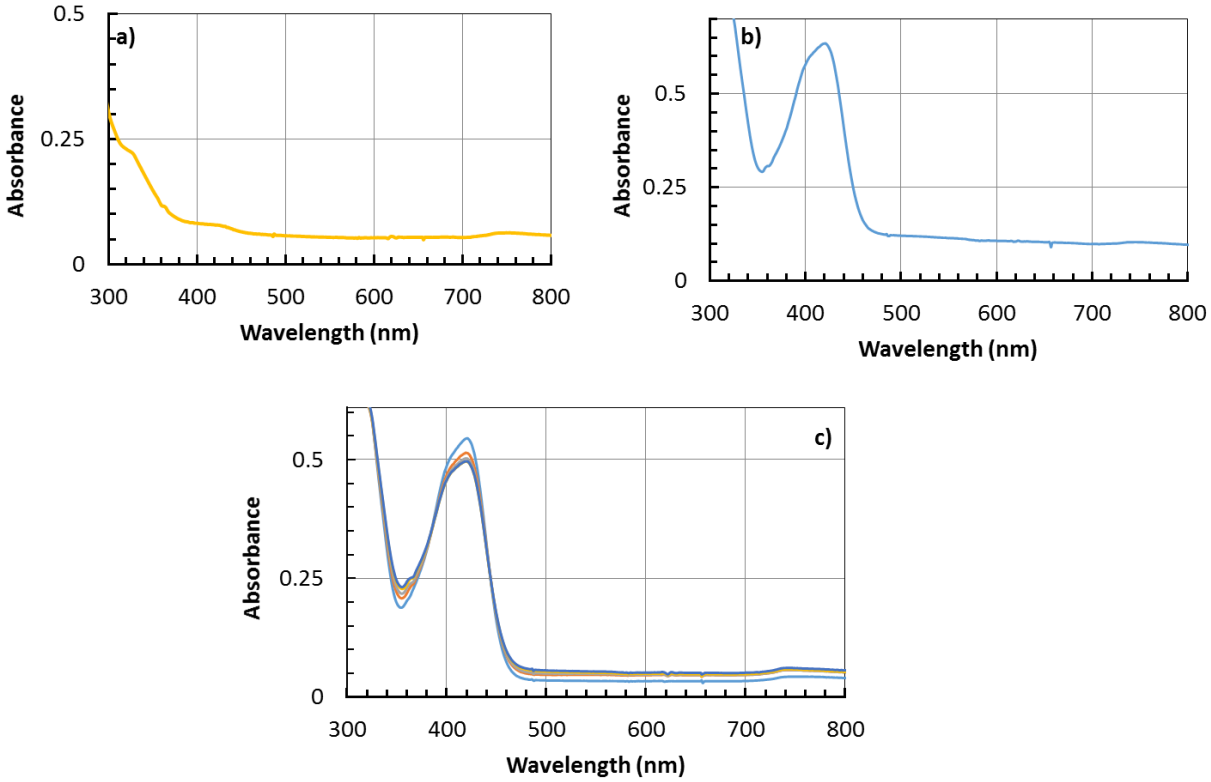

Figure IV-2. Absorbance spectra of (**a**) Sodium Thiosulfate 10^{-3} M, (**b**) Hexacyanoferrate 10^{-3} M (**c**) Mixture of both reagents under illumination: 20 mL of distilled water under visible irradiation for 120 min under N_2 (black spectrum before irradiation and blue spectrum after 120 min irradiation). The spectra were recorded using 2 mm quartz cell.

III- Reduction of hexacyanoferrate in the presence of sodium thiosulfate

The studied reaction is the reduction of ferricyanide or hexacyanoferrate, HC-FeIII, by thiosulfate:

$$2\ Fe(CN)_{6\,(aq)}^{3-} + 2\ S_2O_{3\,(aq)}^{2-} \rightarrow\ 2\ Fe(CN)_{6\,(aq)}^{4-} + S_4O_{6\,(aq)}^{2-} \qquad (1)$$

The redox potential of the couples involved in this reaction are $E^0(Fe(CN)_6^{3-}/Fe(CN)_6^{4-})$ = +0.36 V and $E^0(S_4O_6^{2-}/S_2O_3^{2-})$ = +0.08 V versus the normal hydrogen electrode at 25°C [34]. Although thermodynamically favorable, this reaction needs to be catalyzed. Solutions containing HC-FeIII and ST (without Au-NPs) are stable at room temperature, even under irradiation, while in the presence of Au-NPs and in the absence of irradiation, the reaction takes place as shown by the disappearance of the absorption bands at 310 and 420 nm associated to HC-FeIII (Figure IV-3). The rate of the reaction depends on the size of the Au-NPs.

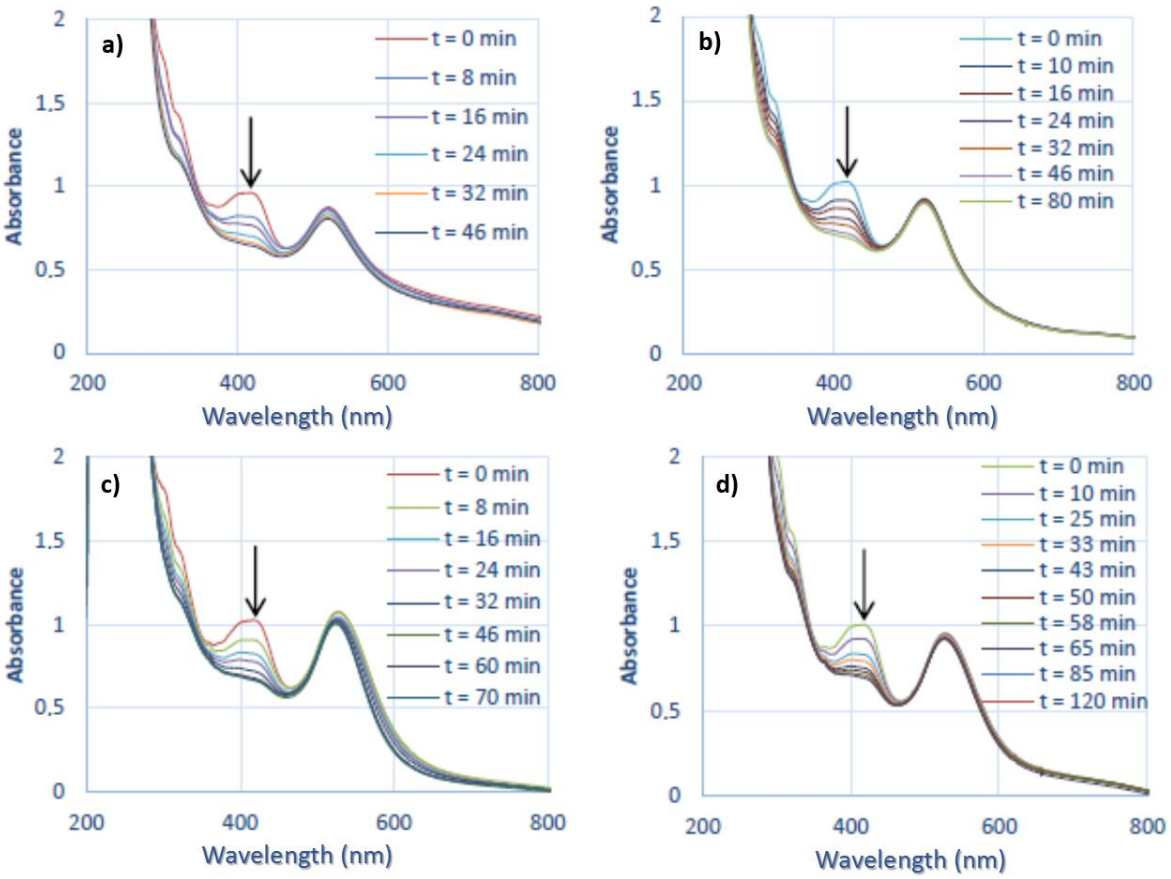

Figure IV-3. Temporal evolution of the UV-visible absorption spectra of deaerated aqueous solutions containing 5×10^{-4} M sodium thiosulfate and 5×10^{-4} M potassium hexacyanoferrate **(a)** in the presence of 15 nm Au-NPs@citrate under irradiation at $\lambda = 520$ nm, **(b)** in the presence of 15 nm Au-NPs@citrate in the dark, **(c)** in the presence of 30 nm Au-NPs@citrate under irradiation at $\lambda = 520$ nm and **(d)** in the presence of 30 nm Au-NPs@citrate in the dark. Optical path length: 1 cm.

III-1- Irradiation using LEDs at 520 nm

Figure IV-3 presents the spectral evolution of solutions containing HC-FeIII, ST and Au-NPs@citrate under LEDs irradiation at $\lambda = 520$ nm, close to the LSPR of Au-NPs. For both sizes of Au-NPs@citrate, the bands at 310 and 430 nm due to HC-FeIII decrease in intensity with irradiation time and disappear after about 45 and 60 minutes of irradiation for 15 nm and 30 nm Au-NPs@citrate, respectively. The LSPR band of the spherical Au-NPs (with a maximum around 515 nm or 525 nm for the solutions containing Au-NPs of 15 and 30 nm respectively) remains quite stable during the whole irradiation time indicating no drastic changes in the Au-NPs morphology.

The kinetics of the reduction reaction of HC-FeIII by ST is followed by the decrease in the absorbance at 420 nm (Figure IV-4). The reduction is faster for the smaller 15 nm Au-NPs@citrate compared to 30 nm Au-NPs@citrate, and for both sizes the reduction is accelerated by the irradiation. These results confirm that Au-NPs play a role of catalysts in this reaction. As catalysis takes place at the surface of the nanoparticles, the kinetics is enhanced with the specific surface area. Considering the average size of the nanoparticles (15 and 30 nm) and assuming that they are quasi-spherical, their specific surface areas are respectively 14.5 m^2 g^{-1} and 7.3 m^2 g^{-1}, respectively.

Moreover, the excitation of the LSPR of the Au-NPs favors the catalytic properties of the Au-NPs. This plasmonic effect could be related to different mechanisms:

1. Electron density exchange between the excited gold nanoparticles and nearby reactants;
2. Effect of the plasmonic near field enhancement on the electron transfer process between HC-FeIII and ST;
3. Temperature increase due to a rapid conversion of the excited surface plasmon resonance into heat that would eventually accelerate the chemical reaction.

It is to note that the temperature increase in the solution during the reaction under irradiation was around 3-4 degrees as measured by a thermos-couple immersed inside the reaction cuvette, but the increase of temperature at the surface of nanoparticles (induced by plasmon resonance) is much higher. Under continuous irradiation, each NP contributes to the global warming of the solution they are surrounded by.

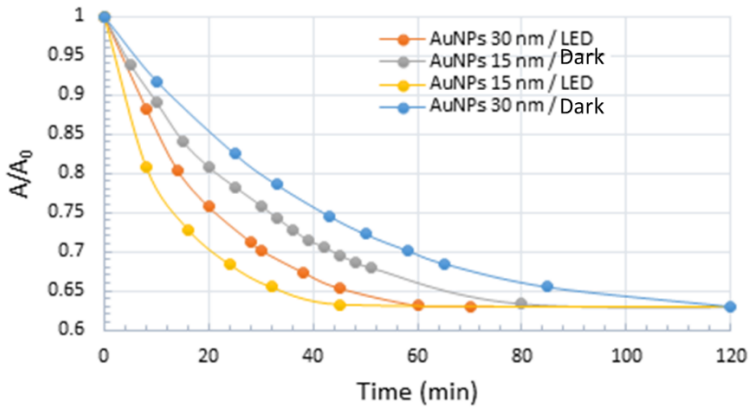

Figure. IV-4. Kinetic trace of the normalized absorbance at 420 nm for the reduction of HC-FeIII in deaerated aqueous solutions containing 5×10^{-4} M sodium thiosulfate and 5×10^{-4} M potassium hexacyanoferrate in the presence of 15 nm or 30 nm Au-NPs@citrate in the dark or under LEDs irradiation at 520 nm.

III-2- Irradiation using a Xe lamp equipped with a 450 nm optical cutoff filter

Similar experiments were performed using a Xe lamp with a 450 nm optical cutoff filter instead of using the LEDs at 520 nm. Under these conditions, in addition to the disappearance of the absorption bands at 310 and 420 nm due to HC-FeIII, changes in the LSPR band of the Au-NPs@citrate are observed (Figure IV-5). For 15 nm Au-NPs@citrate, the LPSR band around 530 nm totally disappears simultaneously as the bands of HC-FeIII (Figure. VI-5a) while for 30 nm Au-NPs@citrate, the LSPR band around 530 nm decreases partially and a new broad band with a maximum around 750 nm appears (Figure. IV-5b). These results indicate that during the reduction reaction upon Xe lamp irradiation the morphology of the Au-NPs@citrate changes dramatically, what is confirmed by TEM images (Figures IV-6 and IV-7).

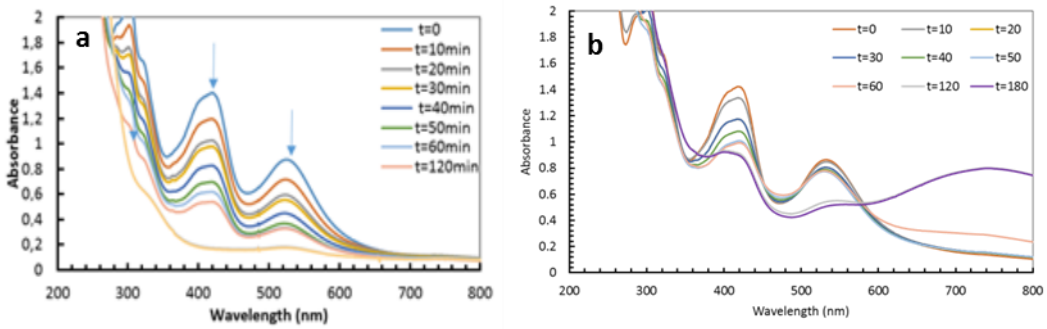

Figure IV-5. Temporal evolution of the UV-visible spectra of deaerated aqueous solutions containing 10^{-3} M sodium thiosulfate and 10^{-3} M potassium hexacyanoferrate under Xe lamp irradiation (equipped with an optical cutoff filter at 450 nm) (**a**) in the presence of 15 nm Au-NPs@citrate and (**b**) 30 nm Au-NPs@citrate. Optical path length: 1 cm.

Figures IV-6 and IV-7 show TEM images of the Au-NPs present at different times during the reduction reaction under Xe lamp irradiation. The TEM images show that Au-NPs reshape with irradiation time: They become more elongated and assemble in necklaces. This reshaping might be due to heating of the Au-NPs by plasmon excitation and to reactions (which are probably catalyzed by the plasmon) at the surface of nanoparticles leading to deligandation of the citrate ions and to chemical complexation of Au with cyanide. These phenomena depend on the initial size of the Au-NPs. Indeed, in the case of the initial 15 nm Au-NPs@citrate, the UV-visible spectra do not exhibit a new plasmon band, which could correspond to elongated nanoparticles or their assembly, in contrast to what is observed for 30 nm Au-NPs@citrate.

This suggests that for the initial smallest 15 nm Au-NPs@citrate, assembly and precipitation of the elongated Au-NPs take place rapidly in seconds or minutes (at the scale of the record of the spectra), while for the initial 30 nm Au-NPs@citrate, oblate NPs and smaller aggregates are formed and remain in suspension.

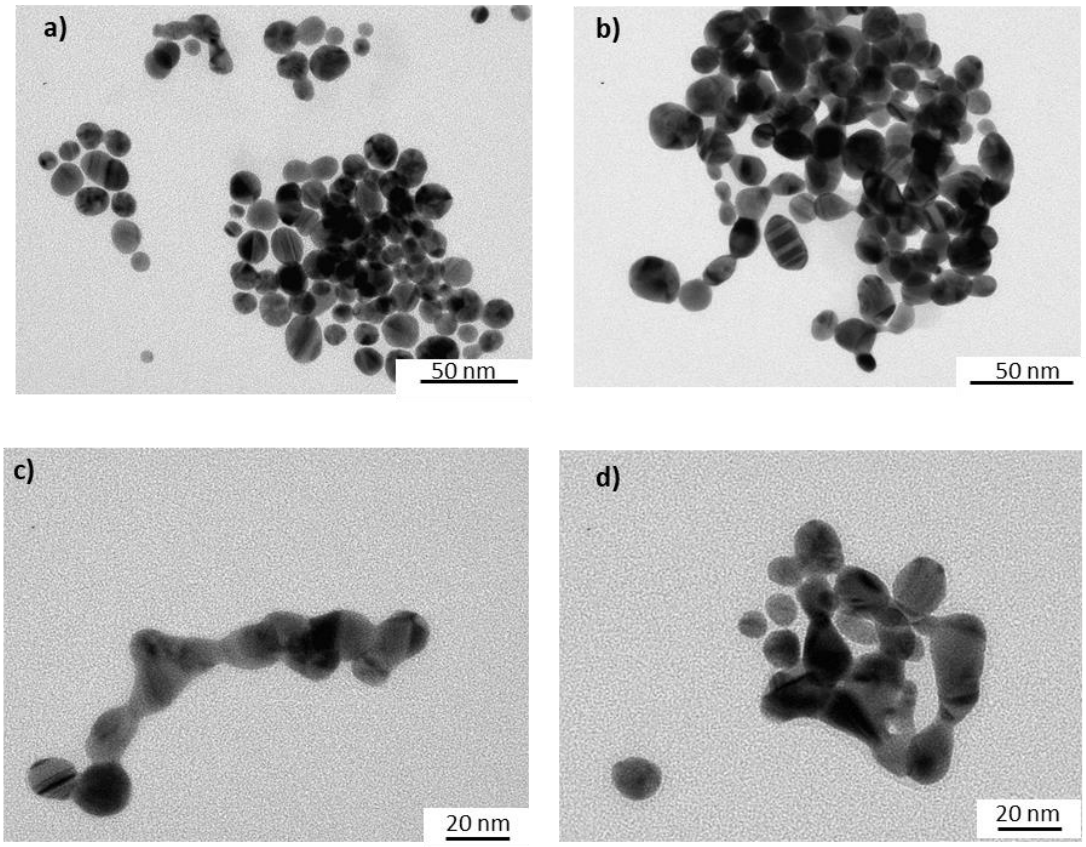

Figure IV-6. TEM images of the initial 15 nm Au-NPs@citrate taken at different times during the reduction reaction of hexacyanoferrate (III) by sodium thiosulfate under irradiation with a Xe lamp equipped with a cutoff filter at 450 nm: (**a**) before irradiation, after (**b**) 30 minutes, (**c**) 120 minutes, and (**d**) 180 minutes of irradiation.

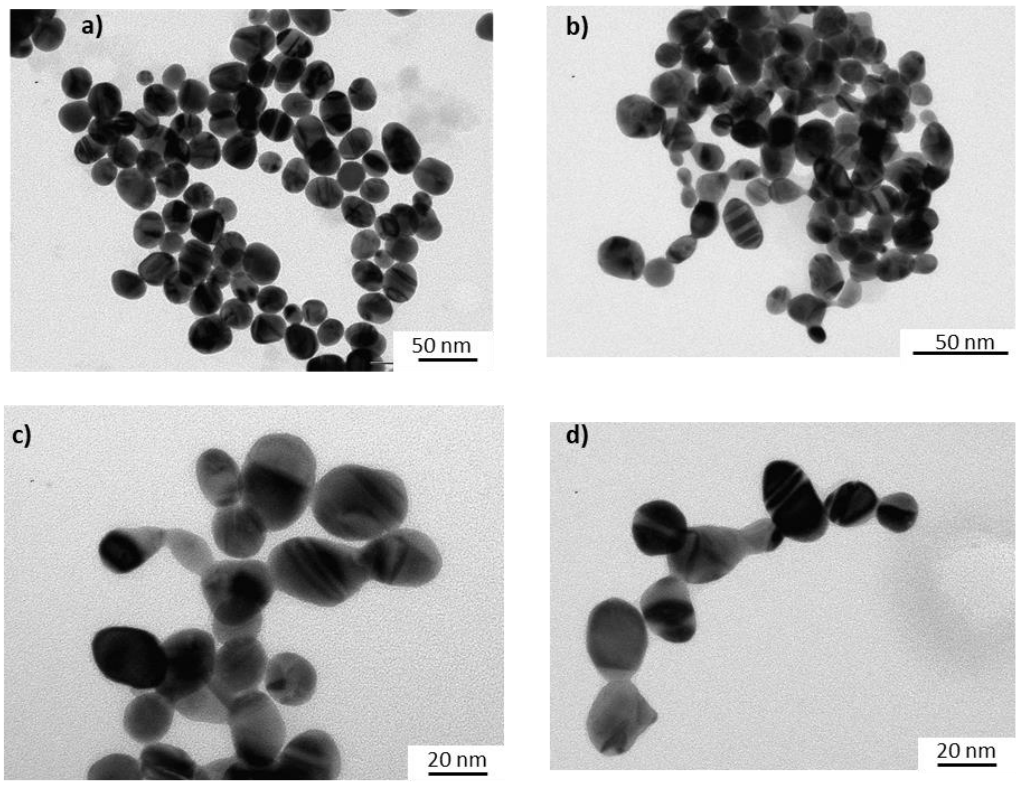

Figure IV-7. TEM images of initial 30 nm Au-NPs@citrate taken at different times of irradiation during the reduction reaction of hexacyanoferrate (III) by sodium thiosulfate under irradiation with a Xe lamp equipped with a cutoff filter at 450 nm: (**a**) before irradiation, and after (**b**) 30 minutes, (**c**) 120 minutes, and (**d**) 180 minutes of irradiation.

IV- Reduction of hexacyanoferrate in the absence of sodium thiosulfate

IV-1- Irradiation using LEDs at λ = 520 nm

Irradiation of solutions containing HC-FeIII and Au-NPs@citrate, but without ST leads to a decrease in the absorption bands at 310 and 420 nm associated to HC-FeIII as well as a decrease in the LSPR of the Au-NPs around 520 nm (Figure IV-8). However, that evolution is very slow compared to the changes observed in the presence of ST under Xe lamp irradiation: While the total reduction of HC-FeIII occurs in less than 1 hour with ST (Figure IV-4), hardly anything happens for 2 hours without ST (Figure IV-9). However, the decrease in absorbance is faster for the 15 nm Au-NPs@citrate than for 30 nm Au-Nps@citrate (Figure IV-9). It is to note that in the dark a tiny decrease in absorbance is observed indicating the absence of reaction and the stability of the solution without irradiation (Figure IV-10).

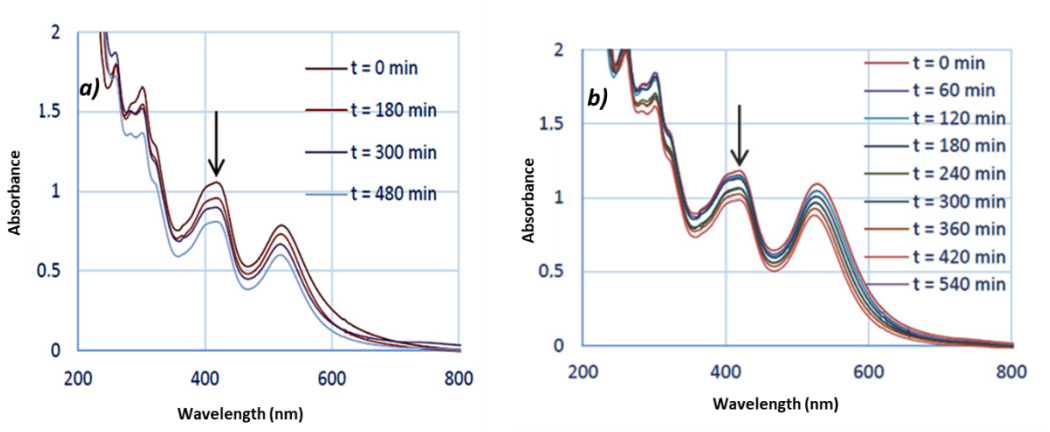

Figure IV-8. Spectral evolution with time of deaerated aqueous solutions containing 5×10^{-4} M potassium hexacyanoferrate under LEDs irradiation at 520 nm) in the presence of (**a** 15 nm Au-NPs@citrate and (**b**) 30 nm Au-NPs@citrate. Optical path length: 1 cm.

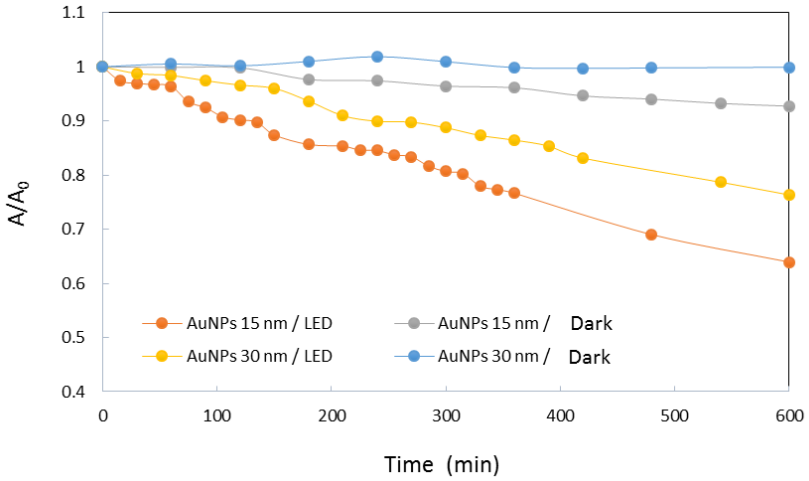

Figure IV-9. Kinetic traces of the normalized absorbance at 420 nm of deaerated aqueous solutions containing initially 10^{-3} M potassium hexacyanoferrate in the presence of 15 nm or 30 nm Au-NPs@citrate and in the dark or under LEDs irradiation at 520 nm.

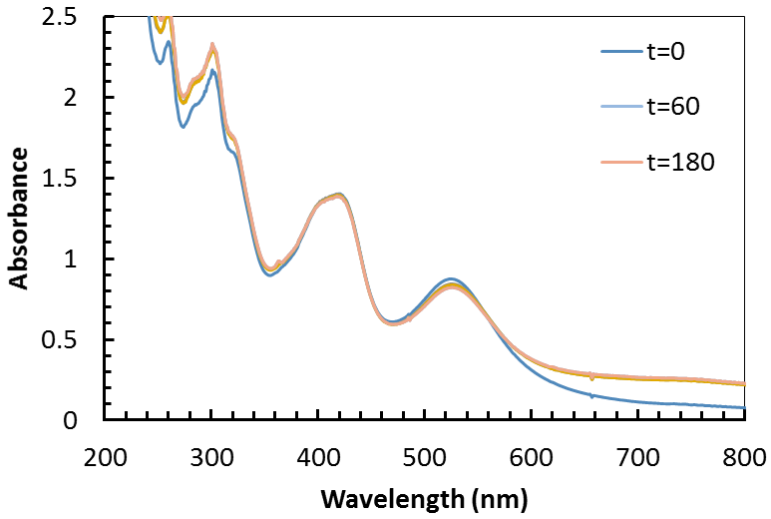

Figure IV-10. Temporal evolution of the absorption spectra of a solution containing 15 nm Au-NPs@citrate and 10^{-3} M potassium hexacyanoferrate III with no irradiation (in dark) for 180 minutes.

The absorbance changes observed under irradiation indicate that reactions occur, which are related to the reduction of HC-FeIII. We show here that this reduction takes place even without a reducing agent such as thiosulfate or borohydrate. In the presence of TS, the reaction is faster and TS plays a role of electron relay. Without TS, the reduction reaction is probably due to hot electrons produced by plasmon excitation or by the reaction with citrate, which can be favored because of the temperature increase on the Au-NP surface subsequent to plasmon excitation. The involvement of citrate ions in the reduction reaction would lead to a loss of stabilizing agents for the Au-NPs, hence the observed change in the LSPR band.

IV-2- Irradiation using a Xe lamp equipped with a 450 nm optical cutoff filter

Figure IV-11 presents the spectral evolution of a deaerated solution containing HC-FeIII and 15 nm Au-NPs@citrate under irradiation by a Xe lamp with a longpass filter at 450 nm. As in the case of the LED irradiation (Figure IV-8), a decrease in the absorbance of the bands at 310, 420 and 520 nm is observed, but this decrease is much faster since after 3 hours, the bands are almost vanished. However, comparison between Figures IV-8a and IV-11 indicates that the presence of ST accelerates the spectral evolution recorded under Xe lamp irradiation and consequently the reaction. But even without ST, reshaping and precipitation due to aggregation of Au-NPs@citrate proceed.

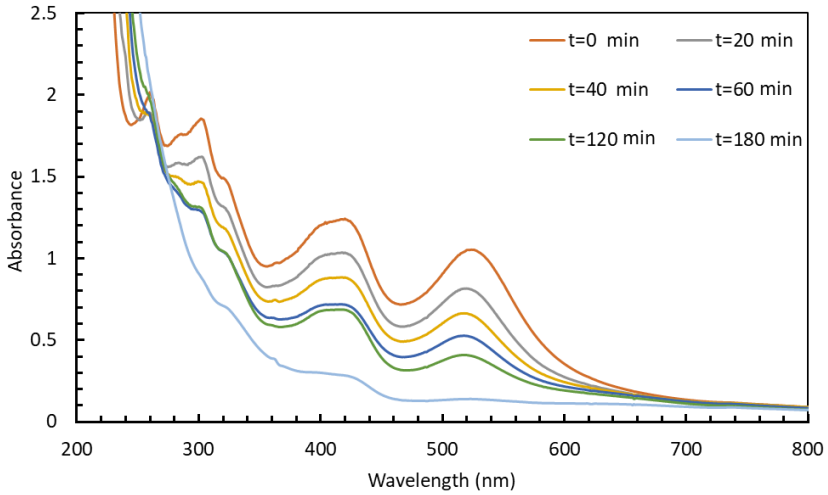

Figure IV-11. Temporal evolution of the absorption spectra of a deaerated aqueous solution containing 5×10^{-4} M potassium hexacyanoferrate in the presence of 15 nm Au-NPs@citrate under Xe lamp irradiation (equipped with an optical cutoff filter at 450 nm). Optical path length: 1 cm.

IV-3- Effect of stabilizing agent of the Au-NPs

In the light of the results presented above, we repeated the experiments using Au-NPs stabilized by a non-reducing agent, and so we replaced citrate by *para*-nitrothiophenol (pNTP) since thiol based compounds are known to be used as stabilizing agents of gold nanoparticles, due to the strong affinity between sulfur and gold atoms. However, it is to keep in mind that during the reaction, the stabilizing agent (pNTP) could also transform [35], and lead to the formation of *para*-aminothiophenol (pATP), but without significant change in the stabilization of the Au-NPs [32, 36].

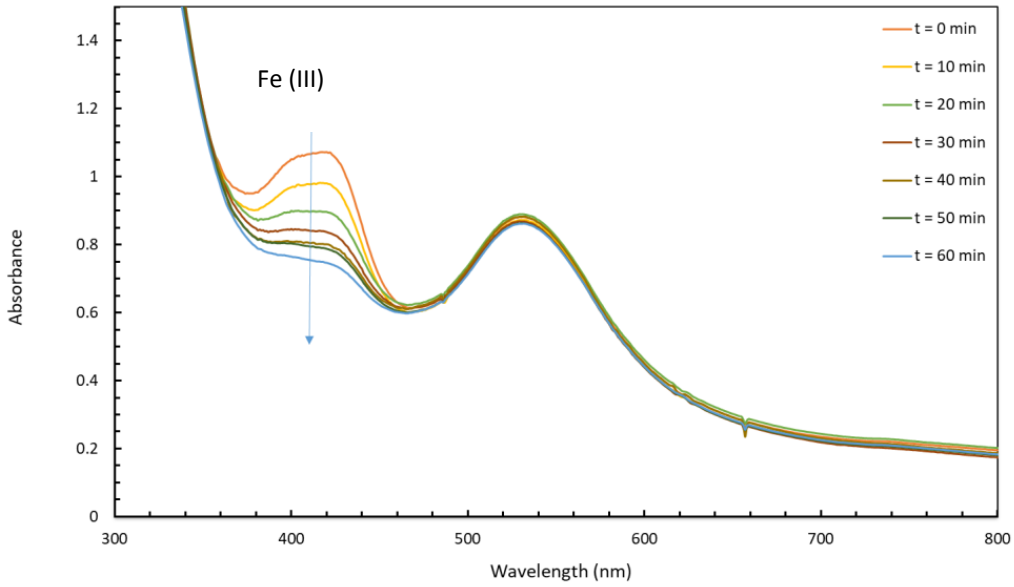

Figure IV-12. Spectral evolution with time of deaerated aqueous solutions containing 10^{-3} M potassium hexacyanoferrate in the presence of 15 nm Au-NPs@pNTP under LEDs irradiation at 520 nm (Optical path length: 1 cm).

Figure IV-12 shows the temporal evolution of the UV-visible spectrum of a deaerated solution containing 15 nm Au-NPs@pNTP and HC-FeIII under LEDs irradiation at 520 nm. In that case, while the band at 420 nm due to HC-FeIII drops, no change is observed in the LSPR band of the Au-NPs. That indicates that the 15 nm Au-NPs@pNTP are stable during the reaction under irradiation, what is confirmed by TEM images (Figure IV-13). It is also worth to notice that the disappearance of the absorption band due to Hc-FeIII is quite rapid, nearly as fast as in the presence of ST (Figure IV-3). That proves that, even without a reducing agent such as ST, reduction of HC-FeIII occurs via plasmon excitation of Au-NPs, and consequently hot electrons are involved.

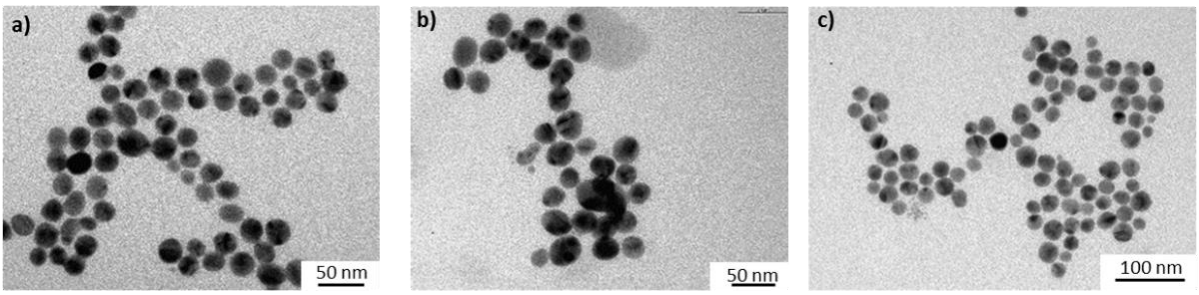

Figure IV-13. TEM images of initial 15 nm Au-NPs@pNTP taken at different times during the reduction reaction of hexacyanoferrate (III) under LEDs irradiation at 520 nm: (**a**) 10 minutes, (**b**) 30 minutes, and (**c**) 60 minutes of irradiation.

V- Discussion

The previous results show the disappearance of HC-FeIII catalyzed by Au-NPs under irradiation in the presence, or not of ST. This disappearance is attributed to the reduction of HC-FeIII. To confirm the reaction and to have some insights into the role played by Au-NPs, X-ray photoelectron spectroscopy XPS analysis were carried out to determine the oxidation states of iron and gold. The XPS wide-scan spectra of 30 nm Au-NPs@citrate after reaction under LEDs irradiation at 520 nm for deaerated solutions containing HC-FeIII with ST or without ST (Figure IV-14) show the presence of gold, iron, carbon, nitrogen, oxygen, potassium and sodium.

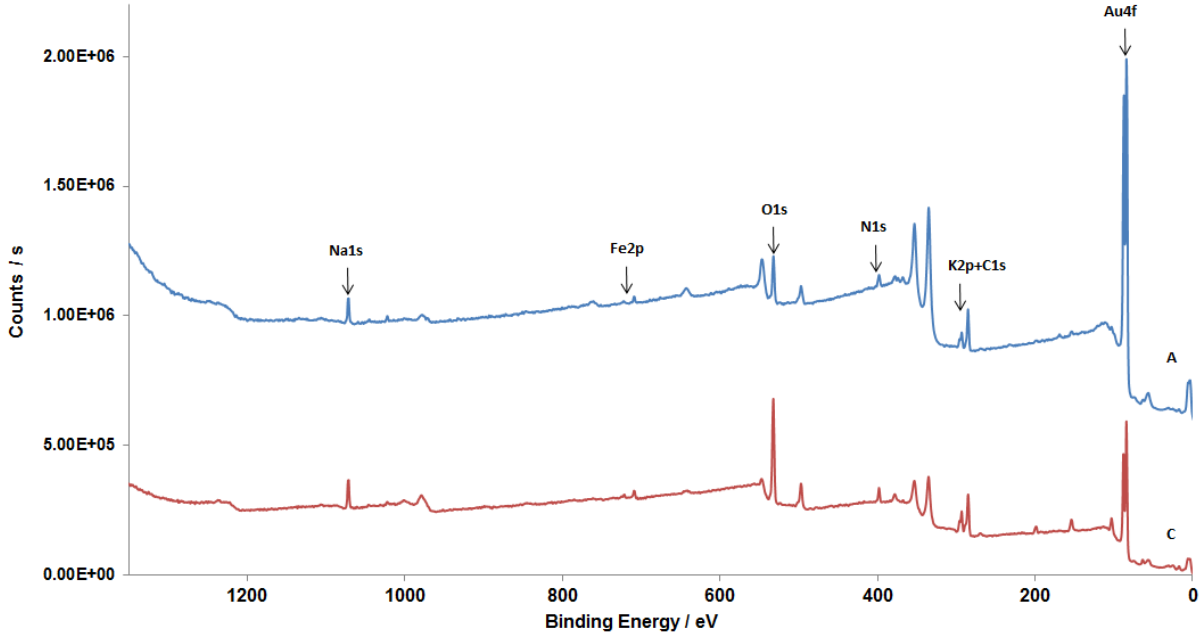

Figure IV-14. XPS wide-scan spectra of 30 nm Au-NPs@citrate after reaction under LEDs irradiation at 520 nm for deaerated solutions containing HC-FeIII with ST or without ST.

Oxygen and carbon are due to citrate ions at the surface of the Au-NPs; Sodium can be related to sodium citrate but also to sodium thiosulfate when present, and potassium and nitrogen comes from potassium hexacyanoferrate. Figure IV-15 presents the XPS spectra recorded for the Au4f, Fe2p and N1s regions.

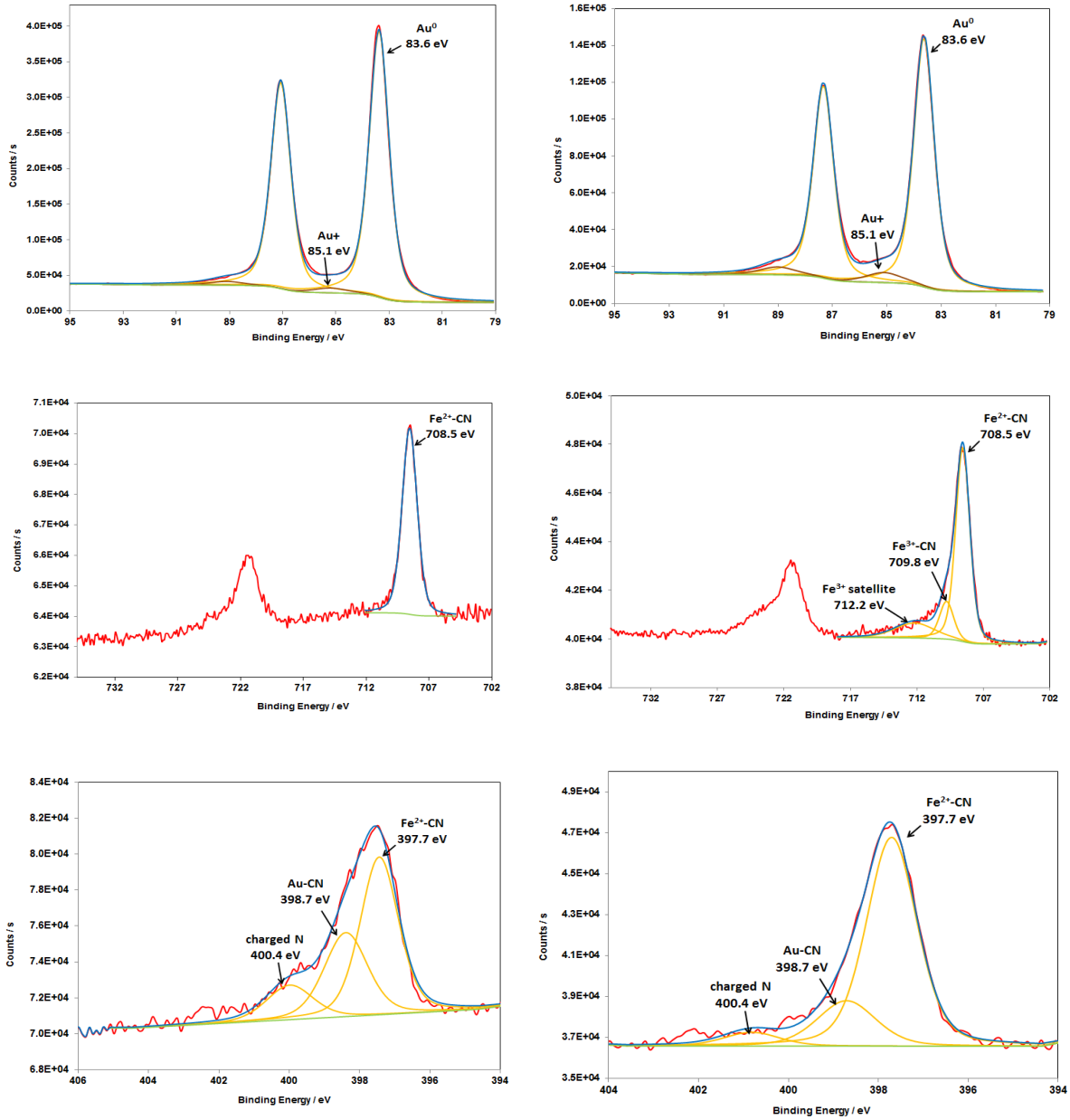

Figure IV-15. XPS spectra of Au4f (top), Fe2p (middle) and N1s (bottom) core levels of 30 nm-Au-NPs@citrate after reaction after reaction under LEDs irradiation at 520 nm (during 60-minutes) for deaerated solutions containing hexacyanoferrate with (left) or without (right) sodium thiosulfate.

The main Au4f signals appear as a doublet separated by 3.7 eV with $Au4f_{7/2}$ and $Au4f_{5/2}$ peaks at 83.6 and 87.3 eV, respectively.[37], what are characteristic values of binding energies for metallic Au atoms (Figure IV-15 top). In the case of the sample without ST, a second doublet is identified at 85.1eV and 89.0 eV (Figure IV-15 top-right) which can be attributed to Au-CN bounds [38,39] rather than to Au-citrate [39-41]. This assumption is supported by the presence of a contribution at 398.7 eV in the N1s spectrum (Figure IV-15 bottom-right), which has an

area equivalent to that of Au^{+} in Au4f [38]. This component at 85.1 eV is also present in the Au4f core-level spectrum of the sample with ST (Figure IV-15 top-left) but to a lesser extent, proving that Au is more protected from oxidation when ST is present.

Investigations of Fe2p core-level spectra corroborate further the effect of ST. A complete reduction of Fe^{III} into Fe^{II} is observed in the presence of thiosulfate (Figure IV-15 middle-left), while in the absence of thiosulfate, only 84% of Fe^{III} has been reduced (Figure IV-15 middle right). In Figure IV-15 middle-left, Fe^{II} is easily identified by the presence of a single doublet located at 708.5 ($Fe2p_{3/2}$) and 721.5 eV ($Fe2p_{1/2}$), typical values for $K_3[Fe(CN_6)]$ [42]. This result confirms the hypothesis that, in the presence of ST, at the end of the reaction (after LEDs irradiation for 60 min), there is a complete reduction of Fe^{III} into Fe^{II} in the present experimental conditions. The presence of a second doublet at 709.8 and 723.7 eV in the spectrum of the sample without ST (Figure IV-15 middle right) is indicative of Fe^{III} [27,43].

The N1s core-level spectrum was decomposed into three contributions, one corresponding to nitrogene in CN bridges, at 397.7 eV, a second contribution at 398.6 eV, which can be attributed to AuCN [29] and a small contribution at 400.4 eV corresponding to charged nitrogen.

The components attributed to AuCN (in the sample with or without ST) shows that the reaction takes place at the surface of Au-NPs@citrate, leading to an oxidation of Au atoms and ligation of Au-NPs@citrate to CN^{-}. This might account for the small changes observed in the LSPR of Au-NPs@citrate in presence of ST and the decrease in LSPR band in the absence of ST, oxidation being more effective in that case. Indeed, it is well-known that cyanides are used to extract gold from mines by its oxidation and complexation [44], as CN^{-} has a great ability to complex with Au and form a stable complex $Au(CN)_2^{-}$. In TEM images, observation of small clusters of Au indicate this partial dissolution. Similar dissolution by cyanide ions has already been invoked in the case of size reduction and reshaping of Pt NPs used as catalysts for electron transfer reaction between hexacyanoferrate and thiosulfate [20, 25].

To summarize XPS discussion, in the presence of ST Au is much less oxidized than in the absence of ST, because in the former case Au-NPs@citrate work mainly as catalysts in the electron transfer from thiosulfate to Fe^{III}. When ST is not present, the reduction of Fe^{III} occurs as shown by UV-visible spectra and XPS analysis. This reduction takes place either by hot electrons induced by plasmon excitation of Au-NPs, or by citrate. In the former case, the electrons are mainly transferred from Au NPs to Fe^{III}, leading to Au^{I}, which will probably be

ligated to CN^- present in the solution. The reduction of Fe^{III} may also be partly due to reduction by citrate, which may become possible because of the temperature increase around the Au-NPs@citrate due to the plasmonic photothermal conversion.

VI- Conclusions

Plasmonic catalysis enables to achieve reactions using solar light with less energy and time consumption. The reduction kinetics of ferricyanide (III) ion into ferrocyanide (II) by Au-NPs is enhanced under visible light excitation. This reduction takes place even without sodium thiosulfate and is due to transfer of hot electrons induced by plasmon excitation. The Au-NPs stabilized by citrate reshape during the reaction. However, the shape of the Au-NPs remains stable when they are stabilized by stronger ligands such as *para*-nitrophenol, and the Au-NPs could then be reused in different catalytic cycles.

This study shed some light on the possible direct applications of catalysis assisted by plasmon of gold nanoparticles excited by visible light. The results demonstrate the effectiveness of using colloidal spherical gold nanoparticles to catalyze redox reactions under visible irradiation.

References

1. Krishnendu, S.; Agasti, S.S.; Chaekyu, K.; Xiaoning, L.; Rotello, V.M. Gold nanoparticles in chemical and biological sensing. *Chem. Rev.* **2012**, *112*, 2739-2779.
2. Lang, X.; Chen, X.; Zhao, J. Heterogeneous visible light photocatalysis for selective organic transformations. . *Chem. Soc. Rev.* **2014**, *43*, 473-486.
3. Haruta, M.; Kobayashi, T.; Sano, H.; Yamada, N. Novel Gold Catalysts for the Oxidation of Carbon Monoxide at a Temperature Far Below 0 °C. *Chem. Lett* **1987**, *37*, 1290 - 1291.
4. Zanella, R.; Giorgio, S.; Shin, C.; Henry, C.; Louis, C. Characterization and reactivity in CO oxidation of gold nanoparticles supported on TiO2 prepared by deposition-precipitation with NaOH and urea. *J. Catal.* **2004**, *222*, 357-367.
5. Huang, X.; Neretina, S.; El-Sayed, M. Gold Nanorods: From Synthesis and Properties to Biological and Biomedical Applications. *Adv. Mater.* **2009**, *21*, 4880-4910.
6. Vincenzo; Amendola, e.a. Surface plasmon resonance in gold nanoparticles: a review. . *J Phys Condens Matter.* **2017**, *29*.
7. Zhang, J.; Wang, L.; Ali, S.; Wang, C.; Wang, L.; Meng, X.; Li, B.; Su, D.; Xiao, F. Wet-Chemistry Strong Metal-Support Interactions in Titania-Supported Au Catalysts. *ACS* **2019**, *141*, 2975-2983.
8. Dohyung, K.; Joaquin, R.; Yi, Y.; Asiri, A.M.; Peidong, Y. Synergistic geometric and electronic effects for electrochemical reduction of carbon dioxide using gold–copper bimetallic nanoparticles. . *Nature. Comm.* **2014**, *5*, 4948.
9. Abidi, W.; Selvakannan, P.; Guillet, Y.; Lampre, I.; Beaunier, P.; Pansu, B.; Palpant, B.; Remita, H. One-Pot Radiolytic Synthesis of Gold Nanorods and Their Optical Properties. . *J. Phys. Chem. C* **2010**, *114*.
10. Linic, S.; Christopher, P.; Ingram, D.B. Plasmonic-Metal Nanostructures for Efficient Conversion of Solar to Chemical Energy. *Nat. Mater.* **2011**, *10*, 911-921.
11. Huang, X.; El-Sayed, M.A. Gold nanoparticles: Optical properties and implementations in cancer diagnosis and photothermal therapy. *Journal of Advanced Research* **2010**, *1*, 13-28.
12. Kim, K.; Lee, I.; Lee, S.J. Photocatalytic reduction of 4-nitrobenzenthiol on Au mediated via Ag nanoparticles. . *Chem. Phys. Lett.* **2003**, *377*, 201-204.
13. Hong, S.; Li, X. Optimal Size of Gold Nanoparticles for Surface-Enhanced Raman Spectroscopy under Different Conditions. *Journal of Nanomaterials* **2013**, *2013*, 1-9.
14. Kowalska, E.M., O.O; Abe, R; Ohtani, B. Visible-light-induced photocatalysis through surface plasmon excitation of gold on titania surfaces. *Physical chemistry chemical physics : PCCP* **2010**, *12*, 2344-2355.
15. Méndez-Medrano, M.G.K., E; Lehoux, A; Herissan, A; Ohtani, B; Bahena, D; Briois, V; Colbeau-Justin, C; Rodríguez-López, J.L; Remita, H. Surface Modification of TiO2 with Ag Nanoparticles and CuO Nanoclusters for Application in Photocatalysis. *J. Phys. Chem. C* **2016**, *120*, 5143-5154.
16. Wang, C.; Astruc, D. Nanogold plasmonic photocatalysis for organic synthesis and clean energy conversion. *Chem. Soc. Rev.* **2014**, *43*, 7188-7216.
17. Huang, X.; El-Sayed, M.A.; El-Sayed, I.H.; Qian, W. Cancer cell imaging and photothermal therapy in the near-infrared region by using gold nanorods. . *J. Am. Chem. Soc.* **2006**, *128*, 2115-2120.
18. Loo, C.; Lin, A.; Hirsch, L.; Lee, M.H.; Barton, J.; Halas, N.; West, J.; Drezek, R. Technology in Cancer Research & Treatment. *ISSN* **2004**, *1533-0346*, 33-40.

19. Xiaohua, H.; Ivan, H., El-Sayed. ; Qian., W.; El-Sayed, M.A. Cancer Cell Imaging and Photothermal Therapy in the Near-Infrared Region by Using Gold Nanorods. *J. Am. Chem. Soc.* **2006**, *128*, 2115.
20. Rong, H.; Y, C.W.; Xiaoyong, W.; Gang, L.; Wei, Z.; Longping, W.; Chen., X.; Kie, Z.; Hou, J.G. Facile synthesis of pentacle gold-copper alloy nanocrystals and their plasmonic and catalytic properties. *Nature Comm.* **2014**, 1-10.
21. Labouret, T.; Audibert, J.-F.; Pansu, R.B.; Palpant, B. Plasmon-Assisted Production of Reactive Oxygen Species by Single Gold Nanorods. *Small* **2015**, *11*, 4475-4479, doi:10.1002/smll.201500509.
22. Narayanan, R.; El-Sayed, M.A. Effect of Catalytic Activity on the Metallic Nanoparticle Size Distribution: Electron-Transfer Reaction between Fe(CN)6 and Thiosulfate Ions Catalyzed by PVP−Platinum Nanoparticles. *J. Phys. Chem.* **2003**, *107*, 12416–12424.
23. Yen, C.W.; El-Sayed, M.A. Plasmonic field effect on the hexacyanoferrate (III)-Thiosulfate electron transfer catalytic reaction on gold nanoparticles: Electromagnetic or Thermal? . *J. Phys. Chem. C.* **2009**, *113*, 19585-19590.
24. Carregal-Romero, S.; Perez-Juste, J.; Herves, P.; Liz-Marzan, L.M.; Mulvaney, P. Colloidal gold-catalyzed reduction of ferrocyanate (III) by borohydride ions: a model system for redox catalysis. *Langmuir : the ACS journal of surfaces and colloids* **2010**, *26*, 1271-1277.
25. Narayanan, R.; El-Sayed, M.A. Shape-Dependent Catalytic Activity of Platinum Nanoparticles in Colloidal Solution. *Nano Lett.* **2004**, *4*, 1343–1348.
26. El-Sayed, N.a.M.A. Shape-Dependent Catalytic Activity of Platinum Nanoparticles in Colloidal Solution. *Nano Letters* **2004**, *4 (7)*.
27. Stefaans, J.G.; Erasmus, E. Electronic effects of metal hexacyanoferrates : An XPS and FTIR study. *Mater. Chem. Phys.* **2018**, *203*, 73-81.
28. Radha Narayanan; El-Sayed, M.A. Shape-Dependent Catalytic Activity of Platinum Nanoparticles in Colloidal Solution. *Nano Letters* **2004**, *4 (7)*.
29. Wang, C.; Astruc, D. Photocatalysis for Organic Synthesis and Clean Energy Conversion. *Chem. Soc. Rev* **2014**, *43*, 7188–7216.
30. Remita, H.; Ibrahim, A.; Sarhid, I.; al., E. Plasmonic catalysis for the Suzuki–Miyaura cross-coupling reaction using palladium nanoflowers. *New J. Chem* **2019**, *43*, 4349-4355
31. Turkevich, J.; Stevenson, P.; Hillier, J. A study of the nucleation and growth processes in the synthesis of colloidal gold. *Discuss Faraday Soc.* **1951**, *11*, 55-57.
32. Pluchery, O.; Remita, H.; Schaming, D. Demonstrative experiments about gold nanoparticles and nanofilms: an introduction to nanoscience. *Gold Bulletin* **2013**, *46*, 319-327.
33. Schaming, O.P.H.R.D. Demonstrative experiments about gold nanoparticles and nanofilms: an introduction to nanoscience. *Gold Bulletin* **2013**, *46*, 319-327.
34. Rumble, J.R.L., David R; Bruno, Thomas J. *CRC handbook of chemistry and physics* 2017.
35. Woehrle, G.H.; Brown, L.O.; Hutchison, J.E. Thiol-functionalized, 1.5-nm gold nanoparticles through ligand exchange reactions: scope and mechanism of ligand exchange. *Journal of the American Chemical Society* **2005**, *127*, 2172-2183.
36. Zhao, L.B.; Zhang, M.; Huang, Y.F.; Williams, C.T.; Wu, D.Y.; Ren, B.; Tian, Z.Q. Theoretical Study of Plasmon-Enhanced Surface Catalytic Coupling Reactions of Aromatic Amines and Nitro Compounds. *J. Phys. Chem. Lett.* **2014**, *5*, 1259-1266.
37. Yuan, L.; Wenwu, S.; Aditya, G.; Nitin, C. Morphological evolution of gold nanoparticles on silicon wires and their plasmonics. *RSC Adv.* **2015**, *5*, 49708-49718.
38. Cook, R.; Crathorne, E.A.; Monhemius, A.J.; Perry, D.L. XPS Study of the Adsorption of Gold (I) Cyanide by Carbons. *Hydrometallugy.* **1989**, *22*, 171-182.

39. Park, J.W.; Shumaker-Parry, J.S. Structural Study of Citrate Layers on Gold Nanoparticles : Role of Intermolecular Intercations in Stabilizing Nanoparticles. *J. Am. Chem. Soc.* **2014**, *163*, 1907-1921.

40. ZHuo, C.K.; Huang, X.; Zhang, P.Y. Sub-Two Nanometer Single Crystal Nanowires. *Nano Lett.* **2008**, *8*, 2041-2044.

41. Mikhlin, Y.; Likhatski, M.; Karacharov, A.; Zaikowski, V.; Krylov, A. Formation of gold and gold sulfide nanoparticles and mesosclae intermediate structures in the reactions of aqueous HAuCl4 with sulfide and citrate ions. *Phys. Chem. Chem. Phys.* **2009**, *11*, 5445-5454.

42. Naumkin, A.V.; Kraut-Vass, A.; Gaarenstroom, S.W.; Powell, C.J. NIST X-ray Photoelectron Spectroscopy Database, NIST Standard Reference Database. *National Institute of Standards and Technology (NIST)* **2000**, *20899*.

43. Grosvenor, A.P.; Kobe, B.A.; Biesinger, M.C.; McIntyre, N.S. Investigation of multiplet splitting of Fe 2p XPS spectra and bonding in iron compounds. *Surf. Interf. Anal.* **2004**, *36*, 1564-1574.

44. Wang, J.; Lu, Y.; Xu, Z. Identifying Extraction Technology of Gold from Solid Waste in Terms of Environmental Friendliness. *ACS Sustainable Chemistry & Engineering* **2019**, *7*, 7260-7267.

Chapter V

Plasmonic catalysis for Suzuki-Miyaura cross-coupling reaction using Palladium nanoflowers

Table of content

I- Introduction

Palladium nanostructures have attracted a lot of interest these last decades because of their applications in catalysis and electrocatalysis, in hydrogen storage, in the field of sensors as well as in nanomedicine [1-7]. Pd is used in a large number of industrially important reactions such as hydrogenation of unsaturated organic compounds and a number of C-C coupling reactions. Moreover, Pd nanoparticles (NPs) are efficient catalysts for environmental pollution abatement and automotive emission control [8-10].

C−C coupling reactions are involved in various organic transformations and polymer syntheses [11-13]. C−C bonds forming reactions (such as the Suzuki−Miyaura [14-16], Heck [17-19], and Sonogoshira [20-22] reactions) are catalyzed by transition metals such as palladium. One of the most important chemical reactions for the pharmaceutical and fine-chemical industries is the Suzuki-Miyaura reaction, a C-C cross-coupling reaction between aryl halides and organoboron compounds that has evolved to become a very useful method to produce highly complex molecules [23]. In the early 1990s, Reetz et al. reported the development of palladium clusters stabilized by alkylammonium cations or polymers and their catalytic activity toward the Suzuki-Miyaura reaction, giving moderate to good yields of the products [24]. A few years later, the group of El-Sayed demonstrated that colloidal Pd nanoparticles were efficient catalysts for the Suzuki-Miyaura reaction in aqueous media, confirming that the reaction is carried out at the surface of the nanoparticles, and that it is easy to separate the nanoparticles from the reaction products due to their solubility in water [25] Palladium-catalyzed C−C coupling reactions involve a thermally activated oxidative addition between the transition metal catalyst and the organic substrates. The more electron-rich is the Pd complex, the faster is this oxidative addition. Very recently, some studies have shown that this charge transfer can be activated by light via a photocatalytic process, allowing a number of different organic transformations [26-28]. A study of light-activated Suzuki-Miyaura reactions mediated by Pd-nanodots stabilized on MoS_2 semiconductor nanosheets led to the observation of very high turnover frequencies, demonstrating the efficiency of the photocatalytic process. Mechanistic studies of this reaction suggested that an efficient electron-hole pair generation in MoS_2 occurs [29]. Pd nanoparticles on semiconducting $(2H)WS_2$ nanosheets, under visible light, have also been shown to catalyze Suzuki-Miyaura reactions at room temperature in protic organic solvents, giving very high yields. Mechanistic studies have shown that the photoexcited electrons produced in the reaction are transferred from the $(2H)WS_2$ nanosheets to palladium nanoparticles, while the photogenerated holes are

transferred to the protic organic solvents, thereby increasing the electron density of the palladium and favoring the oxidative addition of the aryl halide [30]. The plasmonic properties of metal nanostructures can also be used to activate or induce catalytic reactions [31]. Small spherical Pd nanoparticles are known to exhibit a plasmon absorption band in the UV range. Moreover, it has been shown that Pd nanodiscs exhibit broad, localized surface plasmon resonance bands with a higher sensitivity to the disc ratio than those of Ag nanodiscs [32]. Trinh et al. demonstrated direct plasmonic harvesting of visible to NIR light energy using Pd nanoplates (with well-defined and tunable longitudinal surface plasmon resonance (LSPR) peak) in a Suzuki coupling reaction between iodobenzene and phenylboronic acid [33] The authors found that the catalytic activity of the Pd nanoplates was 2.5 and 2.7 times higher than that of Pd octahedrons and cubes, respectively, under illumination. By calculating the increase in temperature of the hot electrons in the Pd nanoplates, it has been shown that the enhanced catalytic activity of the Pd nanoplates was mainly a result of the plasmonic photocatalytic effect by plasmon induced hot electrons. A recent review summarizes the advances in heterogeneous photocatalyzed C-C cross-coupling reactions under visible and near-infrared light irradiation [34].

Here, we have synthesized Pd nanoflowers formed by connected nanosheets displaying a broad absorption plasmon band in the visible and near-IR range [35,36]. We study the application of the plasmonic properties of these palladium nanoflowers under visible light irradiation in Suzuki-Miyaura cross-coupling reactions

II- Pd nanoflowers as catalysts

Pd nanoflowers were synthesized by radiolytic reduction of $Pd^{II}(acac)_2$ in ethanol solution after CO bubbling as detailed in chapter II. Pd^{II} can be reduced by solvated electrons and ethanol radicals induced by solvent radiolysis as well as by CO^- formed by the reaction of CO with solvated electrons [36]. The initially light-yellow solution turned to a dark blue color after irradiation. Figure V-1 shows the UV-visible absorption spectrum of the solution before and after gamma-irradiation. After irradiation, the absorption peak at 326 nm associated to $Pd^{II}(acac)_2$ complex vanishes and a new band appears at 275 nm (associated to free acetylacetone). While small spherical palladium nanoparticles exhibit a plasmon resonance band in the UV range, in our case, a broad plasmon band in the 400–1200 nm region is observed. Pd nanodisks and nanosheets are known to exhibit broad absorption bands in the visible and near infrared regions [36,37].

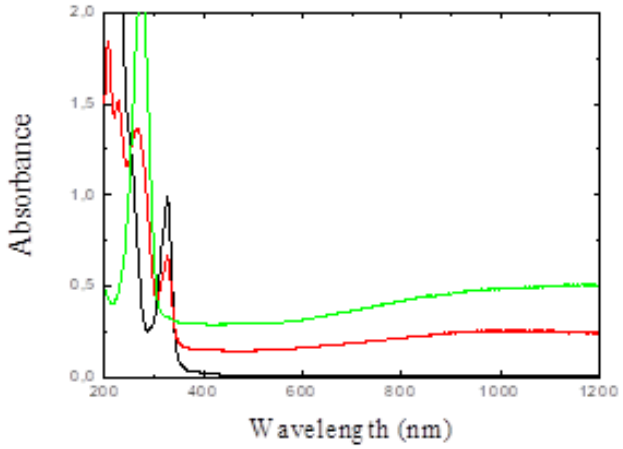

Figure V-1. Absorption spectrum of an ethanol solution containing 10^{-3} mol L^{-1} of $Pd(acac)_2$ under 1 atm of CO for different gamma-irradiation doses: Black line: 0 kGy, red: 2 kGy, green 3 kGy. Dose rate 3 kGy h^{-1}. Optical path = 1 mm.

The TEM images show flower like nanostructures (150 nm). These nanostructures synthesized by radiolysis are formed by very thin Pd nanosheets (petals) with truncated hexagonal shapes (30-50 nm sheet dimensions) (Figure V-2). Most of the sheets originate from a seed and form a flower-like structure. These sheets are very thin so sometimes the borders are rolled. The selected area electron diffraction (SAED) (Figure V-2a inset) can be fully indexed in the cubic system of Pd. A SAED pattern on only one sheet (Figure V-2b inset) shows clearly their good crystallinity. This result indicates the total reduction of the $Pd(acac)_2$ complex. Complete characterization of these nanostuctures has been reported previously [35].

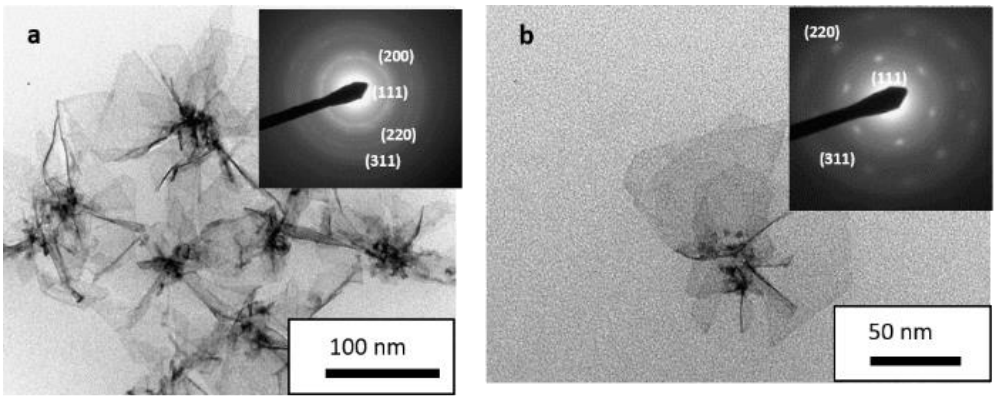

Figure V-2. TEM images of the synthesized Pd nanoflowers; In inset: their electron diffraction patterns.

Previous studies show that CO plays an important role in defining the morphology of the nanosheets and the nanoflowers and intermediate unstable palladium carbonyl clusters are probably involved in the nucleation/growth process [35, 36].

The XPS spectrum of Pd nanoflowers exhibit two main asymmetric peaks at 335 and 340.2 eV (Figure V-3). This double feature, separated by 5.2 eV, is specific to the $3d_{5/2} - 3d_{3/2}$ spin-orbit splitting of Pd3d core shell. The component $Pd3d_{3/2}$ has a more pronounced asymmetry due to the interference coming from the $Pd3d_{5/2}$ plasmon loss peak, at around 342 eV [38,39] The peak positions, aligned following the aliphatic component of C1s set at 284.8 eV, together with their asymmetry and the presence of the plasmon loss peak confirms the metallic nature of Pd.

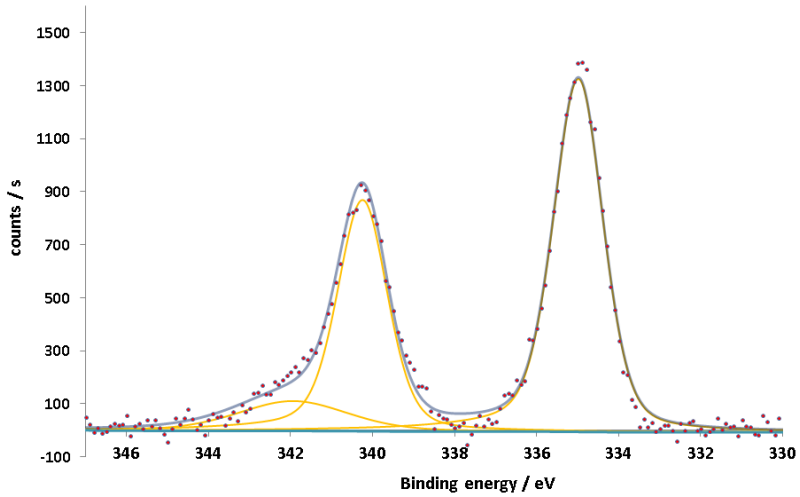

Figure V-3. XPS signals of the Pd3d core levels in the Pd nanoflowers.

It is to note that the generated Pd nanostructures are stable in ethanol solution for few days in the dark and for few hours under light irradiation.

III- Catalytic study of the Suzuki-Miyaura cross coupling reactions

III-1- Experimental details

For the catalytic reaction, a Schlenk tube equipped with a magnetic stirring bar was charged with haloarene (0.54 mmol), boronic acid (0.6 mmol), base (1 mmol) and 4 mL of ethanol solution containing 0.43 mg of palladium nano-sheets. The flask was evacuated and backfilled with argon three times. The reaction mixture was irradiated under stirring with a

300 W Xe lamp equipped with a water cell filter to absorb the near-IR radiation and a 475 nm cut-off filter to avoid direct photoactivation of the aromatic compounds. The mixture was then filtered and analyzed by gas chromatography (GC) or gas chromatography coupled with mass spectrometry (GC-MS).

III-2- Reaction between iodobenzene and phenylboric acid

These Pd nanoflowers exhibiting absorption plasmon in the visible range in ethanol solutions were used as catalysts in Suzuki-Miyaura cross coupling reaction between iodobenzene and phenylboronic acid using Cs_2CO_3 as base (Scheme V-1).

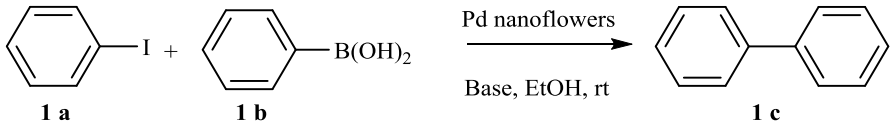

Scheme V-1. Reaction between iodobenzene (1a) and phenyl boric acid (1b) catalyzed by Pd nanoflowers.

The reaction was performed under argon atmosphere, at room temperature, either in the dark or under visible light irradiation (λ>475 nm). The formation of biphenyl was monitored by GC over a period of 240 min (Figure V-4).

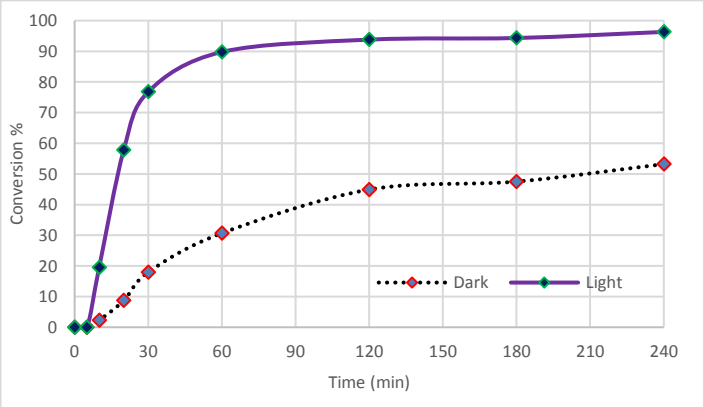

Figure V-4. Catalytic activity of palladium nanoflowers in the dark and under visible light irradiation (λ>475 nm) for the Suzuki-Miyaura coupling reaction. Reaction conditions: iodobenzene (0.54 mmol), phenylboronic acid (0.6 mmol), Cs_2CO_3 (1 mmol) and 4 mL of a 10^{-3} M solution of Pd (0.43 mg) in ethanol. The conversions were calculated from the product content relative to iodobenzene measured by gas chromatography (GC).

After 5 min of latency, light irradiation induces an increase both in the reaction rate and in the conversion. The kinetics of the reaction was much faster and the conversion rate observed for this reaction was dramatically higher under irradiation compared to that carried out in the dark. After 20 min of reaction 57% conversion was observed under irradiation, and only 9% in the dark. The reaction continued to proceed quickly under light illumination to reach 90% conversion at 60 min and 96 % after 240 min, while the reaction in the dark went on slowly up to 53% conversion at 240 min. These results confirm that photocatalysis is indeed taking place. Pd nanoflowers are absorbing in the visible region as shown in Figure 1. The excitation of the plasmon resonance can be converted into heat and hot electrons can be induced on the surface of the nanostructures. These two effects may also be reinforced by the formation of "hot spots", where the electric fields are concentrated. This is likely to accelerate the initial oxidative addition reactions and the subsequent steps of the Suzuki-Miyaura reaction as well, (i.e. the transmetallation and the reductive elimination reactions).

Under similar conditions as those described above, the reaction was carried out using other bases: K_3PO_4, KOH and K_2CO_3 (Figure V-5).

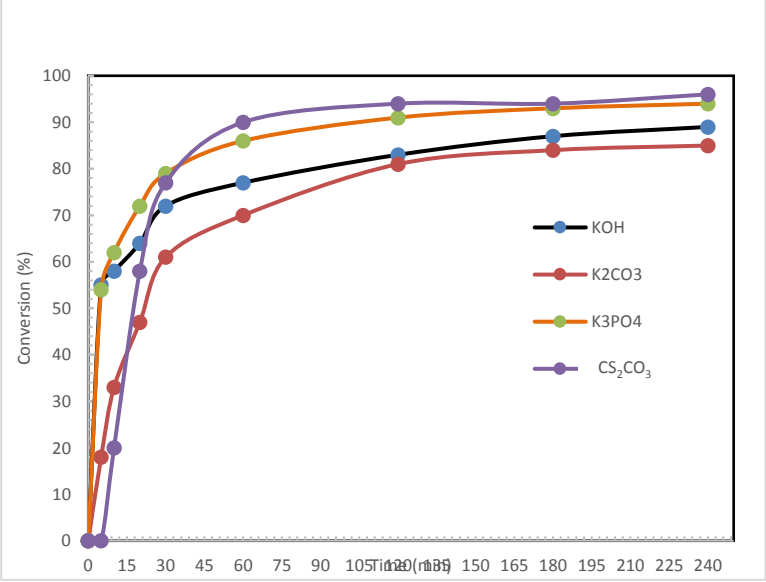

Figure V- 5. Bases effect on the photocatalytic activity of palladium nanoflowers under visible irradiation (λ> 475 nm) on the Suzuki-Miyaura coupling reaction. Reaction conditions: iodobenzene (0.54 mmol), phenylboronic acid (0.6 mmol), base (1 mmol) and 4 mL of a 10^{-3} M solution of Pd (0.43 mg) in ethanol. The conversions were calculated from the product content relative to iodobenzene measured by gas chromatography (GC).

In contrast to Cs_2CO_3, no induction time at the beginning of the reaction is observed by using the other bases. With KOH and K_3PO_4, the reaction initiated very quickly. Over 54% conversion was noted after 5 min. The reaction with K_2CO_3 is the slowest (only 47% conversion after 15 min), and the least efficient with a maximum conversion of 85%. The reactions reach maximum conversions of 89% for KOH and 94% K_3PO_4 after 240 min. To conclude, the best bases for this reaction were found to be Cs_2CO_3 and K_3PO_4.

III-3- Reactions between other haloarenes and phenylboric acid

In order to confirm that the reaction is a true cross-coupling reaction and not a simple homocoupling, other halogenated compounds were employed, such as 4-iodotoluene, 1-iodo-4-nitrobenzene and 1-bromo-4-nitrobenzene. The reactions were carried out under the same conditions, with light irradiation for 240 min and using K_3PO_4 as base (Scheme V-2).

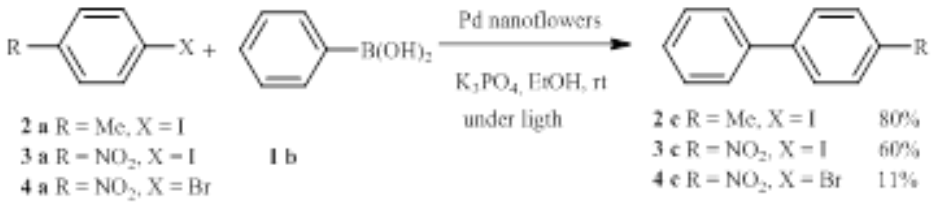

Scheme V-2. Scope of the reaction catalyzed by Pd nanoflowers.

In these reactions only cross-coupling products were observed. The conversion was very good (80%) in the case of 4-iodotoluene, while, surprisingly, the conversion was lower with the very activated 1-iodo-4-nitrobenzene (60% of conversion), and very low with 1-bromo-4-nitrobenzene (11% of conversion). Irradiation of plasmonic Pd nanostructures induces hot electrons and holes, therefore the Pd nanostructures are charged. So, the adsorption of more polar organic halides is favored, which facilitates the first step of the reaction (the oxidative addition of the aryl halide). This can explain the difference in reactivity with 4-iodotoluene, 1-iodo-4-nitrobenzene and 1-bromo-4-nitrobenzene.

III-4- Proposed mechanism

Wang et al. reported plasmonic Suzuki-Miyaura coupling reactions under light activation (using a laser and under solar irradiation) on Au–Pd nanostructures formed by PdNPs on the surface of Au nanorods [40]. They demonstrated that light was absorbed by the Au cores and PdNPs promoted the Suzuki coupling reactions. Au–Pd nanoalloys supported on ZrO_2 tested

for the Suzuki-Miyaura coupling reaction under visible-light illumination gave high yields of the target products, because the activation energy of Suzuki-Miyaura coupling was reduced [41]. In this reported study, plasmon of gold was used to activate the reaction as Au-Pd spherical nanoparticles absorb in the visible range because of Au plasmon. Light absorption due to the LSPR of gold-based nanoparticles was playing an important role in enhancing the catalyst performance. The enhancement of photocatalytic activity was mainly attributed to hot electrons rather than a thermal effect [41]. Pd NPs decorated Au nanorods (NRs) were also used for Suzuki-Miyaura coupling reaction under light illumination, the excitation of plasmon of Au NRs being used to activate the catalytic reaction [42].

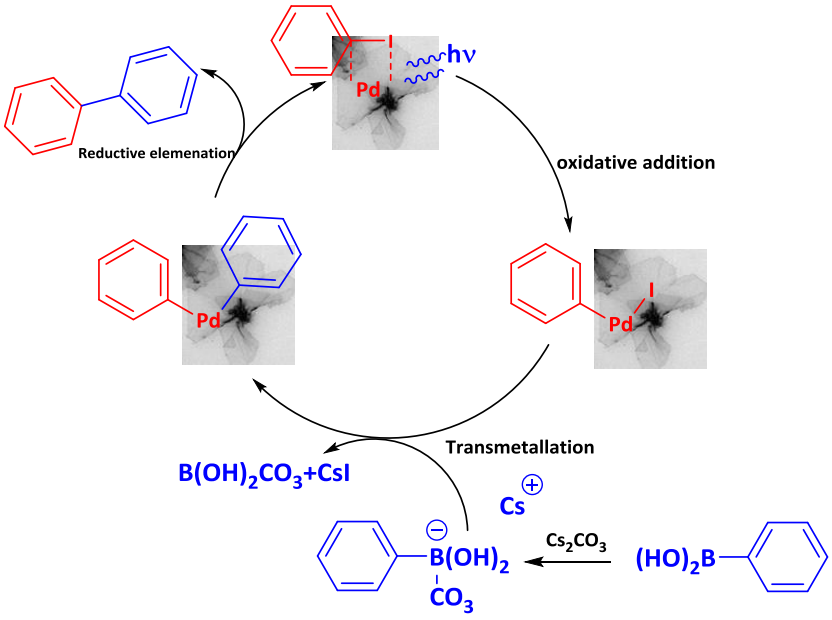

Figure V- 6. Catalytic cycle of Suzuki-Miyaura reaction.

The activation effect of the Suzuki-Miyaura cross-coupling catalyzed by palladium nanosheets can be explained according to the literature [29,41]. The irradiation of the palladium nanosheets generate “hot” electrons, then the electron-rich palladium nanosheets undergo the oxidative addition of aryl halide, followed by transmetallation of in situ formed aryl borate (the boronic acid is transformed after the reaction with base into a borate anion which facilitates the transmetallation). Also, it has been shown that the photogenerated holes in photocatalysts such as g-C_3N_4 or $[Ru(pby)_3]^{2+}$ can activate arylboronic acids by cleaving the C–B bonds or transforming C–B bonds into C–O bonds in the presence of O_2 and H_2O [40, 43]. Finally, reductive elimination generated the biphenyl desired products, which can be

facilitated by “hot” holes. Excitation of plasmon is also converted into heat. The local enhanced temperature on the Pd nanosheets can also be partly responsible of the increase in the reaction kinetics (Figure V-6).

IV- Pd nanoflowers after catalysis

TEM images of the Pd catalysts after 30 minutes of reaction under illumination show evolution of the Pd nanostructures: The nanoflowers and nanosheets are damaged. The cores and the borders resist, but gradually the thinner parts are destroyed to form small Pd nanoparticles (around 4-5 nm) assembled in hexagonal shapes (Figure V-7a and b). Small spherical Pd nanoparticles exhibit a plasmon in the UV and no absorption in the visible range. After 3 h of the catalytic reaction under visible irradiation, no further major change in shape was observed: Small Pd nanoparticles and fragmented sheets are observed in TEM images (Figure V-7c and d). Surprisingly, hexagonal shapes are still observed after 3 h reaction. These Pd nanosheets are probably partly covered by the reaction components during the catalytic reaction, which can contribute in maintaining the initial shape (but in the same time decrease the contrast of part of the nanosheets in TEM observations). This coverage by the reaction component could also contribute in the catalyst poisoning.

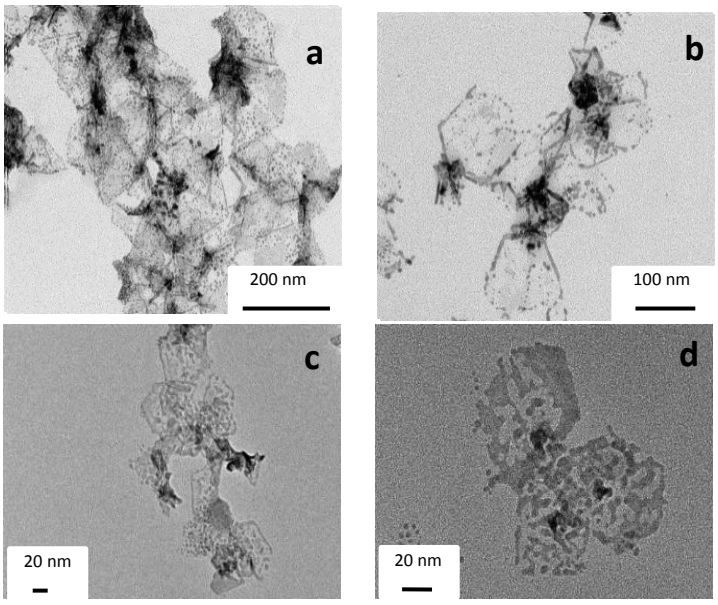

Figure V- 7. TEM images of palladium nanostructures after 30 minutes (a and b) and 3 hours (c and d) of catalytic reaction under visible light showing the evolution of the Pd nanoflowers formed by nanosheets into smaller Pd nanoparticles of few nanometers.

Careful analysis of the conversion rates (Figures V-4 and V-5) shows that the reaction kinetics are fast until about 30 min, then slows down. This behavior can be due to the transformation of Pd nanosheets into small nanoparticles, which cannot be activated under visible light contrary to the Pd nanosheets. Oxidation/reduction of Pd during catalytic cycles can lead to some dissolution or leaching of the Pd during the reaction.

This plasmonic catalysis leads to leaching and reshaping of Pd nanosheets into more thermodynamically stable spherical nanoparticles (Figure V-7). A recent review of Eremin and Ananikov discusses the transformations of molecular catalysts, leaching, aggregation and various interconversions of metal complexes, clusters and nanoparticles that occur during catalytic processes [44]. In the Suzuki-Miyaura cross coupling reactions, a wide range of different Pd species was found in the reaction mixture containing complexes with small and bulky NHC-ligands. Small clusters were detected by MS techniques, and nanoparticles were studied in the precipitate using transmission electron microscopy. There is still a debate in the literature about the question of the true active species in these reactions. It is supposed that very small Pd clusters are more efficient for Suzuki reactions [45-48]. The first step of the Suzuki-Miyaura catalytic cycle corresponds to the addition of the halogene, which induces oxidation of Pd. This oxidation probably leads to partial dissolution (or leaching) of palladium, and this can explain partial reshaping of the Pd nanoflowers.

V- Conclusion

Plasmonic catalysis enables to achieve reactions using solar light with less energy and time consumption. Palladium nanosheets exhibit a broad plasmon absorption band in the visible-near infrared domain. The catalytic activity of Pd nanosheets for Suzuki--Miyaura reactions was remarkably enhanced under visible light irradiation. The reaction was carried out using iodobenzene, phenylboronic acid and Cs_2CO_3 as base, in the dark and under visible light irradiation. Indeed, the results showed that the conversion under light irradiation was 96% versus 53% in the dark. Our finding can be explained by the plasmonic effect, which increases the reactivity of palladium nanostructures. The excitation of the plasmon resonance is converted into heat and hot electrons are induced on Pd surface. To optimize the reaction conditions, different bases were used under light irradiation, the kinetics of the reactions showed that Cs_2CO_3 and K_3PO_4 were efficient bases for this reaction in the presence of palladium nanosheets. Finally, different haloarenes were subjected to the optimized conditions. The highest conversion was obtained with iodotoluene (80%) and surprisingly the

highly activated 1-iodo- or 1-bromo-4-nitrobenzene led to lower conversions. Calculations will be performed to estimate the heat effect induced by plasmon excitation and its contribution on the reaction kinetics. These Pd nanostructures show partial dissolution of Pd and morphological changes during the Suzuki-Miyaura catalytic reaction, and light irradiation induces an enhancement of the kinetics, but could also accelerate Pd dissolution. To enhance the stability of the nanostructures for catalytic applications and increase their turnover frequencies, supporting these nanosheets or modifying them with carbides for example will be tested. These Pd nanoflowers of high surface area could potentially be employed as plasmonic catalysts in other C−C forming reactions, such as Sonogashira, Heck, and Stille reactions. But, studies are still needed to better understand plasmonic palladium-photocatalyzed organic reactions from fundamental and mechanistic points of view in order to design more effective photocatalysts for a larger number of organic reactions.

References

1 Ksar, F.; Sharma, G. K.; Audonnet, F.; Beaunier, P.; Remita, H. Palladium urchin-like nanostructures and their H-2 sorption properties, *Nanotechnology* **2011**, *22*, 305609.

2 Redjala, T.; Remita, H.; Apostolescu, G.; Mostafavi, M.; Thomazeau, C.; Uzio, D. Bimetallic Au-Pd and Ag-Pd clusters synthesised by gamma or electron beam Radiolysis and study of the reactivity/structure relationships in the selective hydrogenation of buta-1,3-diene, *Oil and Gas: Science and Technology* **2006**, *61*, 789-797.

3 Ksar, F.; Surendran, G.; Ramos, L.; Keita, B.; Nadjo, L.; Prouzet, E.; Beaunier, P.; Hagège, A.; Audonnet, F.; Remita, H. Bimetallic Palladium-Gold Nanostructures: Application in Ethanol Oxidation, *Chem. Mater.* **2009**, *21*, 1612-1617.

4 Surendran, G.; Ksar, F.; Ramos, L.; Keita, B.; Nadjo, L.; Prouzet, E.; Beaunier, P.; Dieudonné, Ph.; Audonnet, F.; Remita, H. Palladium nanoballs synthesized in hexagonal mesophases, *J. Phys. Chem. C*. **2008**, *112, 10740-10744*

5 Ghosh, S;. Remita, H.; Kar, P.; Choudhury, S.; Sardar, S.; Beaunier, P.; Roy, P. S.; Bhattacharya, S. K.; Pal, S. K. Facile synthesis of Pd nanostructures in hexagonal mesophases as a promising electrocatalyst for ethanol oxidation, *J. Mater. Chem. A* **2015**, *3*, 9517 – 9527.

6 Ghosh, S.; Teillout, A.-L.; Floresyona, D.; De Oliveira, P.; Hagège, A.; Remita, H. Conducting polymer-supported palladium nanoplates for applications in direct alcohol oxidation *Int. J. Hydrogen Energy* **2015**, *40*, 4951-4959.

7 A. Dumas, P. Couvreur, Palladium: a future key player in the nanomedical field? *Chem. Sci.* **2015**, *6*, 2153-2157.

8 Astruc, D. Palladium nanoparticles as efficient green homogeneous and heterogeneous carbon−carbon coupling precatalysts: A Unifying View. *Inorg. Chem.* **2007**, *46*, 1884-1894.

9 Karimi, B; Abedi, S.; Clark, J.H.; Budarin, V. Highly efficient aerobic oxidation of alcohols using a recoverable catalyst: the role of mesoporous channels of SBA-15 in stabilizing palladium nanoparticles. *Angew. Chem., Int. Ed*, **2006**, *45*, 4776-4779.

10 Kwon, M.S.; Kim, N.; Park, C.M.; Lee, J.S.; Kang K.Y.; Park, Palladium nanoparticles entrapped in aluminum hydroxide: dual catalyst for alkene hydrogenation and aerobic alcohol oxidation. J. *Org. Lett.*, **2005**, *7*, 1077-1079.

11 Schmidt, N. G.; Eger, E.; Kroutil, W. Building Bridges: Biocatalytic C–C-Bond Formation toward Multifunctional Products. *ACS Catal.* **2016**, *6*, 4286−4311.

12 Corrigan, N.; Shanmugam, S.; Xu, J. T.; Boyer, C. Photocatalysis in organic and polymer synthesis. *Chem. Soc. Rev.* **2016**, *45*, 6165−6212.

13 Hussain, I.; Capricho, J.; Yawer, M. A. Synthesis of biaryls *via* ligand-free Suzuki–Miyaura cross-coupling reactions: A review of homogeneous and heterogeneous catalytic develop-ments. *Adv. Synth. Catal.* **2016**, *358*, 3907−3907.

14 Miyaura, N.; Suzuki, A. Palladium-catalyzed cross-coupling reactions of organoboron compounds. *Chem. Rev*. **1995**, *95*, 2457-2483.

15 Suzuki, A. Recent advances in the cross-coupling reactions of organoboron derivatives with organic electrophiles, 1995–1998. *J. Organomet. Chem*. **1999**, *576*, 147-168.

16 Han, F. S. Transition-metal-catalyzed Suzuki–Miyaura cross-coupling reactions: a remarkable advance from palladium to nickel catalysts. *Chem. Soc. Rev*. **2013**, *42*, 5270-5298.

17 de Meijere, A.; Meyer, F. E. Fine Feathers make fine birds: The Heck reaction in modern Garb. *Angew. Chem. Int. Ed.* **1994**, *33*, 2379-2411.

18 Amatore, C.; Jutand, A. Anionic Pd(0) and Pd(II) intermediates in palladium-catalyzed Heck and cross-coupling reactions. *Acc. Chem. Res*. **2000**, *33*, 314-321.

19 Farina, V. High-turnover palladium catalysts in cross-coupling and Heck chemistry: A critical overview. *Adv. Synth. Catal.* **2004**, *346*, 1553-1582.

20 Sonogashira, K. Development of Pd–Cu catalyzed cross-coupling of terminal acetylenes with sp^2-carbon halides. *J. Organomet. Chem*. **2002**, *653*, 46-49.

21 Liang, Y.; Xie, Y. X.; Li, J. H. Modified Palladium-catalyzed Sonogashira cross-coupling reactions under copper-, amine-, and solvent-free conditions. *J. Org. Chem*. **2006**, *71*, 379-381.

22 Chinchilla, R.; Najera, C. The Sonogashira reaction: A booming methodology in synthetic organic chemistry. *Chem. Rev.* **2007**, *107*, 874-922.

23 Maluenda, I.; Navarro, O. Recent developments in the Suzuki-Miyaura reaction: 2010–2014 *Molecules*, **2015**, *20*, 7528-7551.

24 Reetz, M. T.; Breinbauer, R.; Wanninger, K. Suzuki and Heck reactions catalyzed by preformed palladium clusters and palladium. *Tetrahedron. Lett.* **1996**, *37*, 4499-4502.

25 Li, Y.; Hong, X. M.; Collard, D. M.; El-Sayed, M. A. Suzuki cross-coupling reactions catalyzed by palladium nanoparticles in aqueous solution. *Org. Lett.* **2000**, *2*, 2385-2388.

26 Prier, C. K.; Rankic, D. A.; MacMillan, D. W. C. Visible light photoredox catalysis with transition metal complexes: applications in organic synthesis. *Chem. Rev.* **2013**, *113*, 5322−5363.

27 Skubi, K. L.; Blum, T. R.; Yoon, T. P. Dual Catalysis Strategies in Photochemical Synthesis. *Chem. Rev*. **2016**, *116*, 10035−10074

28 Karkas, M. D.; Porco, J. A.; Stephenson, C. R. *J. Chem. Rev.* **2016**, *116*, 9683−9747.

29 Shin, H. H; Kang, E.; Park, H.; Han, T.; Lee, C. H.; Lim, D. K. Photochemical approaches to complex chemotypes: Applications in natural product synthesis. *J. Mater. Chem. A* **2017**, *5*, 24965-24971.

30 Raza, F.; Yim, D. B.; Park, J. H.; Kim, H.-I.; Jeon, S.-J.; Kim, J.-H. Structuring Pd nanoparticles on 2H-WS_2 nanosheets induces excellent photocatalytic activity for cross-coupling reactions under visible Llght. *J. Am. Chem. Soc.* **2017**, *139*, 14767–14774.

31 Linic, S.; Aslam, U.; Boerigter, C.; Morabito, M. Photochemical transformations on plasmonic metal nanoparticles. *Nat. Mater.* **2015**, *14*, 567-576.

32 Langhammer, C.; Yuan, Z.; Zoric, I.; Kasemo, B. Plasmonic properties of supported Pt and Pd nanostructures. *Nano Lett.* **2006**, *6*, 833-838.

33 Trinh, T. T., Sato, R.; Sakamoto, M.; Fujiyoshi, Y.; Haruta, M.; Kurata, H.; Teranishi, T. Visible to near-infrared plasmon-enhanced catalytic activity of Pd hexagonal nanoplates for the Suzuki coupling reaction. *Nanoscale*, **2015**, *7*, 12435-12444.

34 Gu, Q.; Jia, Q.; Long, J.; Gao, Z. Heterogeneous photocatalyzed C-C cross-coupling reactions under visible-light and near-infrared light irradiation. *ChemCatChem*, **2019**, *11*, 669-683.

35 Siril, P. F.; Ramos, L.; Beaunier, P.; Archirel, P.; Etcheberry, A.; Remita, H. Synthesis of ultrathin hexagonal palladium nanosheets. *Chem. Mater*. **2009**, *21*, 5170–5175.

36 Redjala, ; Apostolescu, T. G.; Beaunier, P.; Mostafavi, M.; Etcheberry, A.; Uzio, D.; Thomazeau, T.; Remita, H. Palladium nanostructures synthesized by radiolysis or by photoreduction. *New J. Chem.* **2008**, *32*, 1403-1408.

37 Derai, R.; Remita ; Delcourt, M. O. Pulse radiolysis of $(Rh^{I}(CO)_2Cl)_2$ and $(Rh^{II}(CH_3COO)_2)_2$ solutions under CO or N_2 atmosphere. *Radiat. Phys. Chem.* **1991**, *38*, 483-486

38 Militello, M. C.; Simko, S. J. Elemental Palladium by XPS. *Surface Science Spectra*, **1994**, *3*, 387-394.

39 Kibis, L. S.; Titkov, A.I.; Stadnichenko, A. I.; Koscheev, S. V.; Boronin, A. I. X-ray photoelectron spectroscopy study of Pd oxidation by RF discharge in oxygen. *Appl. Surf. Sci.* **2009**, *255*, 9248-9254.

40 Wang, F.; Li, C. H.; Chen, H. J.; Jiang, R. N.; Sun, L. D.; Li, Q.; Wang, J. F.; Yu, J. C.; Yan, C. H. Plasmonic harvesting of light energy for Suzuki coupling reactions. *J. Am. Chem. Soc.* **2013**, *135*, 5588–5601.

41 Sarina, S.; Zhu, H.; Jaatinen, E.; Xiao, Q.; Liu, H.; Jia, J.; Zhao, J. Enhancing catalytic performance of palladium in gold and palladium alloy nanoparticles for organic synthesis reactions through visible light irradiation at ambient temperatures. *J. Am. Chem. Soc*. **2013**, *135*, 5793–5801.

42 Li, X.-H.; Baar, M.; Blechert S.; Antonietti, M. Facilitating room-temperature Suzuki coupling reaction with light: Mott-Schottky photocatalyst for C-C-coupling. *Sci. Rep.* **2013**, *3*, 1743.

43 Zou, Y.-Q.; Chen, J.-R.; Liu, X.-P.; Lu, L.-Q.; Davis, R. L.; Jørgensen K. A.; Xiao, W.-J. Highly efficient aerobic oxidative hydroxylation of arylboronic acids: photoredox catalysis using visible light. *Angew. Chem., Int. Ed.* **2012**, *51*, 784–788.

44 Eremin, D. B.; Ananikov, V. P. Understanding active apecies in catalytic transformations: from molecular catalysis to nanoparticles, leaching, "cocktails" of catalysts and dynamic systems *Coord. Chem. Rev.* **2017**, *346*, 2-19.

45 Lemo, J.; Heuze, K.; Astruc, D. Synthesis and catalytic activity of DAB-dendrimer encapsulated Pd nanoparticles for the Suzuki coupling reaction. *Inorg. Chem. Acta* **2006**, *359*, 4909-4911.

46 Diallo, A. K.; Ornelas, C.; Salmon, L.; Aranzaes, J. R.; Astruc, D. Homeopathic catalytic activity and atom-leaching mechanism in the Miyaura-Suzuki reactions under ambient conditions using precise “Click” dendrimer-stabilized Pd nanoparticles. *Angew. Chem. Int. Ed.* **2007**, *46*, 8644-8648.

47 Ornelas, C.; Diallo, A. K.; Ruiz, J.; Astruc, D. “Click” polymer-supported palladium nanoparticles as highly efficient catalysts for olefin hydrogenation and Suzuki coupling reaction under ambient conditions. *Adv. Synth. Catal.* **2009**, *351*, 2147-2154.

48 Deraedt, C.; Astruc, D. “Homeopathic” Palladium nanoparticle catalysis of cross Carbon–Carbon coupling reactions. *Acc. Chem. Res.* **2014**, *47*, 494-503.

Conclusion and Perspectives

Sunlight is abundant, free and of environmentally friendly nature. Considerable efforts have been made to use sunlight for ‘‘green’’ chemical synthesis and for environmental applications. Gold nanoparticles have attracted increasing attention because of their unique optical and electronic properties and their various applications in catalysis, electronics, photonics, and nanomedicine. Palladium nanoparticles play a crucial role in catalysis and electrocatalysis. Localized surface plasmon resonance (LSPR) effect of nanostructured materials can be used to induce or activate catalytic or photocatalytic reactions under visible light irradiation. The present work deals with plasmonic photocatalysis with gold nanoparticles and palladium nanostructures. Plasmon of Au nanoparticles and Pd nanostructures were used to assist catalytic reactions respectively for environmental applications and Suzuki-Mayaura reactions.

Redox reactions are very important in environmental catalysis. Therefore, for catalysis assisted by plasmon with Au NPs, we have focused our studies on redox reactions of environmental interest (i) degradation of *para*-nitrothiophenol and (ii) reduction of ferricyanide (III) ion into ferrocyanide (II) ion (Chapter III and Chapter IV, respectively). The Au NPs were synthesized by the Turkevitch method.

In chapter III, we show that the degradation mechanism of *para*-nitrothiophenol (pNTP) is complex as several products were detected by mass spectrometry. The presence of *para*-aminothiophenol (pATP) indicates that the surface-catalyzed reduction of *para*-nitrothiophenol in *para*-aminothiophenol takes place and involves hot electrons. However, to clarify the reduction mechanism, experiments should be conducted under inert atmosphere to get rid of possible oxidation reactions with O_2.

The reduction of ferricyanide (III) ion into ferrocyanide (II) ion catalyzed by spherical Au-NPs is described in chapter IV and the results show that this catalysis is enhanced when Au-NPs were excited at their plasmon. This reduction takes place even without sodium thiosulfate, which demonstrates the implication of hot electrons in this reduction. When Au NPs are stabilized by citrate (a weak ligand), they reshape with catalytic cycles. However, their stabilization with a stronger ligand (pNTP) prevents this reshaping; so, stabilization on support should lead to more stable nanoparticles with cycling, and this can open perspectives in catalysis assisted by plasmon.

In chapter V, we have investigated plasmonic catalysis with Pd nanostructures. Indeed, Pd is an efficient catalyst for hydrogenation reactions, environmental pollution abatement and automotive emission control, and C−C coupling reactions. Pd nanoflowers (synthesized by radiolysis) exhibit absorption in the visible and near infrared regions. The photocatalytic activity of Pd nanoflowers for Suzuki-Miuyara reactions is remarkably enhanced under visible light irradiation. The reaction was carried out using iodobenzene, phenylboronic acid and Cs_2CO_3 as base. Different haloarenes were also used and the highest conversion was obtained with iodotoluene. The excitation of the plasmon resonance is converted into heat and hot electrons are generated. The latter are induced on Pd surface, and are involved in the catalytic mechanism. However, these nanostructures are not very stable with cycling and a dissolution of Pd is observed. To enhance the stability of these nanostructures in catalytic cycles and increase their turnover frequencies, these nanoflowers could be deposited on supports or surface modified with carbides for example. These Pd nanoflowers could also be used for other plasmonic catalytic reactions involving C−C coupling, such as Sonogashira, Heck, and Stille reactions.

Preliminary studies were also conducted in collaboration with Catherine Louis team (Laboratoire de Reactivité des Surfaces, Sorbonne Université) on CO oxidation (into CO_2) with Au nanoparticles deposited on oxides (alumina). This reaction is of great importance in environmental catalysis (application in catalytic convertors for example). However, the catalysts were already too active even without illumination. Future experiments will be conducted with less active catalysts: decreasing the Au loading on Al_2O_3 or using another support such as SiO_2, which leads to less active catalysts. The reactions take place under oxygen. If hot electrons are generated, they would react with O_2 leading to $O_2^{\cdot-}$, which can be analyzed by reduction of cytochrome c. The effect of temperature increase to plasmon excitation will also be studied in collaboration with theoretician physicists from Ecole CentraleSupélec.

Utilization of LSPR in photocatalysis under visible-light irradiation can efficiently improve the photocatalytic activity and also modify the product selectivity. Using plasmonic photocatalysts to convert solar light and to catalyze chemical reactions is promising, and the obtained results are encouraging. More studies are required for the physical understanding of plasmonic photocatalysis from fundamental and mechanistic points of view. For example, the determination of the electron-transfer process from plasmonic nanoparticles to the absorbed molecules or to the semiconductor (where they are deposited) is crucial to the photocatalytic properties. Also, the LSPR absorption is sensitive to size, shape and support, and can affect the

electron-transfer efficiency and the photocatalytic performance. More fundamental studies and calculations are also needed to understand the effect of heat increase (due to plasmon excitation) on the catalytic reactions.

Plasmonic nanoparticles can be used for greener, safer and more effective processes for chemical reactions. Plasmonic catalysis could be extended to various industrial reactions and reactions of environmental interest. As near infrared constitutes about 45% of the solar spectrum, it is also interesting to use nanostructures with plasmon in the near IR (such as Au nanorods or Pd nanoplates) for plasmonic photocatalysis. Fundamental studies on the mechanisms involved in these plasmonic catalytic reactions will also help to design more effective photocatalysts for a large number of reactions of environmental or industrial interest.

Annex

Gas phase oxidation of CO to CO_2 assisted by plasmon of gold nanoparticles

Table of content

Carbon monoxide is a colorless, odorless, tasteless, but highly toxic gas. It combines with hemoglobin to produce carboxy-hemoglobin, which usurps the space in hemoglobin that normally carries oxygen, which becomes ineffective for delivering oxygen to bodily tissues. The oxidation of carbon monoxide had been thoroughly studied during the last thirty years, as it is represents a major challenge to reduce its toxic abundance in the atmosphere. This highly exothermic reaction had been part of the refinery processes, vehicle exhaust emissions, water purification processes, industrial waste, and most importantly, medical and environmental aspects.

$2CO + O_2 \rightarrow 2\ CO_2$ ΔH=-394 kJ/mol

Haruta was the first to report that Au nanoparticles less than 5 nm can catalyze the oxidation of CO into CO_2 in the gas phase at room temperature [1]. had discovered the reactivity of gold nanoparticles in the enhancement of catalysis properties under certain conditions including size and morphology and the presence of an oxide support. The mechanisms of the oxidation still hold a major debate. Possible oxidation could happen on the cationic gold entities found in the medium with the presence of water coming from gas purging flow. Other mechanisms suggest a co-operative role between the support and the noble metal in the oxidation process. The latter mechanisms tend to be more complicated.

This annex gathers the preliminary results obtained on the oxidation of CO assisted by gold plasmon. The aim of the study was to provide a better understanding on energy damping or hot electrons injection into the system as a direct effect of excitation at wavelength matching the plasmon wavelength. This study has been conducted in collaboration with Catherine Louis and Laurent Delannoy (Laboratoire de Réactivité des Surfaces, Sorbonne Université).

I- Synthesis of gold nanoparticles on support

I-1- Deposition-Precipitation (DP) with urea

Deposition-Precipitation (DP) method is widely used by researchers to synthesize metal nanoparticles of controlled size on supports [2]. During thermal treatment, helium is introduced first to push out of any oxygen excess in the U-shaped reactor and valves connected to it. After around 15 minutes of helium purging, H_2 gas is purged at a predetermined flow rate.

A typical synthesis of Au/SiO_2 with a total content of 0.5 wt% is described as below. 1.3 mL of $HAuCl_4$ solution (19.7 mL) was added to a flask with 24.1 mL of distilled water (1 mM total concentration of Au in 25.4 mL of H_2O). Then, 1 g of silica and 38.9 mg of urea were added to the solution and stirred for 3 minutes to form a white suspension The flask was then heated up to 90° C under stirring. The temperature of water bath was kept at 90° C for 2 hours by adding glycerin and continuous magnetic stirring. At this point, the well dispersed suspension turned into a well formed precipitate. Later, 0.194 mL of 2-propanol was added to the suspension in order to scavenge the oxidative ·OH radicals generated during gamma irradiation of water solvent. The suspension was first degassed under N_2 to remove oxygen. The flask was irradiated for 67 minutes with a ^{60}Co panoramic gamma source (dose rate = 4.7 kGy/h). The metal ions (Au III) were reduced by solvated electrons and alcohol radicals induced by solvent radiolysis [3].

I-2- Synthesis after impregnation of gold ions on silica (SiO_2) substrate

One of the frequently used methods to synthesize well dispersed mono/poly layered Au/SiO_2 is direct impregnation of a gold salt solution directly on silica powder [4]. This method consists of carefully wetting a determined weight of silica powder initially with distilled water then later with a solution containing gold atoms. Afterwards, gentle and continuous mixing using a thick glass rod to achieve a relatively homogenous color for all the sample.

In order to prepare Au/SiO_2 4% in mass of Au loading using this method, 3g of SiO_2 (Aerosol 300/30) was wetted to ensure incipient humidity. Later, 7.2 mL of a $HAuCl_4$ solution ($n_{au} = 6.3\times10^{-4}$ mol), till we achieve a homogenous white-yellow powder. The latter powder will be left to dry for 48 to 72 hours.

Then, a urea washing (NH_4OH 30 %) for the dried powder is necessary to ensure controlled diameter of Au/SiO_2 nanoparticles, as Cl^- anion might interfere leading to larger clusters and perhaps the dissolution of silica. Later, a thermal treatment (calcination in sealed oven heated to 300 Celsius) is required to achieve dark-rose nanoparticles.

Different samples on Al_2O_3 and SiO_2 and with loading about 1% were also prepared (Table A-1). The size of the gold nanoparticles is around 2-3 nm.

Sample		Au (%)
Au/SiO_2 1%		0.64
Au/SiO_2_R01 1%		0.67
Au/SiO_2_R02 1%		0.67
	average loading	0.66
Au/Al_2O_3 1%		0.74
Au/Al_2O_3 _R01 1%		0.73
Au/Al_2O_3_R02 1%		0.75
	average loading	0.74

Table A-1. Loading of gold determined by XRF analysis data for the different samples prepared

II- Oxidation of CO

II-1- Reactor

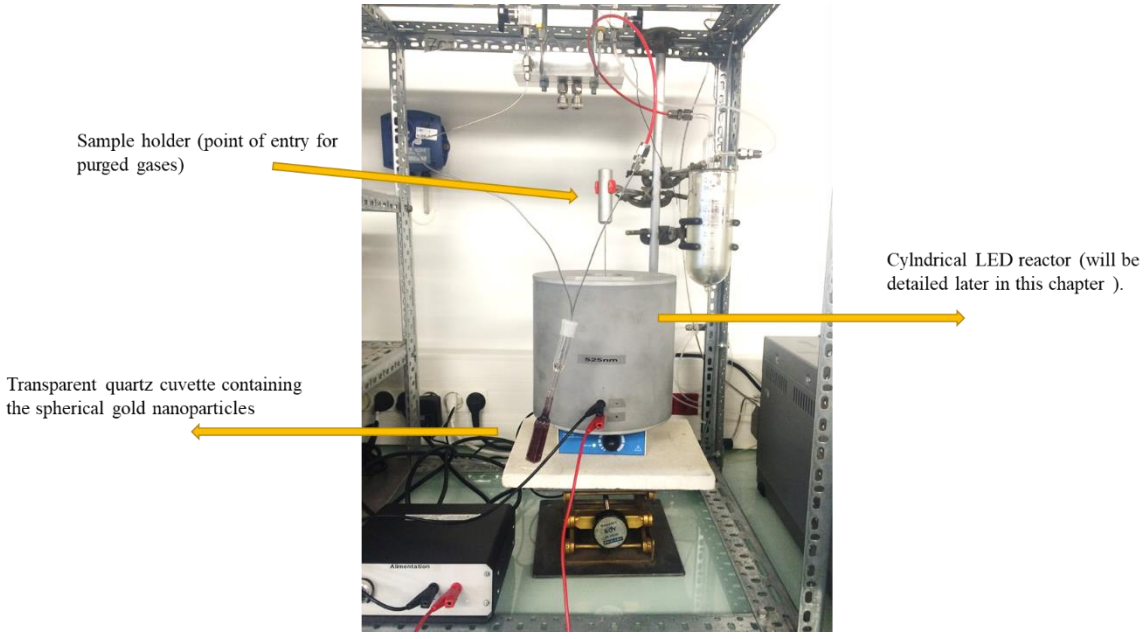

Figure A-1. Experimental setup used to study the oxidation of CO to CO_2 catalyzed by gold nanoparticles either supported on Al_2O_3, and SiO_2 or in solution like above.

Gas is pumped into the U-shaped glass reactor from top. As part of the purging process, Helium and oxygen are purged first for around 50 seconds then CO merged in Helium will be next. The initial and final concentrations of both CO and CO_2 are detected through a micro-gas-chromatography apparatus connected to the output of the reaction setup. Meanwhile, the

temperature variations can be monitored by a thermostat that is positioned carefully on the reactor surface.

II-2- Results

For this experiment, we have to consider different points and raise some questions:

1- Since the reaction is exothermic, how can we separate the heat induced by the SPR from the heat produced during the reaction?

2- In the same manner, do thermal changes inside the LEDs cylinder play a role during the total reaction time?

3- If the catalyst is highly active, is it advisable to deactivate the catalyst?

4- What is the role of reactor position inside the cylinder? How does the intensity of LEDs will modify the final catalytic yield: the concentration of CO_2?

First, it is necessary to check the temperature inside the illuminated reactor (LEDs cylinder) when there is no CO gas flow. We have installed sensitive thermostat at the center of the LEDs sphere to measure the temperature changes as a function of time when the intensity of the LEDs is at its maximum. After 60 min of runtime, a 6 C° rise in temperature is measured at the center of the LEDs reactor, and after 3 hours of runtime, the rise in temperature is 7°C.

First, the catalysis experiment was ready to be carried out using Au/Al_2O_3, 3% Au as catalyst. It seemed favorable to turn on the LEDs cylinder after the conversion of 30% of CO to CO_2, because Au/Al_2O3 3% is considered highly active, with a conversion percentage of almost 95% according to literature and our data. But, the sample is already too active even without illumination (Figure A-2), so no effect of illumination was detected (Figure A-3).

There are several possible explanations for this phenomenon:

1- The elevated activity of catalyst that is blurring the intended plasmonic effect.

2- The temperature keeps rising then stabilizes around 35 C° inside the LEDs sphere, which makes it more difficult to conduct the experiment under optimized conditions.

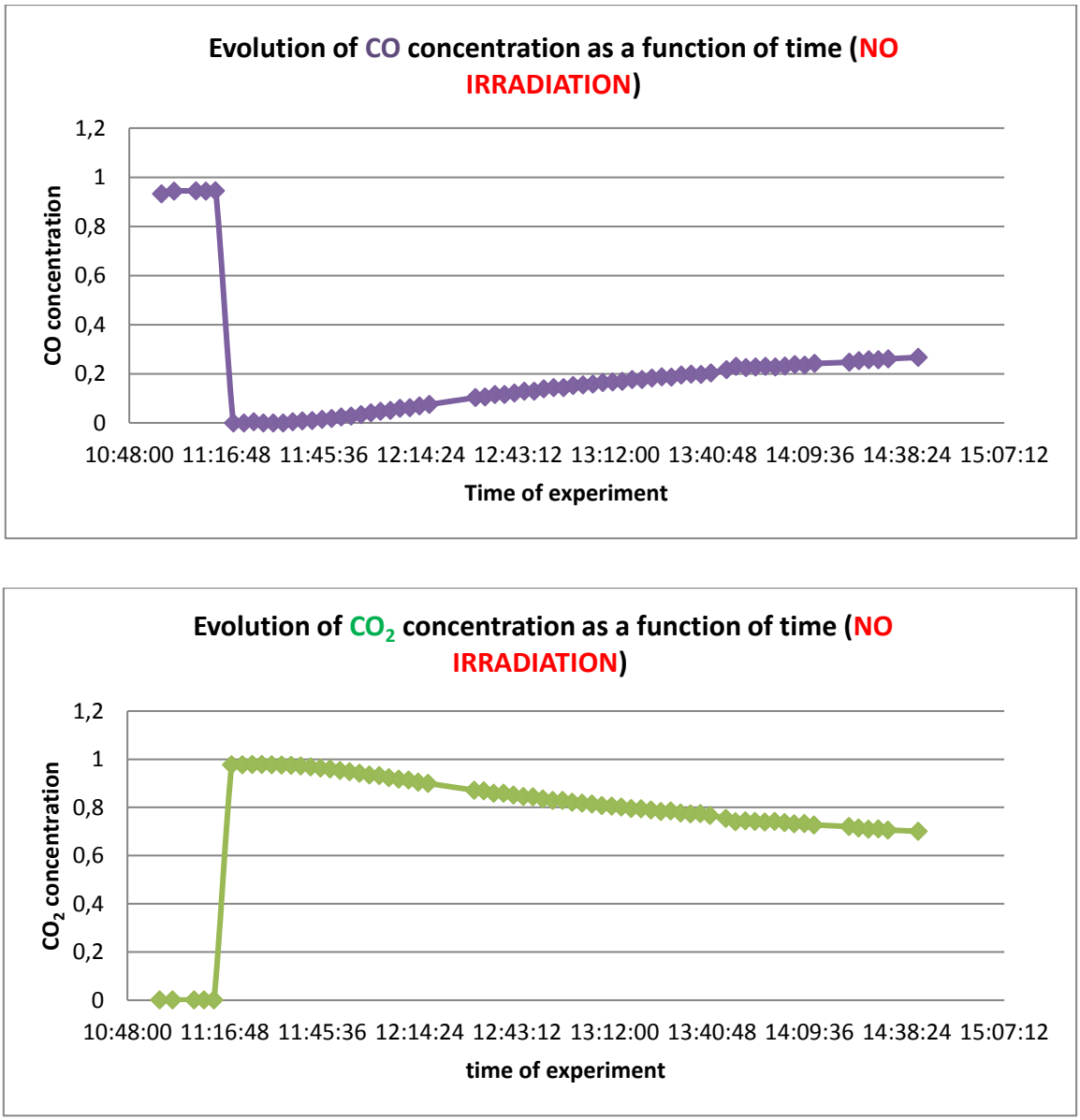

Figure A-2. Evolution of CO and CO_2 as a function of time of reaction without irradiation of LED light source. Note that the high activity of the catalyst made a total conversion with no irradiation; Then the CO_2 concentration started to go down as the activity decreases. The reaction is too fast.

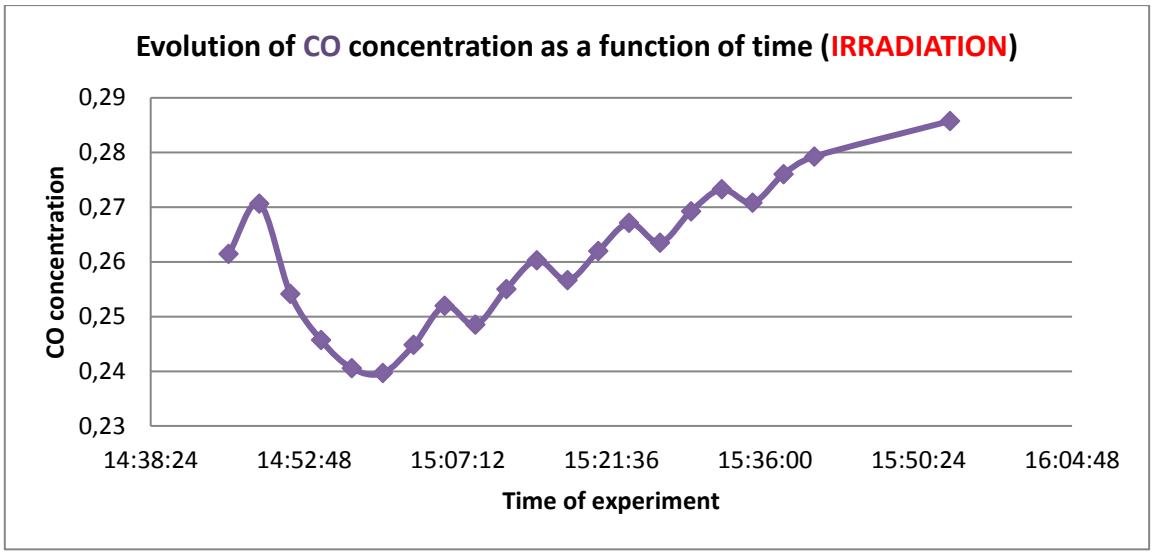

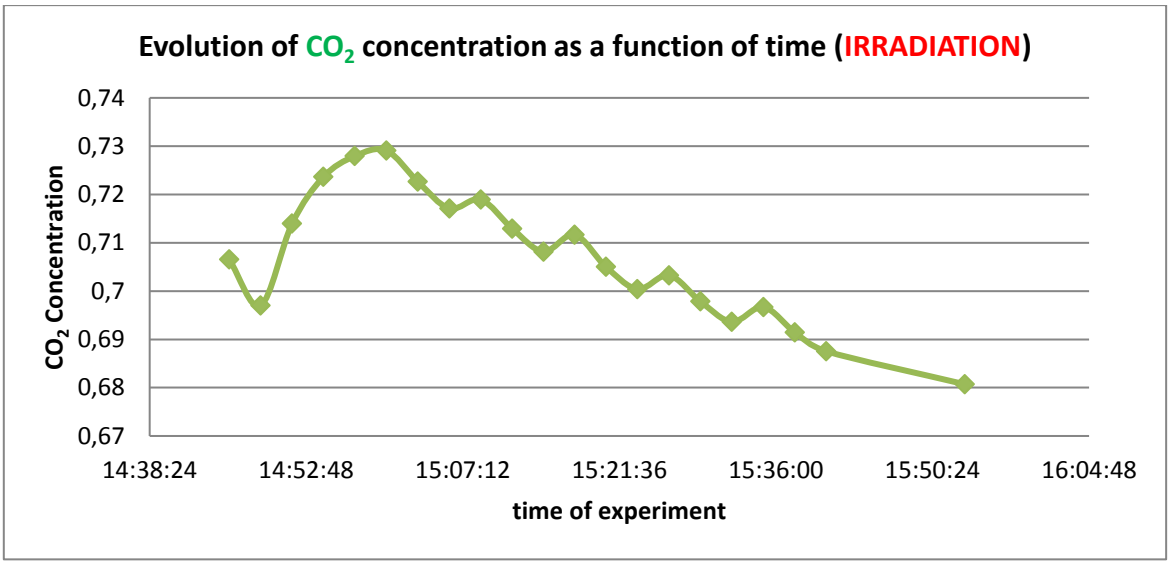

Figure A-3. Evolution of CO and CO_2 concentration as a function of time of reaction under illumination with LEDs light source. Note that because of the high activity of the catalyst, it is very difficult to determine the actual effect of AuNPs plasmon; Obviously as this perturbation is happening; it was not clear to verify this effect.

II-3- Perspectives

The approach would be then to minimize the activity of our catalyst and diffuse the extra temperature by dipping our U-shaped glass reactor into water with ambient temperature to diffuse the extra heat.

Our catalysts were too active, and it was not possible to study the effect of light irradiation. Next experiments will be conducted with less active catalysts by decreasing the Au loading on

Al_2O_3 or using another support such as SiO_2, which leads to less active catalysts. Another possibility is to prepare nanoparticles with larger sizes (3-5 nm).

The experiments could be conducted in a tube filled with distilled water (where the U-shaped reactor will be immersed) at room temperature to minimize the increase of temperature induced by the LED and to diffuse the heat produced by the reaction.

References

1. Haruta, M.; Kobayashi, T.; Sano, H.; Yamada, N. Novel gold catalysts for the oxidation of carbon monoxide at a temperature far below 0 C. *Chemistry Letters* **1987**, *16*, 405-408.
2. Hugon, A.; Kolli, N.E.; Louis, C. Advances in the preparation of supported gold catalysts: Mechanism of deposition, simplification of the procedures and relevance of the elimination of chlorine. *Journal of Catalysis* **2010**, *274*, 239-250.
3. Remita S, R.H.I.W.J., Rao BSM, Eds. . Recent Trends in Radiation Chemistry. *World Scientific* **2018**.
4. Zanella, R.; Giorgio, S.; Shin, C.; Henry, C.; Louis, C. Characterization and reactivity in CO oxidation of gold nanoparticles supported on TiO2 prepared by deposition-precipitation with NaOH and urea. *J. Catal.* **2004**, *222*, 357-367.

Synthèse de thèse en Français.

Catalyse Assistée par Plasmon.

Table des matières

Introduction

Les nanoparticules (NPs) métalliques ont de nombreuses applications en catalyse. Certaines d'entre elles (or, argent, cuivre) présentent une absorption dans le visible résultant de l'excitation du plasmon de surface par un champ électromagnétique extérieur.

Nous proposons dans ce projet de coupler les propriétés catalytiques de nanoparticules à base d'or avec leurs propriétés de résonance de plasmon de façon à assister la réaction catalytique par les électrons chauds générés et par l'effet thermique qui en découle. Cette approche de catalyse assistée par plasmon, est générale et peut être utilisée pour une variété de procédés catalytiques exothermiques et endothermiques impliquant des nanoparticules. Cette catalyse assistée par plasmon permet de réaliser des réactions catalytiques à moindre coût énergétique sous lumière solaire.

Résumé de l'état de l'art

Les plasmons sont des oscillations collectives des électrons confinés dans la bande de conduction des nanoparticules métalliques sous l'action de la lumière. Seul un nombre restreint de métaux présente une résonance de plasmon dans le visible, Il s'agit du cuivre, de l'argent et de l'or (voir Figure 1 en dessus).

Parmi ces métaux, l'or est le plus facile à manipuler car il ne s'oxyde pas. Par ailleurs, les nanoparticules d'or présentent des propriétés catalytiques dans les réactions d'oxydation de molécules telles que CO, COV… pour lesquelles le support oxyde (TiO_2, CeO_2) stabilisant les NPs permet l'activation de l'oxygène. L'or est aussi un catalyseur intéressant pour sa forte sélectivité pour des réactions d'hydrogénation bien que peu actif. Dans ce cas, le support n'intervient pas dans la réaction.

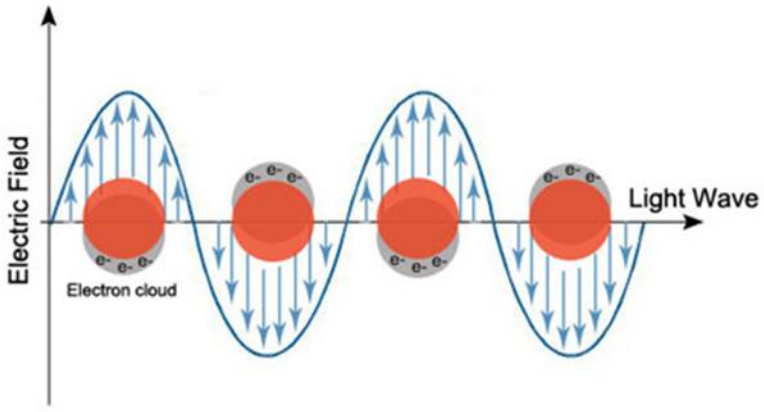

Figure 1- Présentation schématique de la polarisation d'une nanoparticule plasmonique sphérique et de l'oscillation continue due aux interactions de la fonction diélectrique.

Depuis ces cinq dernières années, les propriétés de résonance de plasmon de l'or commencent à être mises à profit pour asssister des réactions catalytiques et photocatalytiques.

La catalyse exaltée par plasmon est un domaine encore très récent et très prometteur [1,2]. L'énergie lumineuse absorbée par les NPs d'or est rapidement convertie en chaleur et des électrons chaux sont générés induisant l'exaltation des propriétés catalytiques. Toutefois peu d'études sont reportées dans la littérature pour étudier la catalyse exaltée par plasmon et comprendre l'origine de cette exaltation.

L'étude de la conversion lumière-chaleur dans les NPs métalliques et du transfert thermique vers leur environnement est assez récente. Grâce aux techniques d'optique ultrarapide, il est possible aujourd'hui d'appréhender les mécanismes d'échanges énergétiques, les mécanismes de transfert d'électron et leur cinétique [3,4]. La dynamique de relaxation thermique de NPs métalliques en matrice suite à l'absorption d'une impulsion lumineuse a pu ainsi être étudiée [4].

En outre, si les particules sont supportées, le transfert de chaleur à partir des particules ne respecte pas les lois de conduction de chaleur classique. Ces deux effets peuvent permettre un échauffement photothermique significatif des nanoparticules avec peu d'énergie optique et sans échauffement significatif du support. L'échauffement par plasmon à l'aide d'un laser permet le contrôle précis de la localisation, l'ampleur et la durée de l'énergie thermique. En revanche, si les nanoparticules sont en solution, l'énergie thermique peut être rapidement transférée au solvant. La Figure-2 schématise deux processus majeurs lies à l'excitation de la bande plasmonique n'un nanoparticule.

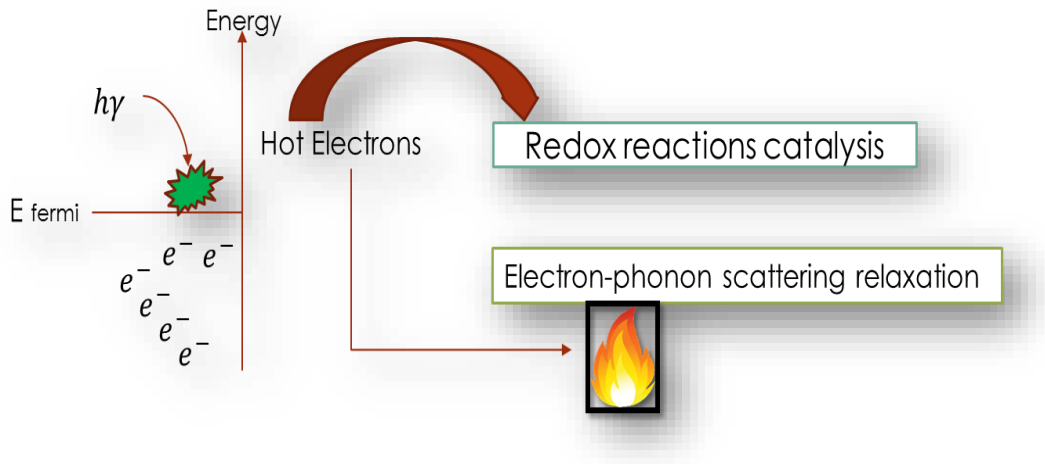

Figure 2- Présentation schématique des deux principales voies possibles d'interaction des électrons chauds avec le milieu entourent.

Ainsi, à des puissances laser assez faibles, une évaporation rapide du solvant peut être obtenue [5]. La possibilité de chauffer directement une nanoparticule de métal noble dans un liquide et de produire une phase vapeur avec un laser de longueur d'onde appropriée permet d'étudier également les réaction en phase gaz. Une telle réaction catalysée par la surface de la NP peut être contrôlée de manière rationnelle (plus ou moins accélérée selon l'énergie et la puissance lumineuse) La résonance plasmon de surface joue le rôle le plus important dans ces réactions catalysées par la surface, et les électrons chauds du plasmon de surface provoquent la réaction catalytique.

Le catalyseur peut être aussi en solution ou en suspension hétérogène déposée sur un support. On peut effectuer la réaction avec des réacteurs éclairés par des lampes, comme ceux que nous avons au LCP a été montré par exemple que l'échauffement par plasmon des nanoparticules d'or en solution fournit non seulement la chaleur de réaction, qui permet de générer à la fois de l'eau mais aussi la vapeur d'éthanol localement sur les catalyseurs en solution dans un mélange eau/éthanol. Les produits de réaction sont CO_2, CO et H_2 et, sont compatibles avec le reformage catalytique de la vapeur d'éthanol.

L'excitation du plasmon peut aussi être mise à profit dans le cas de la photocatalyse. Celle-ci désigne une réaction catalytique induite par l'absorption de photons par un semiconducteur qui génère un électron et un trou (quand l'énergie du photon est supérieure au gap). TiO_2 est le photocatalyseur le plus utilisé mais n'absorbe que dans l'UV. De plus, les rendements quantiques de conversion de la lumière sont faibles à cause des recombinaisons électro-trou élevées. L'ajout de nanoparticules métalliques (Au, Ag, Cu) permet d'augmenter le rendement quantique de conversion de la lumière d'une part, en diminuant la recombinaison-électron trou en piégeant les électrons et d'autre part en générant une activité dans le visible grâce à l'excitation du plasmon qui permet l'éjection d'électron du métal vers la bande de conduction du semiconducteur. En photocatalyse, l'effet prédominent qui permet l'augmentation de l'activité photocatalytique ne semble pas être l'échauffement comme pour la catalyse mais des transferts de charges.

Les processus catalytiques suscitent un intérêt majeur pour la recherche et le développement. Des processus catalytiques photo-activés naturels interviennent dans presque tous les aspects de notre environnement: les cycles de photosynthèse nourrissent et colorent les plantes, les réactions enzymatiques essentielles à la survie des espèces, la décontamination de l'eau à la lumière visible, etc.

Les nanoparticules de nature métallique présentent des propriétés différentes de celles des métaux dans leur structure globale. Plusieurs facteurs contribuent à la différence des propriétés

physico-chimiques telles que la taille, la morphologie, la fonctionnalisation et l'environnement environnant. La Figure 3 montre une solution colloïdale de NPs d'Or. Ces propriétés accordables sont étudiées et appliquées dans un large éventail d'applications.

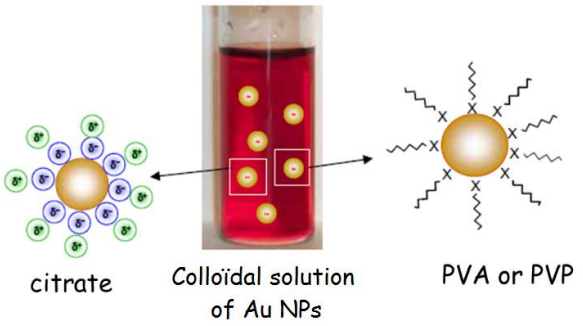

Figure -3 Fonctionnalisation électrostatique (citrate) ou stérique (PVA ou PVP) de nanoparticules d'or sphériques.

Résumé des travaux et principaux résultats

Dans un premier temps, nous avons étudié des réactions catalysées par des nanoparticules d'or synthétisées par la méthode de Türkevich (réduction de complexes d'or par du citrate).

Pour les réactions en solution, des réacteurs photocatalytiques (avec des lampes UV, Visibles ou LEDs) ont permis d'étudier les cinétiques de réaction et les rendements catalytiques. Un exemple d'un reacteur LED développé pendant la thèse est illustré en dessus (Figure-4)

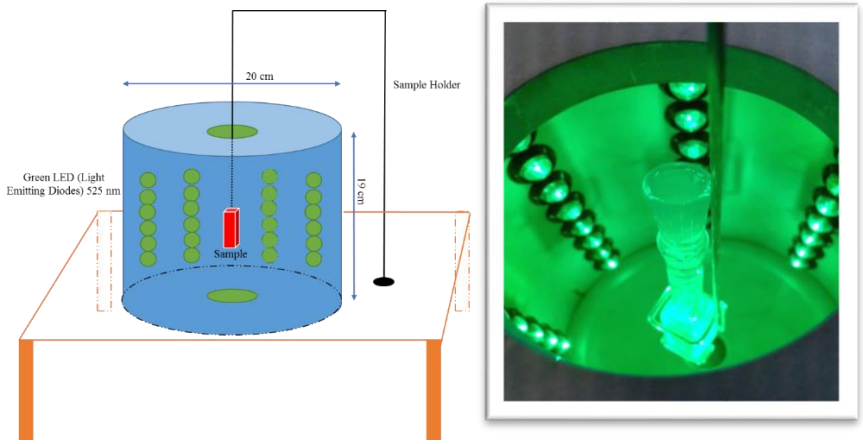

Figure-4 Illustration d'un réacteur LEDs fait maison (à gauche); une photo de l'intérieur du réacteur avec un échantillon de solution irradié dans une cuvette au centre (à droite).

Pour les réactions en phases gaz, des réacteurs du Laboratoire de Réactivité de Surfaces (LRS, Sorbonne Université) (collaboration avec l'équipe de Catherine Louis) ont été adaptés pour

réaliser des films minces et permettre des irradiations sous lumière visible ou sous excitation avec une lampe LEDs de longueur d'onde démission correspondant à celle du plasmon.
Dans un deuxième temps, nous avons étudié en collaboration avec l'ICMMO, des réactions de Suzuki-Miyaura catalysées par des nanofleurs de palladium irradiées dans le visible.

Ce manuscrit est organisé comme suit :
Le premier chapitre est une introduction aux nanosciences. La synthèse et les propriétés des nanoparticules d'or, en particulier le phénomène de résonance localisée du plasmon de surface sont développés. Les applications des nanoparticules d'or dans différents domaines sont présentées. Ce chapitre décrit également l'état de l'art de la catalyse assistée par plasmon.
Le deuxième chapitre est consacré aux matériaux, à la synthèse de nanoparticules métalliques et aux dispositifs expérimentaux utilisés pour étudier les réactions catalytiques. Les différentes techniques utilisées pour la caractérisation des nanoparticules et pour l'analyse des produits de réaction sont également décrites.
Dans le troisième chapitre, on étudie la dégradation du para-nitrothiophénol assistée par du plasmon d'or. Cette dégradation est très efficace avec les nanoparticules d'Or excitées sous lumière visible (Figure 5). Les résultats montrent que le mécanisme de dégradation est complexe car plusieurs produits sont formés. Cependant, il est prouvé que des réactions catalysées en surface impliquant des électrons chauds se produisent lorsque le para-nitrothiophénol (ou une partie de celui-ci) est réduit en para-aminothiophénol.

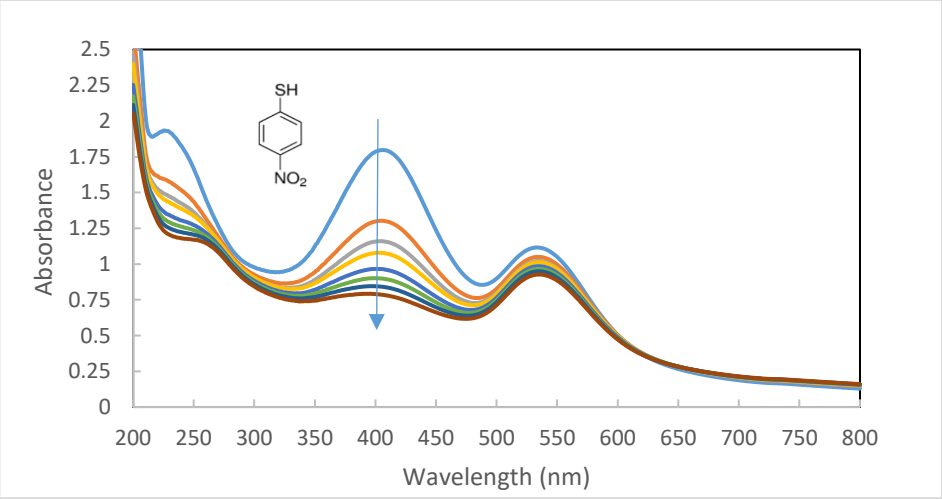

Figure 5- Evolution temporelle des spectres d'absorption d'une solution aqueuse contenant $1{,}64 \times 10^{-4}$ M de pNTP et 30 nm AuNPs ($[Au^0] = 1{,}74 \times 10^{-4}$ M) sous agitation et illumination à 525 nm dans le réacteur photochimique à LEDs pendant 480 minutes.

Dans le quatrième chapitre, nous avons étudié la réduction de l'ion ferricyanure (III) en ferrocyanure (II) catalysée par des nanoparticules d'or sphériques (AuNPs) lorsqu'ielles sont excitées à leur résonance localisée de plasmon. Cette réduction a lieu à température ambiante et sous illumination (lumière visible) même sans utiliser d'agent réducteur. Ce résultat indique à nouveau que des électrons chauds sont impliqués dans le mécanisme de réaction.

Le cinquième chapitre présente l'étude des réactions de couplage croisé Suzuki-Miyaura catalysées par le plasmon de nanofleurs de Pd (voir Figure 6). Les réactions entre les composés benzéniques halogénés et l'acide phényl boronique en présence de diverses bases sont étudiées à l'obscurité et sous irradiation (lumière visible). Il a été démontré que l'activité photocatalytique des nanofleurs de Pd pour les réactions de Suzuki-Miuyara est remarquablement accrue sous irradiation par la lumière visible [6,7].

Enfin, la conclusion générale met en évidence les principaux résultats obtenus au cours de cette thèse avec des nanostructures plasmoniques de Au et de Pd utilisées pour catalyser différentes réactions. Ces travaux ouvrent des perspectives en catalyse exaltée par plasmon, en particulier pour les applications environnementales.

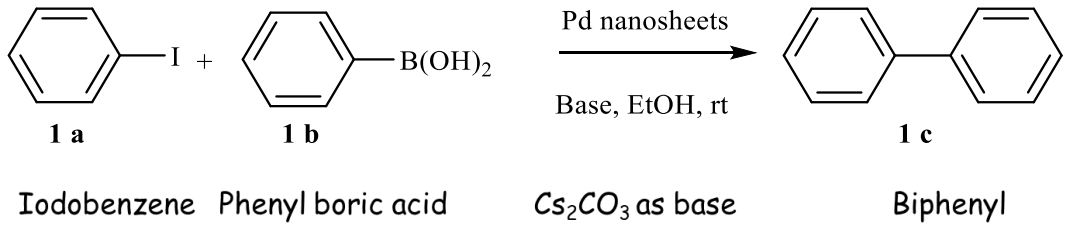

Figure 6- Illustration de la réaction de Suzuki-Miyaura catalysée par des nanofleurs de palladium.

En annexe, des travaux préliminaires sur l'oxydation du CO en CO_2 assisté par le plasmon de nanoparticules d'or (déposées sur différents supports) en phase gazeuse et liquide sont présentés.

Références

1. Linic, P.; Christopher, D.B.I. Plasmonic-Metal Nanostructures for Efficient Conversion of Solar to Chemical Energy. *Nat. Mater.* **2011**, *10*, 911–921.
2. Wang, C.; Astruc, D. Nanogold plasmonic photocatalysis for organic synthesis and clean energy conversion. *Chem. Soc. Rev.* **2014**, *43*, 7188-7216.
3. Govorov, A.O.; Richardson, H.H. Generating heat with metal nanoparticles. *Nano Today* **2007**, *2*, 30-38.
4. Adleman, J.R.; Boyd, D.A.; Goodwin, D.G.; Psaltis, D. Heterogenous Catalysis

Mediated by Plasmon Heating. *Nano Letters* **2009**, *9*, 4417-4423.
5. Dong, B.; Fang, Y.; Chen, X.; Xu, H.; Sun, M. Substrate-, wavelength-, and time-dependent plasmon-assisted surface catalysis reaction of 4-nitrobenzenethiol dimerizing to p,p'-dimercaptoazobenzene on Au, Ag, and Cu films. *Langmuir : the ACS journal of surfaces and colloids* **2011**, *27*, 10677-10682.
6. I.Sarhid; I.Abdellah; Lampre, I.; Huc, V.; Martini, C.; Remita, H. Plasmonic catalysis for the Suzuki–Miyaura cross-coupling reaction using palladium nanoflowers. *New J. Chem* **2019**, *43*, 4349-4355
7. Dumas, A.; Couvreur, P. Palladium: a future key player in the nanomedical field? *Chemical Science* **2015**, *6*, 2153-2157.

Catalysis Assisted by Plasmon

Table of Content

Introduction

Metallic nanoparticles (NPs) have many applications in catalysis. Some of them (gold, silver, copper) have a visible absorption resulting from the excitation of the surface plasmon by an external electromagnetic field. In this project, we propose to couple the catalytic properties of gold-based nanoparticles with their plasmon resonance properties in order to assist the catalytic reaction with the generated hot electrons and the resulting thermal effect. This plasmon-assisted catalysis approach is general and can be used for a variety of exothermic and endothermic catalytic processes involving nanoparticles. This plasmon-assisted catalysis makes it possible to carry out catalytic reactions at lower energy cost under sunlight.

A summary of the state of the art

Plasmons are collective oscillations of electrons confined in the conduction band of metal nanoparticles under the action of light. Only a small number of metals have plasmon resonance in the visible, this is copper, silver and gold (see Figure 1 above). Of these metals, gold is the easiest to handle because it does not oxidize. In addition, the gold nanoparticles have catalytic properties in the oxidation reactions of molecules such as CO, VOC ... for which the oxide support (TiO2, CeO2) stabilizing the NPs allows the activation of oxygen. Gold is also an interesting catalyst for its high selectivity for hydrogenation reactions, although not very active. In this case, the support does not intervene in the reaction.

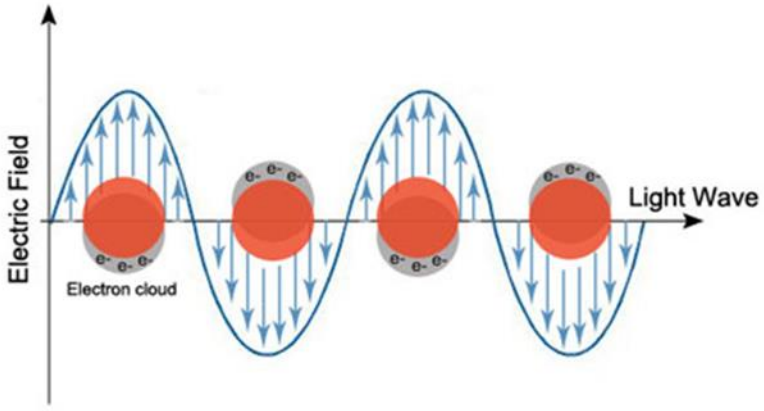

Figure 1- Schematic presentation of the polarization of a spherical plasmonic nanoparticle and the continuous oscillation due to the interactions of the dielectric function.

Since the last five years, the plasmon resonance properties of gold have begun to be used to support catalytic and photocatalytic reactions. Catalysis exalted by plasmon is still a very recent and very promising area [1,2]. The light energy absorbed by the gold NPs is rapidly converted into heat and lime electrons are generated inducing the exaltation of the catalytic properties. However, few studies are reported in the literature to study the catalytic exalted by plasmon and understand the origin of this exaltation.

The study of light-heat conversion in metallic NPs and heat transfer to their environment is fairly recent. Thanks to ultrafast optical techniques, it is now possible to understand energy exchange mechanisms, electron transfer mechanisms and their kinetics [3,4]. The thermal relaxation dynamics of metallic NPs in the matrix following the absorption of a light pulse could thus be studied [4].

In addition, if the particles are supported, the heat transfer from the particles does not respect the conventional heat conduction laws. These two effects can allow a significant photothermal heating of the nanoparticles with little optical energy and without significant heating of the support. Plasmon heating with a laser allows accurate control of the location, magnitude and duration of thermal energy. On the other hand, if the nanoparticles are in solution, the thermal energy can be quickly transferred to the solvent. Figure-2 demonstrate two major processes related to the excitation of the plasmonic band a nanoparticle.

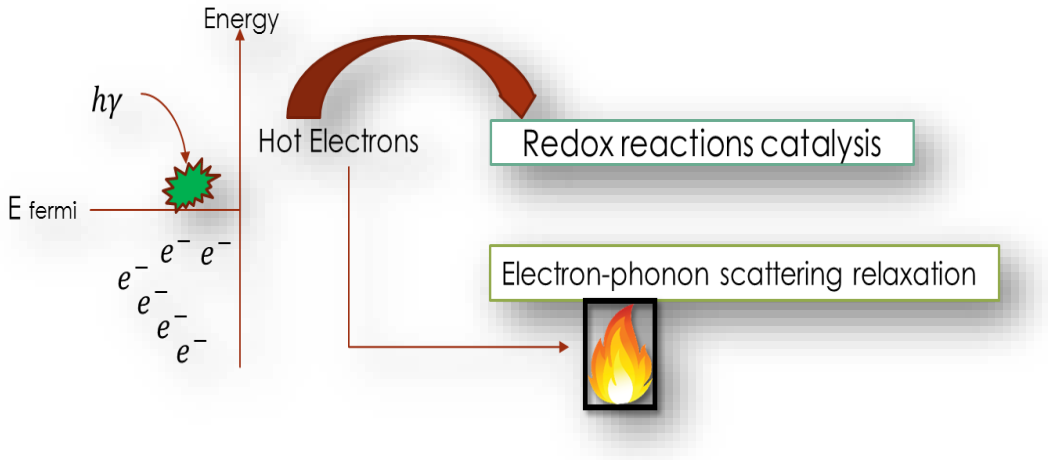

Figure 2- Schematic presentation of the two main possible ways of interaction of hot electrons with the surrounding medium

Thus, at relatively low laser powers, rapid evaporation of the solvent can be obtained [5]. The possibility of directly heating a nanoparticle of noble metal in a liquid and producing a vapor phase with a laser of appropriate wavelength also makes it possible to study the reactions in the gas phase. Such a reaction catalyzed by the surface of the NP can be controlled rationally (more or less accelerated according to the energy and the luminous power) The surface plasmon resonance plays the most important role in these reactions catalyzed by the surface, and Hot electrons from the surface plasmon cause the catalytic reaction.

The catalyst may also be in solution or in heterogeneous suspension deposited on a support. The reaction can be carried out with lamp-lit reactors, such as those we have at LCP has been shown, for example, that the plasmon heating of the gold nanoparticles in solution not only provides the heat of reaction, which makes it possible to generate both water but also ethanol vapor locally on the catalysts in solution in a water / ethanol mixture. The reaction products are CO2, CO and H2 and are compatible with the catalytic reforming of ethanol vapor.

Plasmon excitation can also be exploited in the case of photocatalysis. This refers to a catalytic reaction induced by the absorption of photons by a semiconductor that generates an electron and a hole (when the energy of the photon is greater than the gap). TiO2 is the most used photocatalyst but absorbs only in the UV. In addition, the quantum yields of light conversion are low because of high electro-hole recombinations. The addition of metallic nanoparticles (Au, Ag, Cu) makes it possible to increase the quantum efficiency of light conversion on the one hand, by decreasing the recombination-electron hole by trapping the electrons and on the other hand by generating an activity in the visible thanks to the plasmon excitation which allows the electron ejection of the metal towards the conduction band of the semiconductor. In photocatalysis, the predominant effect that allows the increase in photocatalytic activity does not seem to be heating as for catalysis but charge shifts.

Catalytic processes are of major interest for research and development. Natural photoactivated catalytic processes are involved in almost every aspect of our environment: photosynthetic cycles feed and color plants, enzymatic reactions essential for species survival, decontamination of water with visible light, etc. Nanoparticles of a metallic nature have properties different from those of metals in their overall structure. Several factors contribute to the difference in physico-chemical properties such as size, morphology, functionalization and the surrounding

environment. Figure 3 shows a colloidal solution of gold NPs. These tunable properties are studied and applied in a wide range of applications.

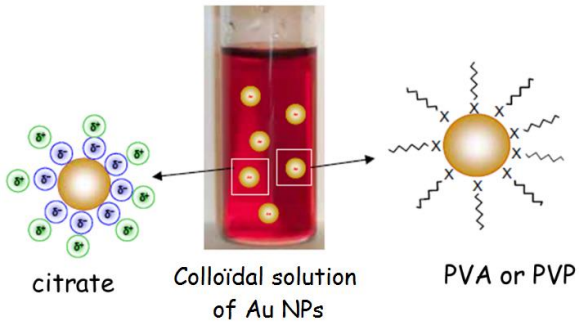

Figure -3 Electrostatic (citrate) or steric (PVA or PVP) functionalization of spherical gold nanoparticles.

Summary of work and main results

In a first step, we studied reactions catalyzed by gold nanoparticles synthesized by the Türkevich method (reduction of gold complexes by citrate).

For the reactions in solution, photocatalytic reactors (with UV, Visible or LEDs lamps) made it possible to study the kinetics of reaction and the catalytic yields. An example of an LED reactor developed during the thesis is shown above (Figure-4)

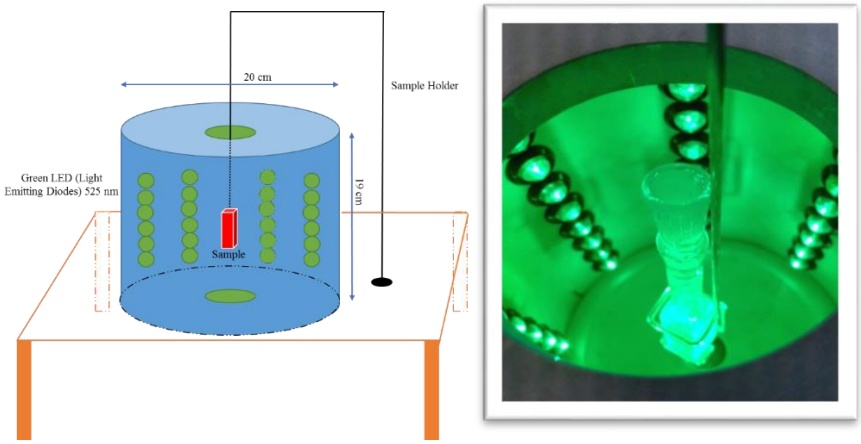

Figure 4 Illustration of a homemade LEDs reactor (left); a photo of the inside of the reactor with a sample of irradiated solution in a bowl in the center (right).

For reactions in the gas phase, reactors from the Surface Reactivity Laboratory (LRS, Sorbonne University) (collaboration with the Catherine Louis team) have been adapted to produce thin films and allow irradiation under visible light or under excitation with a lamp LEDs of wavelength resignation corresponding to that of the plasmon. In a second step, we studied in collaboration with the ICMMO, Suzuki-Miyaura reactions catalyzed by visible palladium nanofillers of palladium.

This manuscript is organized as follows:

The first chapter is an introduction to nanoscience. The synthesis and properties of gold nanoparticles, in particular the phenomenon of localized resonance of surface plasmon are developed. The applications of gold nanoparticles in different fields are presented. This chapter also describes the state of the art of plasmon-assisted catalysis.

The second chapter is devoted to materials, to the synthesis of metallic nanoparticles and to experimental devices used to study catalytic reactions. The various techniques used for the characterization of the nanoparticles and for the analysis of the reaction products are also described.

In the third chapter, we study the degradation of para-nitrothiophenol assisted by gold plasmon. This degradation is very effective with gold nanoparticles excited under visible light (Figure 5). The results show that the degradation mechanism is complex because several products are formed. However, there is evidence that surface catalyzed reactions involving hot electrons occur when para-nitrothiophenol (or a portion thereof) is reduced to para-aminothiophenol.

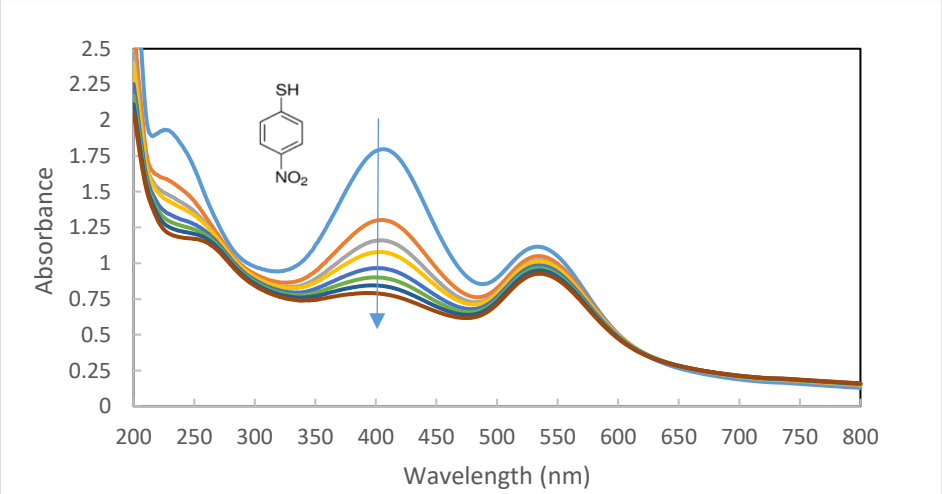

Figure 5 Temporal evolution of the absorption spectra of an aqueous solution containing 1.64 × 10^{-4} M pNTP and 30 nm AuNPs ([Au0] = 1.74 × 10^{-4} M) with stirring and illumination at 525 nm in the photochemical reactor with LEDs for 480 minutes.

In the fourth chapter, we studied the reduction of ferricyanide (III) ion to ferrocyanide (II) catalyzed by spherical gold nanoparticles (AuNPs) when they are excited to their localized plasmon resonance. This reduction takes place at ambient temperature and under illumination (visible light) even without the use of a reducing agent. This result again indicates that hot electrons are involved in the reaction mechanism.

The fifth chapter presents the study of the Suzuki-Miyaura cross-coupling reactions catalyzed by the plasmon of Pd nanoflowers (see Figure 6). Reactions between halogenated benzene compounds and phenyl boronic acid in the presence of various bases are studied in the dark and under irradiation (visible light). It has been shown that the photocatalytic activity of Pd nanofilters for Suzuki-Miuyara reactions is remarkably increased under visible light irradiation [6,7].

Finally, the general conclusion highlights the main results obtained during this thesis with plasmonic nanostructures of Au and Pd used to catalyze different reactions. This work opens perspectives for plasmon-enhanced catalysis, especially for environmental applications.

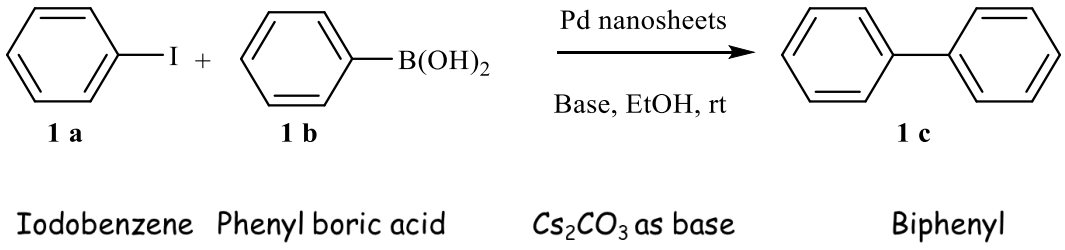

Figure 6 Illustration of the Suzuki-Miyaura reaction catalyzed by palladium nanofillers.

In the appendix, preliminary work on the oxidation of CO2 in CO2 assisted by plasmon of gold nanoparticles (deposited on various supports) in gaseous and liquid phase are presented.

Références

1. Linic, P.; Christopher, D.B.I. Plasmonic-Metal Nanostructures for Efficient Conversion of Solar to Chemical Energy. Nat. Mater. 2011, 10, 911–921.

2. Wang, C.; Astruc, D. Nanogold plasmonic photocatalysis for organic synthesis and clean energy conversion. Chem. Soc. Rev. 2014, 43, 7188-7216.

3. Govorov, A.O.; Richardson, H.H. Generating heat with metal nanoparticles. Nano Today 2007, 2, 30-38.

4. Adleman, J.R.; Boyd, D.A.; Goodwin, D.G.; Psaltis, D. Heterogenous Catalysis Mediated by Plasmon Heating. Nano Letters 2009, 9, 4417-4423.

5. Dong, B.; Fang, Y.; Chen, X.; Xu, H.; Sun, M. Substrate-, wavelength-, and time-dependent plasmon-assisted surface catalysis reaction of 4-nitrobenzenethiol dimerizing to p,p'-dimercaptoazobenzene on Au, Ag, and Cu films. Langmuir : the ACS journal of surfaces and colloids 2011, 27, 10677-10682.

6. I.Sarhid; I.Abdellah; Lampre, I.; Huc, V.; Martini, C.; Remita, H. Plasmonic catalysis for the Suzuki–Miyaura cross-coupling reaction using palladium nanoflowers. New J. Chem 2019, 43, 4349-4355

7. Dumas, A.; Couvreur, P. Palladium: a future key player in the nanomedical field? Chemical Science 2015, 6, 2153-2157.

Titre : Catalyse Assistée par Plasmon

Mots clés : Nanoparticules, Plasmon, Catalyse, Or, Palladium

Résumé : Les nanoparticules (NPs) métalliques ont de nombreuses applications en catalyse. Certaines d'entre elle (or, argent, cuivre) présentent une absorption dans le visible résultant de l'excitation du plasmon de surface par un champ électromagnétique extérieur.
Nous proposons dans ce projet de coupler les proprietes catalytiques de nanoparticules à base d'or avec leurs propriétés de résonance de plasmon de façon à assister la réaction catalytique par les électrons chauds générés et par l'effet thermique qui en découle.
Cette approche de catalyse assiste par plasmon, est générale et peut être utilisée pour une variété de procèdes catalytique exothermiques et endothermiques impliquant des nanoparticules. Cette catalyse assistée par plasmon permet de réaliser des réaction catalytiques à moindre cout énergétique sous lumière solaire.

Les processus catalytique sucitent un interet majeur pour la recherhe et le developpement. Des processus catalytiques photo-actives naturels interviennent dans presque tous les aspets de notre environnement: les cycles de photosynthese nourrissent et colorent les plantes, les reactions enzymatiques essentielles à la suivre des especes, la decontamination d l'eau à la lumiere visible, etc.

Enfin, la conclusion generale met en evidence les principaux resultats obenus au cours de cete these avec des nanostructures plasmonique de Au et de Pd utilisiees pour catalyer differentes reactions. Ces travauz ouvrent des perpectives en catalyse exaltee par plasmon, en particulier pour les applications environnmentales.

Title : Catalysis Assisted by Plasmon

Keywords : Nanoparticles, Plasmon, Catalysis, Gold, Palladium

Abstract : Metallic nanoparticles (NPs) have many applications in catalysis. Some of them (gold, silver, copper) have a visible absorption resulting from the excitation of the surface plasmon by an external electromagnetic field.
In this project, we propose to couple the catalytic properites of gold-based nanoparticles with their plasmon resonance properties in order to assist the catalytic reaction with the generated hot electrons and the resulting thermal effect.
This plasmon-assisted catalysis approach is general and can be used for a variety of exothermic and endothermic catalytic processes involving nanoparticles. This plasmon-assisted catalysis makes it possible to carry out catalytic reactions at lower energy cost under sunlight.

Catalytic processes are a of major interst for research and development. Natural photoactivated catalytic processes are involved in almost every aspect of our environment: photosynthetic cycles feed and color plants, enzymatic reactions essential for species survival, decontamination of water with visible light, etc.

Finally, the general conclusion highlights the main results obtained during this thesis with plasmonic nanostructures of Au and Pd used to catalyze different reactions. This work opens perspectives for plasmon-enhanced catalysis, especially for environmental applications.